Studies on Effects of Metamorphosis and Body Growth on Newt Skeletal Muscle Dedifferentiation

October 2022

YU ZHANYANG

Studies on Effects of Metamorphosis and Body Growth on Newt Skeletal Muscle Dedifferentiation

A Dissertation Submitted to

The Graduate School of Life and Environmental Sciences,

The University of Tsukuba

In Partial Fulfillment of the Requirements

For the Degree of Doctor of Philosophy in Science

YU ZHANYANG

Table of contents

Abstract

Newts can regenerate their limbs throughout their lifespan. To ensure this ability, they switch the stem cell-based cellular mechanism of muscle creation during limb regeneration to a dedifferentiation-based one as they grow beyond metamorphosis. However, which developmental process is essential for muscle dedifferentiation, metamorphosis or body growth, is unknown. To address this issue, I tracked muscle fibers during limb regeneration under conditions in which metamorphosis and body growth were experimentally shifted along the axis of development. Results in this study indicate that a combination of metamorphosis and body growth is necessary for muscle dedifferentiation. On the other hand, *ex vivo* tracking of larval muscle fibers revealed that newt muscle fibers have the ability to dedifferentiate independently of metamorphosis and body growth. These results suggest that newt muscle fibers have an intrinsic ability to dedifferentiate, but that metamorphosis and body growth are necessary for them to exhibit this hidden ability. Presumably, changes in the extracellular environment (niche) during developmental processes allow muscle fibers to contribute to limb regeneration through dedifferentiation. This study can stimulate research on niches as well as gene regulation for dedifferentiation, contributing to a further understanding of regeneration and future medical applications.

Abbreviations

Bp	Base pair
CAGGs	Chicken beta actin promoter with CMV-IE
CarA	Frog (*Xenopus laevis*) cardiac actin promoter
$CreER^{T2}$	Modified Cre recombinase containing the estrogen receptor T2
DAPI	4,6-Diamidino-2-phenylindole
DMSO	Dimethyl sulfoxide
EGFP	Enhanced green fluorescent protein
FA100	4-Allyl-2-methoxyphenol
mCherry	Red fluorescent protein
HS4	Chicken beta-globin core insulator
IgG	Immunoglobulin G
MI	Metamorphosis Inhibition
MIR	Metamorphosis Inhibition Released
Pax7	Paired box protein 7
PBS	Phosphate buffered saline
PCR	Polymerase chain reaction
SMFCs	Skeletal muscle fiber cells
Mono-SMFCs	Mononucleated-skeletal muscle fiber cells
PCNA	Proliferating Cell Nuclear Antigen

BrdU	Bromodeoxyuridine
WE	Wound epithelium

1. Introduction

1.1 The Newt - An Ideal Model for Self-regeneration Study

Regeneration is the ability that organisms can restore their lost body parts. This phenomenon has been studied for more than 200 years, since a famous Italian naturalist Lazzaro Spallanzani documented this phenomenon in various organisms, especially on the salamander's limb, tail, and jaw regeneration (Spallanzani, 1769). But it still has many mysteries remained.

Regenerative ability has been studied in many organisms, such as planarian, hydra, starfish, axolotl, newt and so on (Molina, M.D et al., 2021; Reddy P. C et al., 2019; Cary G.A et al., 2019; Sámano, C et al., 2021; Casco-Robles M. M et al., 2021). Among those organisms, the Japanese fire-bellied newt, *Cynops pyrrhogaster*, is an urodele amphibian which is classified into the family *salamandridae*, can repeatedly regenerate its various complex tissues or body-parts throughout its lifespan. For example, as figure 1 shows, it can regenerate eye tissues (especially the retina and the lens), the limbs, the tail, and so on (Brockes and Kumar, 2002; Tsonis, 2002; Chiba, 2014; Eguchi, G et al., 2011; Koriyama, K et al., 2018).

In contrast to other salamanders like the axolotl which has been recognized as an ideal model for regeneration research for decades, the newt keeps their regenerative ability even after metamorphosis (Wallace, 1981). Previous studies suggested that the newt have evolved a new mechanism that switched terminally differentiated somatic cells into stem-like cells which contribute to tissue regeneration. This process is

so-called reprogramming or dedifferentiation, and it has already been proved in the newt retina and lens regeneration (Saito et al., 1994; Chiba et al., 1997; Tsonis et al., 2004; Islam, M. R et al., 2014; Casco-Robles M. M et al. 2016), and in the newt limb regeneration (Tanaka, H. V et al., 2016; Casco-Robles R. M et al., 2018). Such high regenerative ability is maintained throughout its whole lifespan (Eguchi et al., 2011).

Therefore, the newt is an ideal model for regeneration study, and have huge potential for development of human self-regenerative medicine on how to treat patients with traumatic damage or loss of body parts, or even age-related degenerative diseases (Stocum and Cameron, 2011; Simon and Tanaka, 2013; Joven, A et al., 2019; Matsunami M et al., 2019).

1.2 Adult Newt Limb Regeneration

The newt has exceptional ability to regenerate several kinds of tissues, such as eye tissue (especially retina and lens), limb, tail, jaw, cardiac tissue and so on. Among them, the limb is one of the complex structures, but so impressive to provide us evidence to accomplish human regenerative therapy.

Limb regeneration is an intriguing topic, and it has been researched for long time. It is a complex and long-term process. The overall process of adult newt limb regeneration can be seen in Figure 2. It occurs in two main steps. First, the intact cells dedifferentiate at the wound site into progenitors to form the blastema (Iten and

Bryant, 1973). Second, the blastemal cells will undergo proliferation, patterning, differentiation, and growth using similar genetic mechanisms that deployed during embryonic development (Endo et al., 2004). Ultimately, blastemal cells will generate all the cells for the new structure (Brockes et al., 2001).

When the limb is amputated, the epidermis migrates to cover the stump in 1–2 hours, forming a structure called the wound epithelium (WE) (Satoh et al., 2012). Epidermal cells continuously migrate over the WE, and resulting in a thickened, specialized signaling center called the apical epithelial cap (AEC) (Christensen and Tassava, 2000). Several days later, there are changes in the underlying stump tissues that result in the formation of a blastema (a cell mass accumulated by dedifferentiated cells). Then, a new functional limb is eventually regenerated (Brockes J. P., 1997; Simon A and Tanaka E. M., 2013; Stocum D. L., 2017).

In adult newt limb regeneration, compared to human being, which form scar tissue after injury (Shirakami E et al., 2020). Newt have a non-scar structure maintaining their regeneration capability throughout whole lifespan (Godwin J. W and Rosenthal N., 2014). Focusing on muscle, it undergoes an event called dedifferentiation, and those cells contribute to followed muscle creation. This unique phenomenon draws attention and brings inspiration into development of human regenerative medicine (Chaar Z. Y and Tsilfidis, C., 2006).

1.3 Dedifferentiation

Cell dedifferentiation is the process, by which cells grow reversely from a partially or terminally differentiated stage to a less differentiated stage within their own lineage (Yao, Y et al., 2020).

Larvae of salamanders are, in general, capable of regenerating limbs, primarily from stem or progenitor cells, with the exception of cartilage/bone which is created by the reprogramming or dedifferentiation of mature cells in the dermis of the skin and interstitial tissue (i.e., connective tissue cells) (Tanaka, H. V et al., 2016; Kragl, M et al., 2009; Gerber, T et al., 2018; Lin, T. Y et al., 2021). Focusing on muscle, it is believed that larval muscle is created from muscle progenitor or stem cells, such as satellite cells. However, in most salamanders, regenerative ability of the limbs declines after metamorphosis, although the mechanism is not yet clear (Tsonis, P. A., 1996; Brockes, J. P. et al., 2002; Monaghan, J. R. et al., 2014).

Previous lineage tracing study (Tanaka, H. V et al., 2016; Sandoval-Guzmán, T et al., 2014) by tissue transplantation and muscle tacking study in Japanese fire-bellied newts revealed that, only skeletal muscle contributes to muscle creation through a unique strategy called dedifferentiation.

Muscle dedifferentiation during limb regeneration is a process that fully matured multi-nucleated skeletal muscle fiber cells in the stump migrate and become mono-nucleated skeletal muscle fiber cells which accumulated in blastema (Figure 3). After

this process, resulting cells contribute to muscle creation. This is critical for adult newt muscle regeneration.

Because human being loses regenerative ability, stem cells have no contribution of recovering from body-parts lost, or even age-related damaged disease, so that research on dedifferentiation, with an emphasis on tissue-specific findings, cellular mechanism will provide huge potential for designing new therapeutic strategies for regenerative medicine.

1.4 Cellular Mechanism Switches with Development

Of note, previous studies using muscle fiber cells-tracking system, which demonstrated that, as newt undergone a developmental event called metamorphosis, their lifestyle changed from an aquatic larva mode to a terrestrial adult mode (Figure 4), cellular mechanism for muscle regeneration was switched, from a stem/progenitor-based mechanism to a dedifferentiation-based mechanism. The adult newts (*Cynops pyrrhogaster*) create myogenic cells from multinucleated muscle fibers by dedifferentiation and mobilize them for limb regeneration (Tanaka, H. V et al., 2016).

It has still not been possible to track muscle stem cells in newts, but if they contribute to adult muscle regeneration, their relative contribution to the adult stage is likely to be reduced, as inferred from the increased contribution of

dedifferentiation. Thus, for muscle, dedifferentiation appears to be a mechanism that complements the stem cell-based muscle creation capacity, thereby ensuring limb regeneration in the adult stage.

1.5 Metamorphosis and Body Growth

However, it remains to be determined, during natural development, which developmental event is regulating muscle dedifferentiation ability.

As one possibility, metamorphosis, which makes newt adapt to terrestrial environment has been considered. The metamorphosis of amphibians is an elaborate process involving substantial histological and physiological changes. For example, shrank tail fin, degradation of external respirational organ (gills) and newly developed lungs as amphibian adapts from aquatic to terrestrial environment (Fabre, A. C et al., 2020; Bonett, R. M et al., 2017; Denoël, M et al., 2019). Metamorphosis is initiated internally and maintained by the thyroid hormone (TH), and the process is obligatory. TH elicits extensive cellular, biochemical, and morphological changes to occur during metamorphosis. Events that occur during metamorphosis, including altered gene expression, morphogenesis, tissue restructuring, and extensive cell death, result from differential response of tissues to TH (Page, R. B et al., 2009; Ajduković, M et al., 2021; Johnson, C. K et al., 2013; Crowner, A et al., 2019).

Another possibility is growth. As the newts grow, their body size is gradually getting big, when the newts age over 1.5 years and size bigger than 8 cm, they become reproductive (Maranouchi et al., 2000). Therefore, during growth, not only body size and cell number increase, also possibly growth hormone or sexual hormone may change the microenvironment and give rise muscle dedifferentiation competency.

1.6 Purpose and Goal of This Study

In this study, to address the question as to determine which process is essential for muscle dedifferentiation, naturally developing newts as well as experimentally modified newts such as those grown in a condition that inhibited metamorphosis examined (Chiba, C et al., 2012). Combined with muscle nucleus-tracking system (Casco-Robles M. M et al., 2010; Casco-Robles M. M et al., 2011) and CRISPR/Cas9 albino newts, I was able to clarify the muscle behavior during limb regeneration and uncover the mechanism that what makes muscle dedifferentiation ability unleashed. Solving these questions, could provide fundamental basis for uncovering the molecular mechanism of dedifferentiation, and potentially connects to new therapeutic strategies for muscle damage disease (Relaix, F et al., 2021).

2. Materials and Methods

Experiments presented herein were performed at University of Tsukuba. All methods were carried out in accordance with the Regulations on the Handling of Animal Experiments in Tsukuba university. All experimental protocols were approved by the Animal Care and Use Committee in university (University of Tsukuba, 120119, 170110). Moreover, all methods were performed in accordance with the ARRIVE guidelines.

2.1 Animals

The Toride-Imori line of the Japanese fire-bellied newt *Cynops pyrrhogaster* was used in this study. The adult newts for egg collection were reared at 18 °C under natural light in the University of Tsukuba. Fertilized eggs (F0) were obtained from these animals (total body length: males, ~9 cm; females, 11–12 cm, see Figure 4) naturally or artificially (see below), and allowed to develop at 18-20 °C in special laboratory rooms unless otherwise noted. For albino F1 newts, fertilized eggs were artificially obtained from albino F0 newts (> 5 years old) matured in the laboratory (Figure 6). All wild-type F0 and albino F1 newts examined in this study were obtained from the University of Tsukuba. Developmental stages of larvae were determined according to previous criteria. In this study, newts (~3 cm, total body length, see Figure 4) immediately after metamorphosis that had just started to eat

food, were defined as ‘juveniles’ (see Figure 18), while those that reached ~6 cm (total body length) were considered as ‘preadolescence’ (see Figure 23).

2.2 Anesthesia

An anesthetic, FA100 (4-allyl-2-methoxyphenol; DS Pharma Animal Health, Osaka, Japan) dissolved in tap water (v/v) was used at room temperature (22 °C). Before limb amputation, animals were anesthetized in the following conditions (FA100, time) unless otherwise noted: swimming larvae, 0.025%, 30 min; juveniles, 0.025%, 30 min; preadolescences, 0.05%, 30 min; MI giant larvae, 0.05%, 60 min; MIR juveniles, 0.05%, 60 min; adults, 0.1%, 60 min. This anesthesia was also applied to monitor cells in living animals, when taking pictures of animals, *in vitro* fertilization, and the endpoint.

2.3 Limb Amputation

Following anesthesia, pre-metamorphic newts (swimming larvae and MI giant larvae) were transferred to plastic cups containing newt normal saline solution (115 mM NaCl, 3.7 mM KCl, 3 mM $CaCl_2$, 1 mM $MgCl_2$, 18 mM D-glucose, 10 mM HEPES and 0.001% phenol red; adjusted to pH 7.5 with 0.3N NaOH) until amputations. Post-metamorphic newts (juveniles, preadolescences, MIR juveniles and adults) were rinsed with filtered tap water and dried on a paper towel.

A forelimb of each animal was amputated under a dissecting microscope (M165 FC; Leica Microsystems, Wetzlar, Germany) using a surgical blade (No. 19, Futaba, Tokyo, Japan) for swimming larvae, juveniles, and preadolescences, while a microtome blade (C35, Feather Safety Razor, Osaka, Japan) was used for MI giant larvae, MIR juveniles and adults. To track the skeletal muscle fiber cells (SMFCs) during limb regeneration in all cases, I performed amputation in the middle of the forearm, which positions near the middle of ulna and radius.

Pre-metamorphic amputees were allowed to recover in a plastic cup (φ86 × 40 mm; one animal per cup) containing filtered tap water at 18-20 °C and then reared in the same condition. Post-metamorphic amputees were placed in a Tupperware box (W: 14.1 cm D: 21.4 cm, H: 4cm; one animal per box) containing crumpled pieces of half-dried paper towel, allowed to recover at 14 °C overnight, then reared in the same box at 18–20 °C. The cups and moist boxes were cleaned every other day to avoid contamination. Feeding was restarted as soon as the digits appeared on the regenerating forelimb. Post-metamorphic newts were returned to the moist container after feeding for 3 h.

2.4 Transgenesis for muscle fiber nucleus-tracking

Construct design

To track the nuclei of muscle fibers, a plasmid vector *pCreERT2<CarA-CAGGs>[EGFP]mCherry (I-SceI)*2 was modified so that a nuclear localization signal (MAPKKKRKV; DNA sequence: 5'-ATGGCTCCAAAGAAGAAGCGTAAGGTA-3') (Kalderon, D et al., 1984) was added to N-terminal end of mCherry, using conventional molecular cloning procedures.

This cassette comprises the Cre driver and *LoxP* reporter constructs in opposite directions (see Figure 5). The reporter construct *CAGGs>[EGFP]N-mCherry* expresses EGFP, whose gene is flanked by *loxP* sites and followed by the *N-mCherry* gene, under the control of a universal promoter (*CAGGs*). The driver construct *CreERT2<CarA* expresses inducible Cre recombinase (Cre-ERT2) under the control of a cardiac actin promoter (*CarA*; from M11 cardiac actin promoter pCarA, Addgene 171482), allowing the specific expression of N-mCherry in mature skeletal muscle fibers of limbs via Cre-mediated recombination of the floxed EGFP in the presence of an inducer tamoxifen. Each construct was flanked by chicken β-globin HS4 2× core insulators (kindly provided by Dr. Gary Felsenfeld at the National Institute of Health, Bethesda, MD, USA). The transgene cassette was flanked by I-*Sce*I recognition sites, allowing its insertion into the newt genome. Note that the plasmid was cloned and amplified in the Stbl3 strain of *Escherichia coli* (One Shot Stbl3 chemically

competent *E. coli*, C7373-03; Thermo Fisher Scientific, Inc., Waltham, MA, USA) at 28°C. This step was essential to ensure the integrity of the plasmid due to its complexity.

CRISPR/Cas9 albino parental (F0) newts

Albino parental newts were provided by Dr.Takeshima, detailed information described as following. Albino parental newts were created by a knock-out of the tyrosinase gene at Nagoya University (3LBA-29, The 37th Annual Meeting of the Molecular Biology Society of Japan, 2014;https://www.mbsj.jp/meetings/annual/2014/program/LBA.pdf; for details, see Figure 6).

To collect eggs, adult male and female Toride-Imori newts were transferred from the University of Tsukuba in advance. Following *in vitro* fertilization (for detailed procedures, see next section), one-cell stage embryos were injected, as in transgenesis (see below), with 10 nl of solution containing 400 pg of sgRNA, which was designed to target 5'-CCTTCTCTTTTGGGAACGCGAAC-3', based on the *C. pyrrhogaster* tyrosinase sequence (accession number LC062599, DDBJ) that cloned in-house, and 2 ng of recombinant CAS9 His tag NLS protein (CP01; PNA Bio Inc., Newbury Park, CA, USA). A primer set (forward: 5'-GTGTGGACGACCGGGAAG-3'; reverse: 5'-GCTTAGCAGGTCGGCTACTG-3') was used to evaluate the deletion

of the target site. The F0 albino mutants screened at Nagoya University were transferred to the University of Tsukuba, and reared for longer than 5 years.

Egg collection

Fertilized eggs of wild type newts were routinely obtained early in the morning using a two-tank system in a semi-natural condition, as described previously (Casco-Robles M.M et al., 2011). For one-cell embryos of albino F0 newts, *in vitro* fertilization was performed as following. A pair of adult male and female newts (> 5 years old) in the reproductive state were injected subcutaneously with 100 μl gonadotropin (HCG, 3,000U; Asuka Seiyaku, Tokyo, Japan) every two days for one week prior to *in vitro* fertilization.

The animals were anesthetized, dried in paper towels, and placed in surgical chambers. First, the oviducts containing eggs were excised from the female, and ~30 mature eggs enveloped by the chorion were carefully transferred into a Petri dish and stored at 14 °C. Meanwhile, the vas deferens containing sperm was excised from the male and transferred into another Petri dish on ice. The vas deferens was gently homogenized in 1 ml 1x MMR solution (100 mM NaCl, 2 mM KCl, 2 mM $CaCl_2$, 1 mM $MgSO_4$, 5 mM HEPES, 0.1 mM EDTA; pH7.4 adjusted with 0.3N NaOH) on ice to release the sperm. The dish containing the eggs was returned to room temperature (18-20 °C). Then, the sperm-MMR suspension was diluted with the same volume of

distilled water, and immediately poured over the eggs. The eggs were allowed to stand for 15 min, rinsed twice with 1x MMR solution, and allowed to stand for another 30 min. The fertilized eggs were rinsed twice with 0.2 x MMR solution, allowed to stand for 1 h, and then used for microinjection.

Microinjection

Transgenesis was carried out according to the I-*Sce*I protocol: Following dejellying, one-cell-stage embryos were injected with a construct/enzyme mixture (80 ng/μl DNA construct; 0.5 U/μl I-*Sce*I (catalogue number: R06945; New England Biolabs, Tokyo, Japan); 1× I-*Sce*I buffer (New England Biolabs); 0.01% phenol red) at 4–8 nl per embryo, and then reared until they reached the developmental stages to be examined (Casco-Robles M. M et al., 2011).

Tamoxifen-induced recombination

Swimming larvae at St. 53 were temporarily incubated in rearing solution (0.1 × Holtfreter's solution) containing 4 μM(*Z*)-4-hydroxytamoxifen (4-OHT; H7904-5MG; Sigma-Aldrich Japan K.K., Tokyo, Japan; master mix: 100–300 μM in dimethyl sulfoxide) for 24 h.

In this study, prior to the administration of 4-OHT, animals that expressed EGFP evenly throughout the body or exclusively in muscle fibers were pre-screened, as

done previously (Tanaka, H. V. et al., 2016). After 4-OHT administration, animals that specifically expressed N-mCherry in nuclei of striated muscle fibers were screened. Recombination efficiency and specificity were assessed using tissue sections (see Figure 7-12). The ratio of mCherry nuclei to all nuclei in EGFP-positive muscle fibers was calculated by tracing the outline of the muscle fiber with a line on the image and counting the nuclei in it. This was done using five sections per forelimb of one individual, and the average of the five sections was used as the representative value for that individual. The values in the forelimbs of the juveniles ranged from 17 to 42% (30.8 ± 4.8%, n=5), as described in Results. Based on previous evaluations, 4-OHT-induced recombination should have occurred on average in less than 10% of all cassettes inserted into the genomic DNA of muscle cells. This indicates that all nuclei of a muscle fiber might not always undergo recombination. In fact, even in muscle fibers with a large number of nuclei with N-mCherry fluorescence, most of them continuously expressed EGFP in the cytoplasm. Note that in the current conditions, unlike a previous report, spontaneous recombination in pre-metamorphic limb regeneration was not observed (Figure 8).

2.5 Control of Metamorphosis and Body Growth

To shift the onset time of metamorphosis in the delay direction along the axis of development (see Figure 28), swimming larvae at St. 58 were reared in filtered tap water containing 0.2 g/L thiourea (208-01205; Fujifilm Wako Chemicals, Osaka, Japan) at room temperature (18-20 °C), as described previously (Chiba, C. et al., 2012). The animals were fed then transferred into fresh thiourea-containing rearing water, every other day. They grew up with preserved larval characteristics. In this study, I used MI giant larvae which achieved a total body length of ~6 cm, corresponding to the size of preadolescences.

To induce metamorphosis, MI giant larvae were simply transferred into plain tap water (Chiba, C. et al., 2012). They metamorphosed over ~2 months. In this study, I referred to the post-metamorphic giant juveniles that started to eat food as MIR juveniles.

To shift the onset time of metamorphosis in the advance direction along the axis of development, swimming larvae at St. 57 were reared in filtered tap water containing 100 nM T_3 (Figure 37) This solution was prepared by diluting 100 μM T_3 (3,3,5-triiodo-L-thyronine sodium salt; T6397-100MG; Sigma-Aldrich Japan K.K.) dissolved in 1N NaOH to 1,000-fold. Importantly, this larval stage had not completed digit formation (a transitional stage from four to five digits) in the hind limbs, and was estimated to be at 2-3 months before metamorphosis.

To slow the growth of the body as well as to increase the time resolution for recognizing the phenomenon of dedifferentiation, juveniles were reared after limb amputation at 12 °C (Figure 21), which was lower than the standard rearing

temperature (18-20 °C) in which the total body length of animals and the size of blastema reached the values for 12 °C in about 20 days.

2.6 Tissue Preparation

To examine the localization of EGFP and N-mCherry fluorescence in normal and regenerating forelimbs, they were amputated under anesthesia and fixed in a modified Zambony's fixative (2% paraformaldehyde and 0.2% picric acid dissolved in phosphate-buffered saline solution (PBS, pH 7.5)) at 4 °C for 2 h or 4-6 h depending on the size of the limb (for swimming larvae and juveniles, 2 h; for preadolescences, MI giant larvae, MIR juveniles, and adults, 4-6 h), except for Pax7 immunohistochemistry in which adult limbs were fixed for 3 h. Limb samples were washed thoroughly with PBS at 4 °C (5 min × 2, 10 min × 2, 15 min × 2, 30 min × 2 and 1 h × 2) and then allowed to soak in 30% sucrose in PBS at 4 °C.
They were embedded into Tissue-Tek O.C.T. Compound (4583; Sakura Finetek USA, Inc., Torrance, CA, USA), frozen at ~−20 °C in a cryostat (CM1860; Leica) and serially sectioned from end to end at ~20 μm thickness (e.g., for adult limbs, 120-140 sections). Tissue sections were attached to gelatin-coated coverslips, air-dried and stored at −20 °C until use. All sections, except those for immunohistochemistry, were washed thoroughly with PBS and examined for fluorescence.

2.7 Immunohistochemistry

Tissues were immunofluorescently labelled. Primary antibodies were mouse monoclonal anti-Pax7 antibody (1:200; PAX7-c; Developmental Studies Hybridoma Bank, University of Iowa, Iowa, IA, USA), mouse monoclonal anti-myosin heavy chain antibody (1:200; MF20-c; Developmental Studies Hybridoma Bank) and rabbit polyclonal anti-PCNA antibody (1:500; ab18197; Abcam, Tokyo, Japan), and for control, rabbit polyclonal anti-collagen type IV antibody (1:500; 600-401-106-0.1; Rockland Immunochemicals, Gilbertsville, PA 19525, USA).

Secondary antibodies were goat anti-mouse IgG (H+L) antibody conjugated with Alexa Fluor 405 (1:200; A-31553; Thermo Fisher Scientific) and goat anti-rabbit IgG (H+L) antibody conjugated with Alexa Fluor 405 (1:500; ab175652; Abcam).

Tissue sections on coverslips were rinsed thoroughly (PBS, 1% Triton X-100 in PBS and PBS; 15 min each), incubated in a blocking solution (3% normal goat serum (S-1000-20; Vector Laboratories, Burlingame, CA, USA)/1% Triton X-100 in PBS) for 2 h, washed twice in PBS and then incubated in primary antibody diluted with blocking solution for 15 h at 4 °C. After washing thoroughly, samples were incubated in secondary antibody diluted with blocking solution for 4 h and washed thoroughly. The tissues on the coverslip were immersed into 90% glycerol in PBS or into VECTASHIELD mounting medium (H-1400; Vector Laboratories) and placed on a glass slide so that the tissues were mounted under the coverslip. Except for the

immunohistochemistry, cell nuclei in the tissues were stained with 4,6-diamidino-2-phenylindole (DAPI, 1:50,000; D1306; Thermo Fisher Scientific).

2.8 Explant Culture of Larval Muscle

For the control culture medium, 80% Leibovitz's L-15 medium (41300-039; Gibco, Thermo Fisher Scientific) containing 10% charcoal/dextran stripped fetal bovine serum (charcoal/dextran-treated FBS; Lot#: AC10233363; Cat#: SH30068; Hyclone, Cytiva, Tokyo, Japan) was used. For the test culture medium, T_3 was added to the control medium at a final concentration of 100 nM. In this case, 100 μM T_3 dissolved in 1N NaOH was diluted with control culture medium at 1 μM and filter sterilized (28SP020RS; ADVANTEC, Tokyo, Japan). Aliquots of this solution (10x T_3 stock) were stored at -20 °C until use. The 10x T_3 stock was diluted to 1x T_3 (i.e., 100 nM) with control culture medium immediately before use.

In this study, transgenic swimming larvae at St. 57 (n=16) were used for muscle explant culture (Figure 37, left penal). To sterilize the larvae, poly(vinylpyrrolidone)-iodine complex (PVP-I; PVP1-100G; Sigma-Aldrich Japan K.K.) solution, which was dissolved in MilliQ water at 10% (w/v) and filter sterilized, was used. Following anesthesia in 0.1% FA-100 for 10-20 min, the larvae were placed on a piece of paper towel (4 cm x 4 cm) soaked in 1-2 ml of PVP-I solution in a 60 mm plastic dish for 30 sec. After washing the larvae by transferring them twice to another dish containing

fresh sterilized PBS, they were placed on a surgical plate in a 35 mm plastic dish containing PBS. Under a dissecting microscope (SZ61; Olympus, Tokyo, Japan), the forelimb was amputated below the shoulder. The limb sample was immobilized to a surgical plate by pinning it to the hand, and the skin was carefully peeled off using fine forceps. A portion of the *M. flexor antebrachii et carpi radialis* (FACR) (Walthall, J. C and Ashley-Ross, M. A., 2006), the most anterior flexor muscle of the forearm, was excised and transferred to a dish containing culture medium (one explant per dish).

In this study, I used a collagen type I-coated glass base dish (27 mm; 4970-011; AGC Techno Glass, Shizuoka, Japan) and filled it with 1 ml of culture medium. The lid of the dish was sealed with Parafilm (Bemis, Illinois, Chicago, USA), transferred into an incubator (25 °C), and allowed to stand for 1 week. At one week after the start of culture, in which about 50% of explants successfully adhered to the bottom of the dish, I started to monitor the behavior of muscle fibers in those adherent explants under a fluorescence inverted microscope (BZ-X800; EYENCE, Osaka, Japan). To minimize possible phototoxicity, observations were made in Low Photobleach Mode for less than 30 min per day and repeated every other day. Half of the medium in the dish was carefully refreshed every 4 days.

Note that muscle explants examined in this study were harvested from different individuals (i.e., one explant per larva) with one exception, where two muscle

explants from the same individual were cultured in the presence of 100 nM T_3 (T37 and T37-2 in see table). The volume of the adherent explant was estimated, as a sphere, from the cross-sectional area of the explants measured from the bottom of the culture dish on day 7 (for the control condition, range: 0.0108-0.0373 mm^3, mean ± SEM: 0.0217 ± 0.0057 mm^3, *n*=4; for the test condition, range: 0.0133-0.0263 mm^3, mean ± SEM: 0.0177 ± 0.0023 mm^3, *n*=5; there were no significant differences in the means between samples). The mean luminance of N-mCherry fluorescence in the adherent explant on day 7, which reflects the recombinant efficiency, was as follows: for the control condition, range: 17.74-39.05, mean ± SEM: 27.48 ± 5.244, *n*=4; for the test condition, range: 19.35-28.38, mean ± SEM: 22.774 ± 1.608, *n*=5; there were no significant differences in the means between samples.

To evaluate mitotic activity of iv-mono-SMFCs, two other muscle explants were cultured in medium containing 10% normal fetal bovine serum (FBS; Lot#: AJF10577; Cat#: SH30071.03; Hyclone, Cytiva, Tokyo, Japan) for 27 days, and further cultured in the same medium containing 10 μM BrdU (5-bromo-2′-deoxyuridine; B5002-100MG; Sigma-Aldrich Japan K.K.) for 15 h.

The cultures were fixed in 2% paraformaldehyde in PBS (pH 7.5) for 20 min, and then BrdU-incorporated nuclei were labelled with sheep polyclonal anti-BrdU antibody (1:500; ab1893; Abcam) and donkey anti-sheep IgG (H+L) antibody conjugated with Alexa Fluor 350 (1:500; A-21097; Thermo Fisher Scientific) as done

for tissue sections except for the blocking solution in which normal donkey serum (017-000-001; Jackson ImmunoResearch, West Grove, PA, USA) was used.

2.9 Image Acquisition and Analysis

To monitor EGFP and N-mCherry fluorescence in the forelimbs during development and regeneration in living albino newts, I used a fluorescence dissecting microscope (M165 FC; Leica) with specific filter sets for EGFP (Leica GFP-Plant; exciter: 470/40 nm; emitter: 525/50 nm) and mCherry (exciter: XF1044, 575DF25; emitter: XF3402, 645OM75; Opto Science, Tokyo, Japan). Images or videos were taken while changing the focal plane with a digital camera (C-5060; Olympus) attached to the microscope and stored in a computer.

To track muscle fibers in explant cultures by N-mCherry fluorescence, I used the all-in-one fluorescence inverted microscope system (BZ-X800; EYENCE) with filter sets for EGFP (OP-87763; exciter: 470/40 nm; emitter: 525/50 nm) and TRITC (OP-87764; exciter: 545/25 nm; emitter: 605/70 nm). Using the images acquired, the size of the cross-sectional area of the explants and their mean luminance of mCherry fluorescence were measured in Adobe Photoshop 2021 (Adobe Systems, San Jose, CA, USA). To measure mean luminance, fluorescence images of explants were taken using a 4X objective lens at the same intensity (100% in Low Photobleach Mode) and exposure time (1.2 sec).

All tissue sections were examined for fluorescence by a charge-coupled device camera system (DP73; cellSens Standard 1.6; Olympus) attached to a microscope (BX50; Olympus). Images of tissues shown in the figures were acquired through a confocal microscope system (LSM700; ZEN 2009, ver. 6.0.0.303; Carl Zeiss, Oberkochen, Germany) with filter sets for EGFP (Filter Set17; exciter: BP 485/20 nm; emitter: BP 515-565 nm), mCherry (Filter Set20; exciter: BP 546/12 nm; emitter: BP 575-640 nm) and DAPI (Filter Set49; exciter: G 365 nm; emitter: BP 445/50 nm), unless otherwise noted.

Images were analyzed by Adobe Photoshop 2021 and with software for image acquisition systems. Figures were prepared using Adobe Photoshop 2021. Statistical analysis was made using BellCurve for Excel (ver 3.22, Social Survey Research Information, Tokyo, Japan).

3. Results

3.1. Muscle fiber nucleus-tracking system

3.1.1 The Reason to develop nucleus-tracking system

In this study, I developed a nucleus-tracking system that specifically labels the nuclei of multinucleated skeletal muscle fibers in forelimbs with a fluorescent protein, N-mCherry.

Besides, in our laboratory, a newt cytoplasmic muscle tracking system has already been created (Figure 13). However, there are several reasons to make it for nucleus tracking system. For example, a 3D confocal image (Figure 14) from cytoplasmic tracking newt shows that, muscle dedifferentiation could be detected, but because of changed morphology and fragmentation of muscle fibers, precise localization of muscle originated cells in blastema is impossible. Further, cells isolation for omics research was extremely difficult. Therefore, to overcome such difficulties and increased the resolution of cell tracking and further studies, I developed a muscle fiber nucleus-tracking system.

3.1.2 Evaluation of the System

Transgene Cassette.

To address above issue, I introduced a NLS (Nuclear Localization Signal) element (sequence, ATGGCTCCAAAGAAGAAGCGTAAGGTA) into cytoplasmic-tracking transgene cassette (Figure 5).

For detail, the transgene cassette pCreER^{T2}<CarA-CAGGs>[EGFP]NLS-mCherry (ISce1) expresses inducible Cre recombinase in muscle fiber cells, under control of a muscle-specific promotor, Cardiac actin promotor. In the presence of tamoxifen, fluorescent marker which under a universal promotor CAGGs, switches from EGFP to nuclear localized mCherry (N-mCherry), via a loxp system. Therefore, this cassette enables to label the nuclei of multinucleated skeletal muscle fibers by N-mCherry.

Transgenesis.

To create transgenic newts, purified DNA plasmid was micro-injected into one-cell stage fertilized eggs. Two weeks later, embryos' development reached blastula stage, embryos showing EGFP fluorescence were selected and reared till stage 53, which larval newts' complete development of forelimb and start to develop hindlimb (Figure 15). Of note, animal survival rate at here is higher than 80%, and among them, up to 40% of larvae with EGFP fluorescence.

For the following nucleus tracking experiments, I selected newts in which EGFP was expressed with medium intensity throughout the body, and newts with mosaic pattern in which EGFP was exclusively expressed in muscle to rule out the contamination of non-muscle cells.

When animal reached stage 53, 4-OHT (4-hydroxy tamoxifen) was applied by rearing larvae in 4-OHT contained water for 24 hours. For this system, recombination did not occur in any tissue in the absence of tamoxifen (Figure 7). but after larvae applied to 4-OHT, recombination occurred, and nuclei of SMFCs become N-mCherry positive (Figure 8, 9), it shows clearly beads on string appearance. About the efficiency of N-mCherry fluorescent muscle nuclei, in this study, I only calculated the ratio of nuclei that N-mCherry positive in SMFCs, rather than recombination itself. Because of the reason that a part of N-mCherry fluorescence caused not by directly recombination, but those nuclei in same fiber are recombinant. In these recombination-induced animals, 17-42% (30.8±4.8%, n=5) of all nuclei in EGFP muscle fibers in the forelimb showed mCherry fluorescence.

3.1.3 Labeling Specificity of Muscle Nuclei

To validate that those mCherry fluorescent nuclei are located in muscle fibers, I acquired high magnified images by confocal microscopy (Figure 10). Images showed that mCherry fluorescent nuclei are clearly localized in skeletal muscle fibers. And

MHC immunohistochemistry result (Figure 11) re-confirmed the N-mCherry positive cells' muscle fiber localization.

Further, to exclude the possibility that residual myogenic stem cells, in other name satellite cells which express Pax7, have been involved in nucleus-tracking system, I performed immunohistochemistry (Figure 12, *n*=5). And as result, Pax7 positive satellite cells, never labelled by N-mCherry.

As a Summary, this system allowed mesenchymal cells (named mono-SMFCs) originating from skeletal muscle fibers to be tracked, by their fluorescent nucleus during limb regeneration (see below). Fluorescent nuclei help to distinguish mono-SMFCs from each other while they migrate to compose the blastema and create new muscles in regenerating limbs.

3.1.4 Albino Newts Enabled Live Monitor

This system was applied to wild-type newts as well as CRISPR/Cas9 albino newts (Figure 16). Albino mother newts (F0) were provided by Dr. Takeshima. Differ to wild-type newts that fertilized eggs collected by two tank semi-natural system, *in vitro* fertilization was applied to obtain one-cell stage fertilized eggs. Combined with transgenesis, albino muscle-nucleus tracking newts enabled to monitor those fluorescent nuclei alive (Figure 17), even during limb regeneration.

3.2 Body Growth is Necessary for Limb Muscle Dedifferentiation

3.2.1 Natural Metamorphosis Do Not Allow Muscle Dedifferentiation

Because metamorphosis makes newt adapt to terrestrial environment from aquatic environment, as well as metamorphosis do change newt limb regeneration mechanism, such as their digits formation pattern changed during limb regeneration (Kumar, A et al., 2015), from a preaxial dominance to a postaxial dominance (Figure 18). Therefore, at first, I hypothesized that dedifferentiation might be controlled only by metamorphosis. If this is true, then N-mCherry cells will appear in juvenile's blastema.

To verify this hypothesis, I examined muscle dedifferentiation during limb regeneration using muscle-nucleus tracking newts. First, larval newt limb regeneration was examined. As results, living monitors (Figure 19) show no N-mCherry cells observed in their blastema. In larval regenerated limb, there are no N-mCherry cells detected (Figure 20). These results consistent with previous study that, no muscle contribution during larva limb regeneration.

Then, limb regeneration on post-metamorphic newts were examined. First, juveniles undergone metamorphosis, which have 3-4cm body size were applied to amputation. However, contrary to the hypothesis, there is no N-mCherry cells detected in albino juvenile blastema (Figure 21). Plenty of blastema samples were prepared for sections (n=25), but no N-mCherry cells observed in juvenile blastema in

any case (Figure 22). Therefore, natural metamorphosis is not sufficient to muscle dedifferentiation.

3.2.2 Preadolescence Newt Shows Muscle Dedifferentiation Capacity

I continued to examine muscle dedifferentiation during limb regeneration as newt grown up. Surprisingly, I found that once the newts reached the size of 6 cm, and age of over 1.1 years, amount of N-mCherry mono-SMFCs (mononucleated skeletal muscle fiber cells) were detected in their blastema. Live monitor from albino preadolescence clearly shows appearance of N-mCherry nuclei in their blastema (Figure 23). Consistent with live monitor, cryosection images show clear detection of N-mCherry mononucleated cells in preadolescence blastema (Figure 24). PCNA labelling of sections suggested that mono-SMFCs in blastema were mitotically active (73–100%, 88.2±2.2%, n=4 (3 sections each); figure 25). So far, as a conclusion, growth is required to muscle dedifferentiation.

3.2.3 Body Growth Matters but Not Aging

However, about growth, size or aging, which one is critical for preadolescence are unknown. Therefore, I set an experiment to clarify this issue. Studies show that, for the newt, low temperature have effect to slow down body size growth while maintaining their aging (Tattersall, G. J et al., 2012; Y. L. Werner, 2016). Therefore, I kept juvenile in low temperature, and let it reach preadolescence age but only have small size. And made amputation to examine muscle dedifferentiation during limb regeneration. Live image of regenerated limb (Figure 26) shows that there is no N-mCherry mono-SMFCs detection, even though few N-mCherry cells over the amputation plain were observed. It was possibly caused by muscle extension or fusion, but not dedifferentiation (See below).

At this time point, this newt reached body size of 6.8cm, therefore another amputation was performed. Look at its blastema and regenerated limb, big mount of mono-SMFCs were detected in both cases (Figure 27). This same to preadolescence as well as normal adult newt which showing muscle dedifferentiation capacity. Therefore, I clarified the conclusion that body growth is necessary to muscle dedifferentiation, but not aging.

3.3 Metamorphosis is Necessary for Limb Muscle Dedifferentiation

3.3.1 Body Growth is not a Sole Condition for Muscle Dedifferentiation

As above, Body growth is necessary for limb muscle dedifferentiation. However, whether it is a sole condition for muscle dedifferentiation is unknown.

To address this question, I examined muscle dedifferentiation of metamorphosis inhibited (MI) giant larva newt. MI giant larva were prepared by rearing normal larva in water containing thiourea, which is an inhibitor of thyroid hormone synthesis (Chiba, C et al., 2012). MI giant larva have big body size that related to preadolescence, but not undergo metamorphosis. They maintain larval feature in which during limb regeneration digit formed preaxially (Figure 28). If body growth is a sole condition for muscle dedifferentiation, N-mCherry cells should appear during their limb regeneration.

In one particular case, a MI giant larva has strong fluorescent expression but low level of pigmentation. It enables to live monitor its blastema during limb regeneration. As a result, there is no N-mCherry nuclei detected in blastema (Figure 29). Consistent with the live monitor result, cryosection image (Figure 30) shows no N-mCherry cells detected in blastema. Further, there is no N-mCherry cells detected in regenerated limb (Figure 31), which indicate that same to normal larva, there is no muscle contribution during larval limb regeneration even in MI giant larva. Taken together, I conclude that, body growth is not a sole condition for muscle dedifferentiation.

3.3.2 MI Giant Larva Acquired Muscle Dedifferentiation after Metamorphosis

At this point, I am forced to re-examine the necessity of metamorphosis by inducing metamorphosis of MI giant larva and examining their limb regeneration. To induce metamorphosis of MI giant larva newt, I used the method to simply rear them in plain water (Figure 32). One month later, Transformation starts. For example, their gill begins to degrade. Two months after switching rearing water, metamorphosis inhibition was fully released, and MIR (metamorphosis inhibition released) juvenile were used for examination. Of note, MIR newt digit formed post axially, which is an adult feature (Figure 32).

If metamorphosis is necessary for muscle dedifferentiation, then N-mCherry cells should appear in limb regeneration of MIR juveniles. But, unexpected, there is no N-mCherry cells observed in their blastema (Figure 33). But as limb morphogenesis progressed, big mount of N-mCherry mononucleated SMFCs appeared. Those N-mCherry cells seemed to migrate distally along the space between cartilage and skin (Figure 34). Therefore, I conclude that, in MIR newt, metamorphosis is required for muscle dedifferentiation, but delayed.

3.3.3 Delayed Metamorphosis Responsible for Delayed Dedifferentiation

In comparison to normal preadolescences, there is a slight delay before the mono-SMFCs show up. Note that, during this time, MIR juveniles are undergoing metamorphosis. In fact, their skeleton is still made of cartilage.

Therefore, as a possible explanation, delayed metamorphosis may be responsible for this delayed muscle dedifferentiation. To verify this possibility, I examined MIR newts' limb regeneration 6 month later. As a result, mono-SMFCs were observed in the blastema of MIR newts (Figure 35). So, this verified the possibility that delay comes from delayed metamorphosis.

Taken together, by examining naturally developing newts and metamorphosis inhibition newts, I conclude that a combination of metamorphosis and body growth is required for muscle dedifferentiation (Summarized in Figure 36).

3.4 Newt Limb Muscles are Capable of Dedifferentiation Before Metamorphosis

From the conclusion that was reached above, a new question arose, namely whether, in nature, newts acquire the ability of muscle dedifferentiation through metamorphosis but suppress that capacity until they grow up to preadolescence. As a possibility, thyroid hormones would be able to induce dedifferentiation in pre-metamorphic muscles *ex vivo*, where the muscles can be free from inhibition by body growth.

To address this issue, next I cultured explants of larval muscles in the presence of a physiologically active thyroid hormone, triiodothyronine (T_3). For this experiment, I used swimming larvae at St. 57, which had not completed digit formation in their hind limbs and were estimated to be 2-3 months before metamorphosis. Of note, these larvae already had the competence of metamorphosis. When reared in T_3-containing tap water, they exhibited metamorphosis-like transformation over 2 weeks, even though they died thereafter (Figure 37).

I separated muscle explants (0.078-0.16 mm^3) from forelimbs of muscle nucleus tracking swimming larvae, and cultured them in a collagen-I-coated dish (1 explant/dish) (Figure 38). Here I used a culture medium containing charcoal/dextran stripped fetal bovine serum for the control, and added T_3 at 100 nM to the medium from the beginning of culture. In this study, T_3 was administered over the culture period because the expression level of T_3 receptors might still be low at

this early developmental stage (Gao, X., et al. 2017). In both control and test conditions, half of the explants adhered on the substrate within 1 week (Figure 39, ratio of adhered explants: control, 4/8; test, 5/9), and fibroblast-like mesenchymal cells immediately migrated from these explants. The total number of cells that expanded on the substrate gradually increased in both conditions, with no statistical difference between them (Figure 40, 41).

In these conditions, I monitored the behavior of muscle fibers. It is important to note here that muscle fibers at this stage were typically striated, suggesting their maturation with sarcomeres, and that N-mCherry fluorescence was always observed in the nuclei of muscle fibers, validating the specificity of cell tracking system (Figure 39).

As a result, contrary to the hypothesis, pre-metamorphic muscle fibers exhibited a dedifferentiation-like behavior regardless of the presence of T_3. In both conditions, single cells with an N-mCherry nucleus (named iv-mono-SMFCs) appeared at the circumference of the explant (Figure 42, 43). The ratio of the attached explants from which the iv-mono-SMFCs appeared in 23 days was 3/4 in the control and 4/5 in the test, and the total number of iv-mono-SMFCs that appeared from all of the attached explants in the same culture period was 7 in the control and 15 in the test. These cells migrated on the substrate of the culture dish. The shape of these cells was not distinguishable from other migrating mesenchymal cells. The date of appearance and

the length of time the cells could be followed varied from cell to cell (see table 1). In all these cells, no cell division was observed. Further, Iv-mono-SMFCs migrated from a muscle explant during culture for 23 days were further cultured in the presence of 10 μM BrdU for 15 hours that showed cell cycle entry (See figure 47).

For most iv-mono-SMFCs, it was hard to trace them back to the original muscle fibers because of the uniform EGFP expression in the explant and changes to the shape of muscle fibers. However, in one particular case, where a single muscle fiber in the explant was attached to the bottom of the culture dish, I successfully tracked the muscle fiber (Figure 44). In this case, the muscle explant was cultured in the presence of 100 nM T_3. After the explant became attached to the substrate of the culture dish, two nuclei in the muscle fiber gradually moved along the fiber toward the periphery of the explant, and finally met at the peripheral end of the fiber. During this process, the striated pattern of the muscle fiber disappeared (see Figure 44, lowest panel). The peripheral end of the muscle fiber formed a protrusion containing two nuclei (Figure 44). The protrusion extended further on the substrate of the culture dish. The leading end of the protrusion seemed to tow the residual part of the muscle fiber that was finally pulled out of the explant. The resulting cell with two nuclei stayed at the same place for as long as 2 hours but finally disappeared.

In another case, I observed a similar protrusion in the control condition (Figure 45). In this case, the protrusion gave rise to two mononucleated cells. The cell which

retained its connection with the explant shrank, then died. However, the other cell which migrated forward survived and displayed an elongated morphology. Interestingly, this cell fused to other migrating mesenchymal cells within half a day to form a flat multinucleated cell, and survived for as long as one month (Figure 46). And this cell fused to other cells originally have no fluorescence, but those cells gradually showed fluorescence after fusion, this gives an explanation of fluorescent cells observed over amputation plain, in juvenile blastema.

4. Discussion

In this study, I addressed whether metamorphosis or body growth is essential for newts to dedifferentiate muscle fibers to mobilize them for limb regeneration. Explant cultures of larval muscles revealed that newt muscle fibers are capable of dedifferentiation independently of metamorphosis, although more cases are needed to know the processes of muscle fiber cellularization. Actually, there are few reports that have traced the processes by which newt striated muscle fibers give rise to mono-SMFCs (Sandoval-Guzmán, T et al., 2014; Tanaka, H. V et al., 2016).

On the other hand, investigations of naturally developing and metamorphosis–controlled newts demonstrated that muscle dedifferentiation requires a combination of metamorphosis and body growth until preadolescence size. Note that this study does not exclude the possibility that metamorphosis induces muscle dedifferentiation only at early larval sizes, because larvae die when forced to metamorphose in a premature state. However, even if this were the case, it would have nothing to do with the physiological function of dedifferentiation. Age and sexual maturity are unlikely to directly affect the ability of muscle dedifferentiation.

Taken together, I conclude that newt muscle fibers have an intrinsic dedifferentiation capacity, but this capacity is suppressed until, or is unleashed as, the newt grows into preadolescence beyond metamorphosis.

In fact, as demonstrated in our previous study (Tanaka, H. V et al., 2016), juvenile muscle fibers grafted in the forelimbs of preadolescents, which were referred to as

adults in that study, exhibited dedifferentiation and contributed to muscle creation during limb regeneration.

As shown in this study, digit patterning during forelimb regeneration is obviously switched through metamorphosis (see Figure 18). Besides, in newts' eyes, retinal regeneration by reprogramming of retinal pigment epithelium (RPE) cells is observed in juveniles, although at this stage the contribution of RPE cells is still considerably less than that of stem cells at the ciliary marginal zone (Casco-Robles M. M et al., 2016).

However, in juvenile limb regeneration, only N-mCherry nuclei in muscle fibers extending distally over the amputation plane were observed (see Figure 21, 26). If mono-SMFCs participate in the extension of muscle fibers, there should be a leading mono-SMFC that adds, as soon as it divides, its daughter cell to a distal tip of muscle fiber, although it was not detected in this study. I do not completely rule out the possibility that dedifferentiation is merely invisible. However, independent of this, muscle dedifferentiation is a very minor player during juvenile limb regeneration.

Thus, it seems that muscle dedifferentiation is designed to function in life after preadolescence. What is it that changes through metamorphosis and body growth that permits muscle dedifferentiation? If muscle stem cells, such as satellite cells, continue to play a role in muscle creation during limb regeneration after metamorphosis, then interestingly, in contrast to dedifferentiation, the relative contribution of stem cells to

muscle creation seems to be limited by something that changes with metamorphosis and body growth.

The most reasonable explanations are changes in the extracellular microenvironment, or ‘niche’. It is known that the changes in niche associated with developmental stages affect the number and properties of stem cells, decreasing their contribution to tissue turnover or repair/regeneration (Relaix, F et al., 2021). Interestingly, transverse sections (8 serial sections, each 20 μm) of the forearm near the elbow and visualized satellite cells by Pax7 immunohistochemistry reveal that, density of satellite cells in adult muscle is much lower than that in juvenile muscle. Although the total number of Pax7+ cells per section was not significantly different between juveniles and adults, the number of Pax7+ cells/muscle area (mm^2) was significantly reduced in adults due to the increase of muscle size as the body grows (For detail see figure 48) Newts may be able to compensate for their reduced stem cell capacity with dedifferentiated cells, thereby enabling lifelong body part regeneration. It is fascinating to hypothesize that in newts, the extracellular environment, which inhibits the involvement of muscle stem cells in limb regeneration, conversely promotes dedifferentiation of muscle fibers (Figure 49). Further, even if the extracellular environment is primarily important, the possibility of stem cell-mediated control of dedifferentiation is also worth considering. However, the exact extent of the contribution of stem cells to muscle creation in post-

preadolescence newts is not known. In future research, it is essential to track stem cells along with muscle fibers.

This study foresees those studies associated with developmental events, such as metamorphosis and body growth, and will be essential in the future to assess regenerative abilities and to elucidate their mechanisms. From this point of view, it is necessary to reevaluate whether the cells of frogs and other salamanders have an equivalent dedifferentiation capacity to that of newts.

Furthermore, it is necessary to determine the extracellular environment that liberates the ability of cells to dedifferentiate. This could lead to techniques to artificially control cell dedifferentiation and to research on new cells that are performed in *in vivo* environments where stem cells cannot work.

5.References

Spallanzani L: Prodromo di un opera da imprimersi sopra la riproduzioni animali, 1769 [An Essay On Animal Reproductions (1769), translated from Italian by M. Matty, 1769, Kessinger Publishing (2010).]

Molina, M.D.; Cebrià, F. (2021) Decoding Stem Cells: An Overview on Planarian Stem Cell Heterogeneity and Lineage Progression. Biomolecules., *11*, 1532.

Reddy P. C., Gungi A., Unni M. (2019b). "Cellular and Molecular Mechanisms of Hydra Regeneration," in *Evo-Devo: Non-model Species in Cell and Developmental Biology* (Cham, Switzerland: Springer;), 259–290. 10.1007/978-3-030-23459-1_12

Cary G.A., Wolff A., Zueva O.. et al. (2019) Analysis of sea star larval regeneration reveals conserved processes of whole-body regeneration across the metazoa. *BMC Biol.*, 17, 1–19.

Sámano, C., González-Barrios, R., Castro-Azpíroz, M., Torres-García, D., Ocampo-Cervantes, J. A., Otero-Negrete, J., & Soto-Reyes, E. (2021). Genomics and epigenomics of axolotl regeneration. *The International journal of developmental biology*, *65*(7-8-9), 465–474.

Casco-Robles, M. M., Yasuda, K., Yahata, K., Maruo, F., & Chiba, C. (2021). Reviewing the Effects of Skin Manipulations on Adult Newt Limb Regeneration: Implications for the Subcutaneous Origin of Axial Pattern Formation. *Biomedicines*, *9*(10), 1426.

Brockes, J. P. and Kumar, A. (2002). Plasticity and reprogramming of differentiated cells in amphibian regeneration. Nat. Rev. Mol. Cell Biol., *3*, 566–574.

Tsonis, P. A. (2002). Regenerative biology: the emerging field of tissue repair and restoration. Differentiation, *70(8)*, 397-409.

Chiba, C. (2014). The retinal pigment epithelium: an important player of retinal disorders and regeneration. Exp. Eye. Res., *123*, 107-114

Eguchi, G., Eguchi, Y., Nakamura, K., Yadav, M. C., Millán, J. L., & Tsonis, P. A. (2011). Regenerative capacity in newts is not altered by repeated regeneration and ageing. *Nature communications*, *2*, 384.

Koriyama, K., Sakagami, R., Myouga, A., Hayashi, T., & Takeuchi, T. (2018). Newts can normalize duplicated proximal-distal disorder during limb

regeneration. *Developmental dynamics: an official publication of the American Association of Anatomists*, *247*(12), 1276–1285.

Wallace, H. (1981). Vertebrate limb regeneration (p. 320). (New York: Wiley Press)

Saito, T., Kaneko, Y., Maruo, F., Niino, M., & Sakaki, Y. (1994). Study of the regenerating newt retina by electrophysiology and immunohistochemistry (bipolar- and cone-specific antigen localization). J. Exp. Zool., *270(6)*, 491-500.

Chiba, C., Matsushima, O., Muneoka, Y., & Saito, T. (1997). Time course of appearance of GABA and GABA receptors during retinal regeneration in the adult newt. Brain Res. Dev. Brain Res., *98(2)*, 204-210.

Tsonis, P. A., Madhavan, M., Tancous, E. E., & Del Rio-Tsonis, K. (2004). A newt's eye view of lens regeneration. Int. J. Dev. Biol., *48(8-9)*, 975-980.

Islam, M. R., Nakamura, K., Casco-Robles, M. M., Kunahong, A., Inami, W., Toyama, F., Maruo, F., & Chiba, C. (2014). The newt reprograms mature RPE cells into a unique multipotent state for retinal regeneration. *Scientific reports*, *4*, 6043.

Casco-Robles, M. M., Islam, M. R., Inami, W., Tanaka, H. V., Kunahong, A., Yasumuro, H., Hanzawa, S., Casco-Robles, R. M., Toyama, F., Maruo, F., & Chiba, C. (2016). Turning the fate of reprogramming cells from retinal disorder to regeneration by Pax6 in newts. *Scientific reports*, *6*, 33761.

Tanaka, H. V., Ng, N., Yang Yu, Z., Casco-Robles, M. M., Maruo, F., Tsonis, P. A., & Chiba, C. (2016). A developmentally regulated switch from stem cells to dedifferentiation for limb muscle regeneration in newts. *Nature communications*, *7*, 11069

Casco-Robles, R. M., Watanabe, A., Eto, K., Takeshima, K., Obata, S., Kinoshita, T., Ariizumi, T., Nakatani, K., Nakada, T., Tsonis, P. A., Casco-Robles, M. M., Sakurai, K., Yahata, K., Maruo, F., Toyama, F., & Chiba, C. (2018). Novel erythrocyte clumps revealed by an orphan gene Newtic1 in circulating blood and regenerating limbs of the adult newt. *Scientific reports*, *8*(1), 7455.

Stocum, D. L., & Cameron, J. A. (2011). Looking proximally and distally: 100 years of limb regeneration and beyond. Dev. Dyn., *240(5)*, 943-968.

Simon A, Tanaka, E. M. (2013). Limb regeneration. *Wiley Interdiscip* Rev. Dev. Biol*., 2(2)*, 291-300.

Joven, A., Elewa, A., & Simon, A. (2019). Model systems for regeneration: salamanders. *Development (Cambridge, England)*, *146*(14), dev167700.

Matsunami, M., Suzuki, M., Haramoto, Y., Fukui, A., Inoue, T., Yamaguchi, K., Uchiyama, I., Mori, K., Tashiro, K., Ito, Y., Takeuchi, T., Suzuki, K. T., Agata, K., Shigenobu, S., & Hayashi, T. (2019). A comprehensive reference transcriptome resource for the Iberian ribbed newt Pleurodeles waltl, an emerging model for developmental and regeneration biology. *DNA research : an international journal for rapid publication of reports on genes and genomes*, *26*(3), 217–229.

Iten, LE, Bryant SV. (1973). Forelimb regeneration from different levels of amputation in the newt, Notophthalmus viridescens: length, rate, and stages. *Wilhelm Roux'Archiv für Entwicklungsmechanik der Organismen,* 173(**4**), 263-282.

Endo, T., Bryant, S. V., & Gardiner, D. M. (2004). A stepwise model system for limb regeneration. Dev. Biol., *270(1)*, 135-145.

Brockes, J. P., Kumar, A., & Velloso, C. P. (2001). Regeneration as an evolutionary variable. J. Anat., *199(1&2)*, 3-11.

Satoh, A., Bryant, S. V., & Gardiner, D. M. (2012). Nerve signaling regulates basal keratinocyte proliferation in the blastema apical epithelial cap in the axolotl (Ambystoma mexicanum). Dev. Biol., *366(2)*, 374-381.

Christensen, R. N., & Tassava, R. A. (2000). Apical epithelial cap morphology and fibronectin gene expression in regenerating axolotl limbs. Dev. Dyn., *217(2)*, 216-224.

Brockes J. P. (1997). Amphibian limb regeneration: rebuilding a complex structure. *Science (New York, N.Y.)*, *276*(5309), 81–87.

Simon, A., & Tanaka, E. M. (2013). Limb regeneration. *Wiley interdisciplinary reviews. Developmental biology*, *2*(2), 291–300.

Stocum D. L. (2017). Mechanisms of urodele limb regeneration. *Regeneration (Oxford, England)*, *4*(4), 159–200.

Shirakami, E., Yamakawa, S., & Hayashida, K. (2020). Strategies to prevent hypertrophic scar formation: a review of therapeutic interventions based on molecular evidence. *Burns & trauma*, *8*, tkz003.

Godwin, J. W., & Rosenthal, N. (2014). Scar-free wound healing and regeneration in amphibians: immunological influences on regenerative success. *Differentiation; research in biological diversity*, *87*(1-2), 66–75.

Chaar, Z. Y., & Tsilfidis, C. (2006). Newt opportunities for understanding the dedifferentiation process. *TheScientificWorldJournal*, *6 Suppl 1*, 55–64.

Yao, Y., & Wang, C. (2020). Dedifferentiation: inspiration for devising engineering strategies for regenerative medicine. *NPJ Regenerative medicine*, *5*, 14.

Kragl, M., Knapp, D., Nacu, E., Khattak, S., Maden, M., Epperlein, H. H., & Tanaka, E. M. (2009). Cells keep a memory of their tissue origin during axolotl limb regeneration. *Nature*, *460*(7251), 60–65.

Gerber, T., Murawala, P., Knapp, D., Masselink, W., Schuez, M., Hermann, S., Gac-Santel, M., Nowoshilow, S., Kageyama, J., Khattak, S., Currie, J. D., Camp, J. G., Tanaka, E. M., & Treutlein, B. (2018). Single-cell analysis uncovers convergence of

cell identities during axolotl limb regeneration. *Science (New York, N.Y.)*, *362*(6413), eaaq0681.

Lin, T. Y., Gerber, T., Taniguchi-Sugiura, Y., Murawala, P., Hermann, S., Grosser, L., Shibata, E., Treutlein, B., & Tanaka, E. M. (2021). Fibroblast dedifferentiation as a determinant of successful regeneration. *Developmental cell*, *56*(10), 1541–1551.e6.

Tsonis, P. A. (1996). *Limb Regeneration* Cambridge Univ. Press.

Brockes, J. P., & Kumar, A. (2002). Plasticity and reprogramming of differentiated cells in amphibian regeneration. *Nature reviews. Molecular cell biology*, *3*(8), 566–574.

Monaghan, J. R., Stier, A. C., Michonneau, F., Smith, M. D., Pasch, B., Maden, M., & Seifert, A. W. (2014). Experimentally induced metamorphosis in axolotls reduces regenerative rate and fidelity. *Regeneration (Oxford, England)*, *1*(1), 2–14.

Sandoval-Guzmán, T., Wang, H., Khattak, S., Schuez, M., Roensch, K., Nacu, E., Tazaki, A., Joven, A., Tanaka, E. M., & Simon, A. (2014). Fundamental differences in

dedifferentiation and stem cell recruitment during skeletal muscle regeneration in two salamander species. *Cell stem cell*, *14*(2), 174–187.

Fabre, A. C., Bardua, C., Bon, M., Clavel, J., Felice, R. N., Streicher, J. W., Bonnel, J., Stanley, E. L., Blackburn, D. C., & Goswami, A. (2020). Metamorphosis shapes cranial diversity and rate of evolution in salamanders. *Nature ecology & evolution*, *4*(8), 1129–1140.

Bonett, R. M., & Blair, A. L. (2017). Evidence for complex life cycle constraints on salamander body form diversification. *Proceedings of the National Academy of Sciences of the United States of America*, *114*(37), 9936–9941.

Denoël, M., Drapeau, L., Oromi, N., & Winandy, L. (2019). The role of predation risk in metamorphosis versus behavioural avoidance: a sex-specific study in a facultative paedomorphic amphibian. *Oecologia*, *189*(3), 637–645.

Page, R. B., Monaghan, J. R., Walker, J. A., & Voss, S. R. (2009). A model of transcriptional and morphological changes during thyroid hormone-induced metamorphosis of the axolotl. *General and comparative endocrinology*, *162*(2), 219–232.

Ajduković, M., Vučić, T., & Cvijanović, M. (2021). Effects of thiourea on the skull of *Triturus* newts during ontogeny. *PeerJ*, *9*, e11535.

Johnson, C. K., & Voss, S. R. (2013). Salamander paedomorphosis: linking thyroid hormone to life history and life cycle evolution. *Current topics in developmental biology*, *103*, 229–258.

Crowner, A., Khatri, S., Blichmann, D., & Voss, S. R. (2019). Rediscovering the Axolotl as a Model for Thyroid Hormone Dependent Development. *Frontiers in endocrinology*, *10*, 237.

Maranouchi, Junsuke, Hiroaki Ueda and Osamu Ochi. (2000). Variation in age and size among breeding populations at different altitudes in the Japanese newts, *Cynops pyrrhogaster*. Amphibia-Reptilia. 21 (3):381-396.

Chiba, C., Yamada, S., Tanaka, H., Inae-Chiba, M., Miura, T., Casco-Robles, M. M., Yoshikawa, T., Inami, W., Mizuno, A., Islam, M. R., Han, W., Yasumuro, H., Matsumoto, M., & Takayanagi, M. (2012). Metamorphosis inhibition: an alternative rearing protocol for the newt, Cynops pyrrhogaster. *Zoological science*, *29*(5), 293–298.

Casco-Robles, M. M., Yamada, S., Miura, T., & Chiba, C. (2010). Simple and efficient transgenesis with I-SceI meganuclease in the newt, *Cynops pyrrhogaster*. Dev. Dyn., *239(12)*, 3275-3284.

Casco-Robles, M. M., Yamada, S., Miura, T., Nakamura, K., Haynes, T., Maki, N., ... & Chiba, C. (2011). Expressing exogenous genes in newts by transgenesis. Nat. Protoc., *6(5)*, 600-608.

Relaix, F., Bencze, M., Borok, M. J., Der Vartanian, A., Gattazzo, F., Mademtzoglou, D., Perez-Diaz, S., Prola, A., Reyes-Fernandez, P. C., Rotini, A., & Taglietti (2021). Perspectives on skeletal muscle stem cells. *Nature communications*, *12*(1), 692.

Kalderon, D., Roberts, B. L., Richardson, W. D., & Smith, A. E. (1984). A short amino acid sequence able to specify nuclear location. Cell, *39(3)*, 499-509.

Walthall, J. C., & Ashley-Ross, M. A. (2006). Postcranial myology of the California newt, Taricha torosa. *The anatomical record. Part A, Discoveries in molecular, cellular, and evolutionary biology*, *288*(1), 46–57.

Kumar, A., Gates, P. B., Czarkwiani, A., & Brockes, J. P. (2015). An orphan gene is necessary for preaxial digit formation during salamander limb development. *Nature communications*, *6*, 8684.

Tattersall, G. J., Tyson, T. M., Lenchyshyn, J. R., & Carlone, R. L. (2012). Temperature preference during forelimb regeneration in the red-spotted newt Notophthalmus viridescens. *Journal of experimental zoology. Part A, Ecological genetics and physiology*, *317*(4), 248–258.

Y. L. Werner. (2016) The effects of temperature on regeneration speed: a comment on Saccucci et al., 2016. Journal of Zoology 300, 237–238

Gao, X., Lee, H. Y., Li, W., Platt, R. J., Barrasa, M. I., Ma, Q., Elmes, R. R., Rosenfeld, M. G., & Lodish, H. F. (2017). Thyroid hormone receptor beta and NCOA4 regulate terminal erythrocyte differentiation. *Proceedings of the National Academy of Sciences of the United States of America*, *114*(38), 10107–10112.

6. Figures and legends

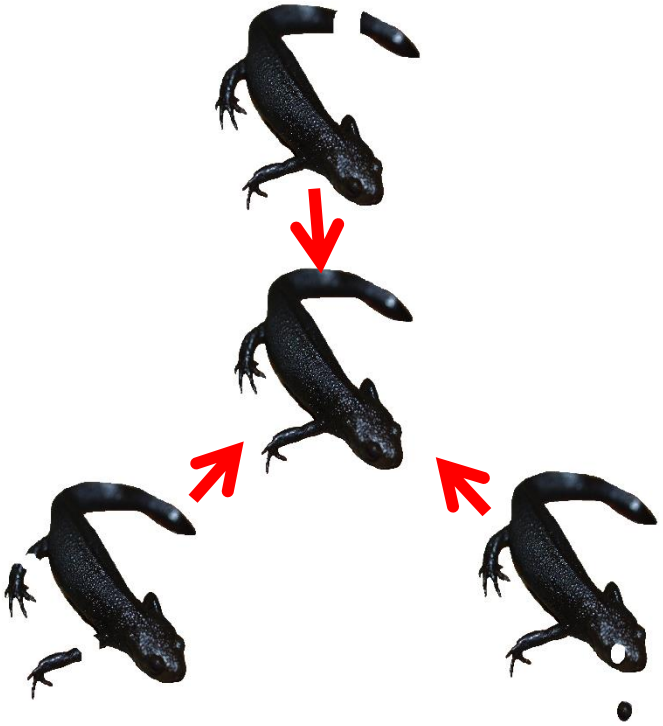

Figure 1. The newt has the ability to regenerate their lost body parts, such as the eye tissues, the limbs, the tail and so on. The animal showed here is the Japanese fire bellied newt, *Cynops pyrrhogaster.*

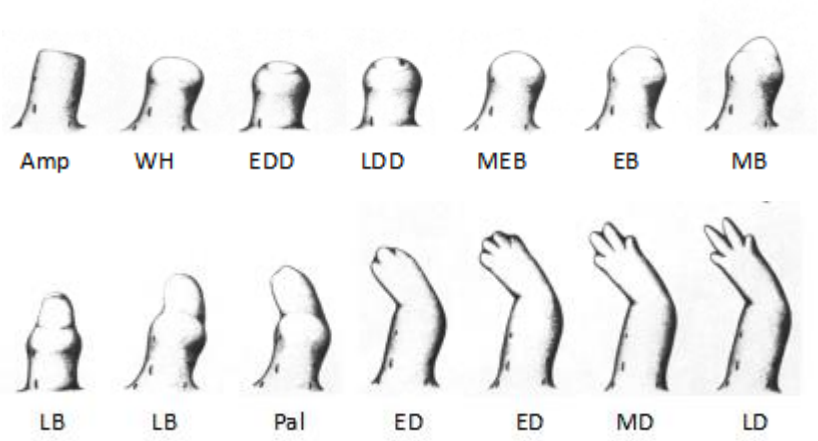

Figure 2. Illustration of adult newt limb regeneration (Modified from Ten and Bryant, 1973). Upper figures representing early limb regeneration from amputation (Amp) to medium blastema (MB) formation. Lower figures representing the processes of patterning (Pal) and differentiation (ED, MD, LD).

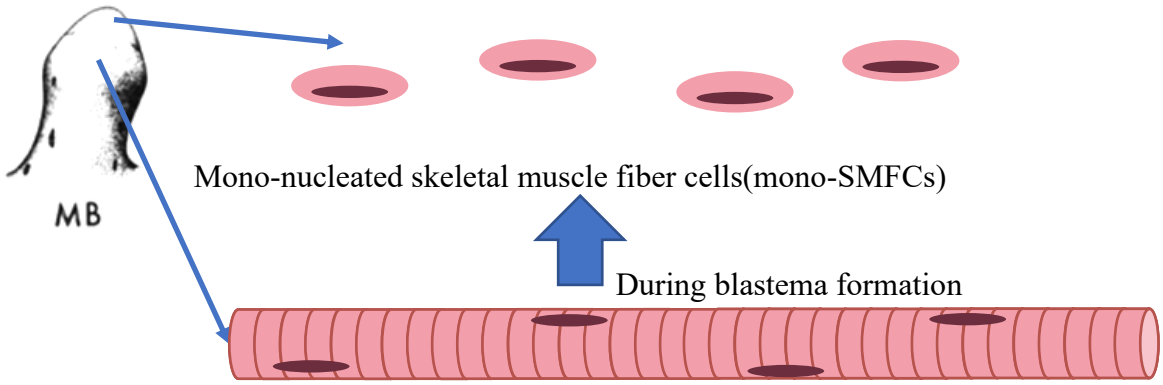

Figure 3. Illustration of newt muscle dedifferentiation. In adult Japanese fire-bellied newt limb regeneration, during blastema formation, fully matured multi-nucleated skeletal muscle fiber cells (SMFCs) migrate and become mono-nucleated skeletal muscle fiber cells (mono-SMFCs). Resulting cells contribute to following muscle creation.

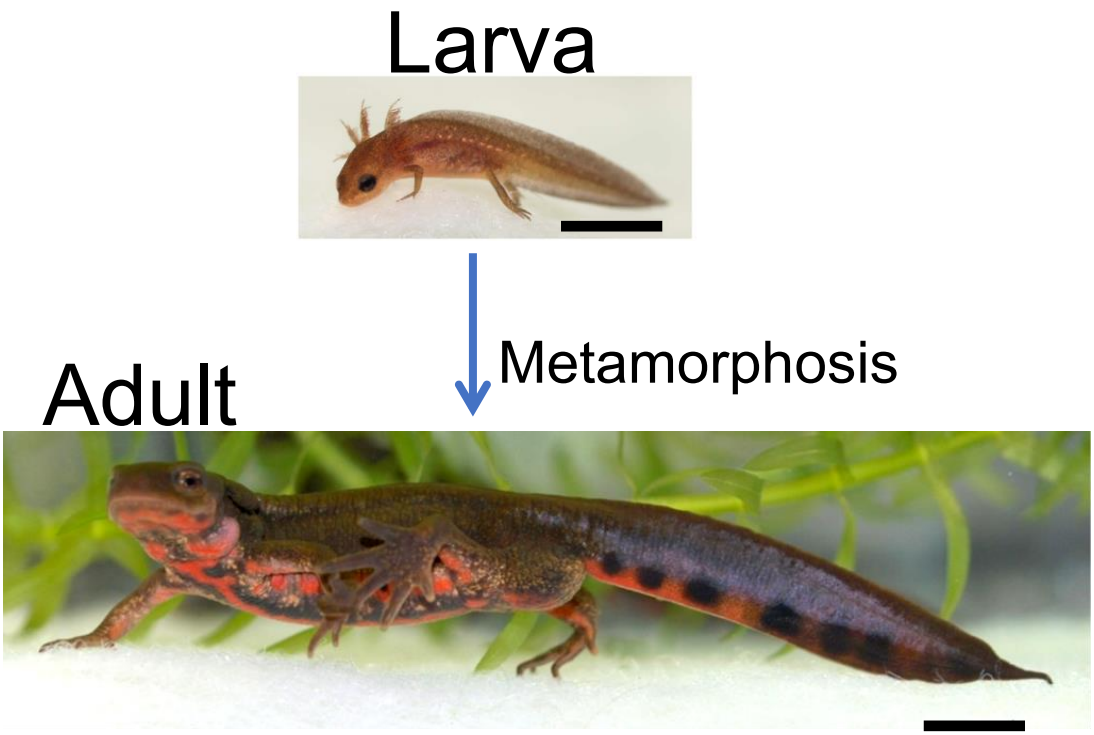

Figure 4. Images of a pre-metamorphic swimming larva and an post-metamorphic adult newt. Size comparison between larva newt and a metamorphosed adult newt. Scale bar, 1cm.

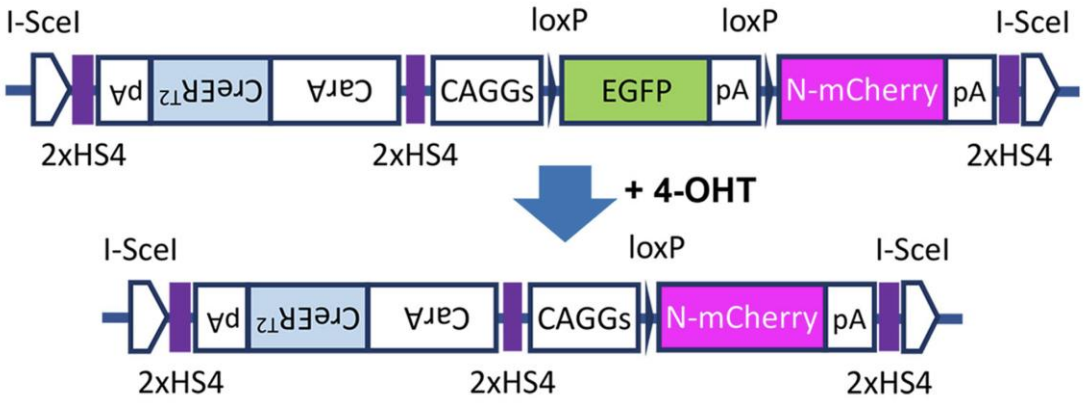

Figure 5. Images of a swimming larva and an adult newt. A transgene cassette for conditional gene expression in muscle fibers. To label the nuclei of skeletal muscle fibers and mono-SMFCs, a nuclear-localized derivative of mCherry (N-mCherry) was used. This cassette expresses inducible Cre-recombinase (CreER^{T2}) in mature skeletal muscle fibers under the control of the cardiac actin promoter (*CarA*). In the presence of 4-hydroxy tamoxifen (4-OHT), a fluorescent marker, which is expressed under the control of the universal promoter *CAGGs*, is switched from EGFP to N-mCherry via the *loxP* system. *CAGGs* makes it possible to monitor skeletal muscle fibers and their derivatives during limb regeneration. *I-SceI*: I-*Sce*I meganuclease recognition sequence. *2xHS4*: insulator sequence.

a

GTCTCCGATGTGATGTGTGGGGGTGGCGGGTCGGAGGGTATTTGTAATCGTGCTGGGGTGTTGCAGGTAAGCCCGCTATGCA
GAAGGCGCGATGATGGTGTGGGGCCTGGCTGTTTGCGTGCTGCTGTGGGCTCTGCCCTGCCGGGCCCAGTTCCCGCGGCC
CTGCGCCTCCTCCCAGGCTCTACTCAGCAAGGAGTGCTGCCCGGTGTGGGACGGCGATGGCTCTCCCTGTGGCCAGCTCTCC
GGCCGCGGCAGTTGCCAGGCCGTGGAGGTGTCCCAGGCCCCCAACGGACCCCAGTTTCCGTTTTCGGGTGTGGACGACC
GGGAAGACTGGCCCCTCGTCTTCTACAACCGCACCTGCCACTGCGTGCCGCCCTTCAGCGGCTTCCAGTGCGGGGAGTGCG
CCTTCGGGCGCTGGGGTCCGGACTGCGCGGAATCGCGCGTGCAGGTGCGCAAGAGCATCACTCAGCTCAGCGCCACCGAGA
GCGCCCGACTCCTGGCCTACCTGAACCTGGCCAAACGCACCACCAACCCCGACTACGTGATCTCCACTGGGACCTACGAGCA
GATGGACAACGGGTCCCGGCCGCTCTTCGCCGATATCAGCGTCTACGACCTCTTTGTCTGGATTCACTACTACGCGTCCCGGG
ACACATGGGTGCCAGCGGGGGGCGAGGAGGAGACTGTGGTGTGGAGAAACATCGACTTCGCCCACGAAGCGCCCGCCTTCC
TGCCGTGGCACCGGTTCTACCTTCTCTTTTGGGAACGCGAACTCCAGAAGGTGACGGGAGATGAGAACTTTACCAT
CCCCTACTGGGACTGGAGGGGCGCCCAGGGCTGCGAGGTCTGCACCGACCAGCTGATGGGGGCGCGGCACCCGACAGTA
GCCGACCTGCTAAGCCCGGCTTCCTTCTTCTCCTCCTGGCAGATCATTTGCAGCAAGGCTGAAGAGTATAACAATCTACG

b

c

ACCGGTTCTACCTTCTCTTTTGGGAACGCGAACTCCAGAAGGT	WT	
ACCGGTTCTACCT TTTGGGAACGCGAACTCCAGAAGGT	5b Del	[10/16]
ACCGGTTCTACCTTCTCCA GAACTCCAGAAGGT	10b-Del/2b-Mut	[5/16]
ACCGGTTCTACCTTCTACCTTGGGAACGCGAACTCCAGAAGGT	3b-Mut	[1/16]

Figure 6. Generation of albino newt *Cynops pyrrhogaster* by CRISPR/Cas9 genome editing. (**a**) The upper half of the cDNA sequence (accession number: LC06259) encoding the *C. pyrrhogaster* tyrosinase. Red: initiation site; yellow: CRISPR target site; purple: PAM sequence; blue: PCR primer region. (**b**) Tyrosinase-knockout newts with complete albinism one year after genome editing. Females of this batch showed natural spawning in the following year. (**c**) Mutation patterns on the target site. The uppermost sequence is the wild type (WT). Three mutation patterns were observed (5b Del, 10b-Del/2b-Mut and 3b-Mut). Red letters: mutated bases. Numbers in brackets indicate the frequency of appearance of each pattern. Note that the newts in (**b**), which belong to 5b Del, were used as the parent newts for the following transgenic experiments.

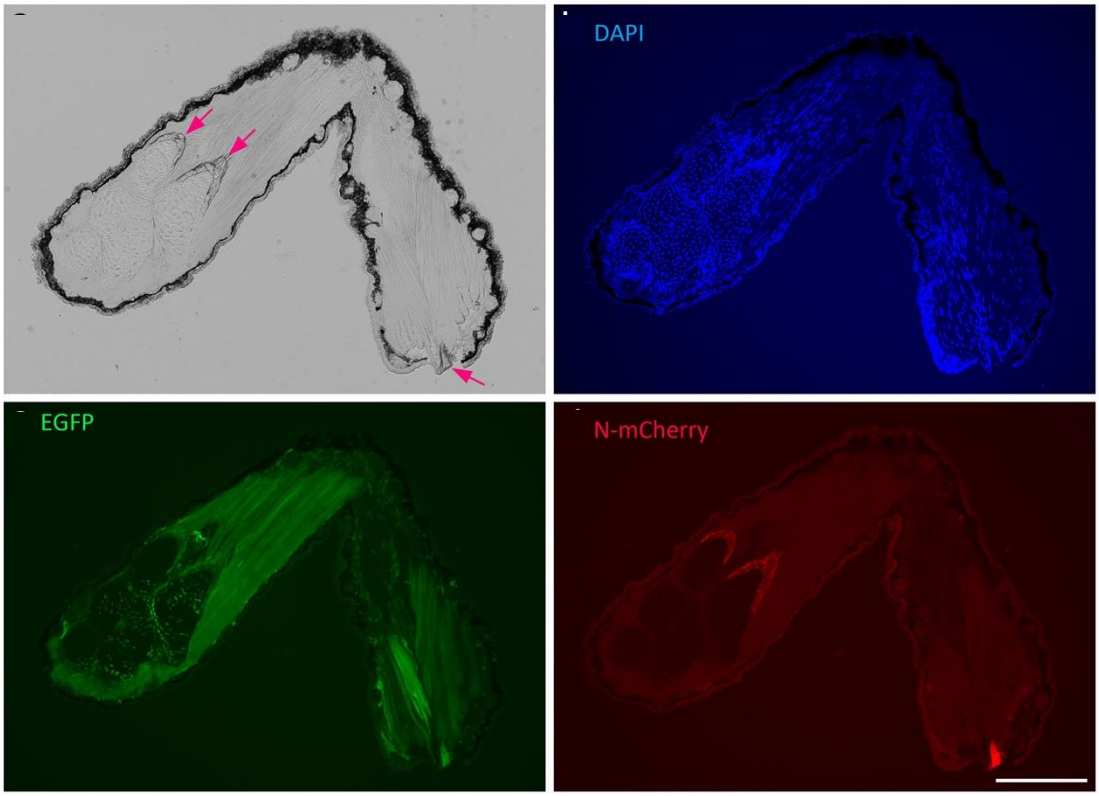

Figure 7. Control without induction of Cre-mediated recombination by 4-OHT.

A section of the forelimb of a juvenile. This animal was not reared in 4-OHT containing water at swimming larva stage (St. 53). Arrows indicate areas of ossification, where autofluorescence can be seen. The image was acquired with the KEYENCE BZ-X800 fluorescence microscope. Scale bar: 500 μm. I made serial sections of five swimming larvae without 4-OHT administration, but never observed mCherry fluorescence in their body.

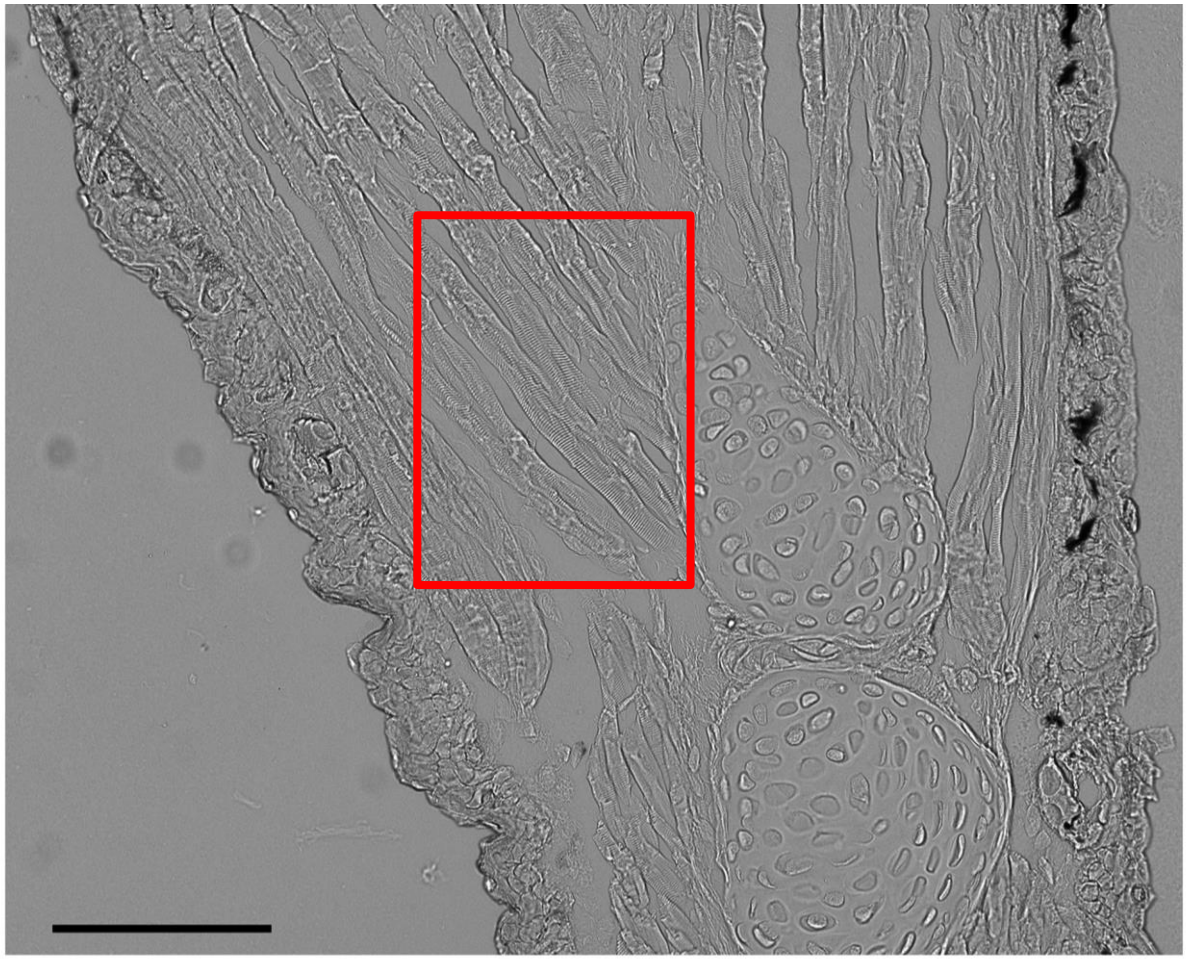


EGFP
N-mCherry
DAPI

Figure 8. Muscle fiber-specific expression of N-mCherry. A representative image showing muscle fiber-specific expression of N-mCherry in the forelimbs of swimming larvae (St. 58) after induction of recombination with 4-OHT at St. 53 (*n*=10). Upper panel is a transmitted light image of a section of the forelimb. Sarcomeres are found in skeletal muscle fibers. The image was acquired with the KEYENCE BZ-X800 fluorescence microscope. Scale bar: 200 μm. lower panel is a merged image of EGFP, N-mCherry and DAPI (nuclei) fluorescence in the same section.

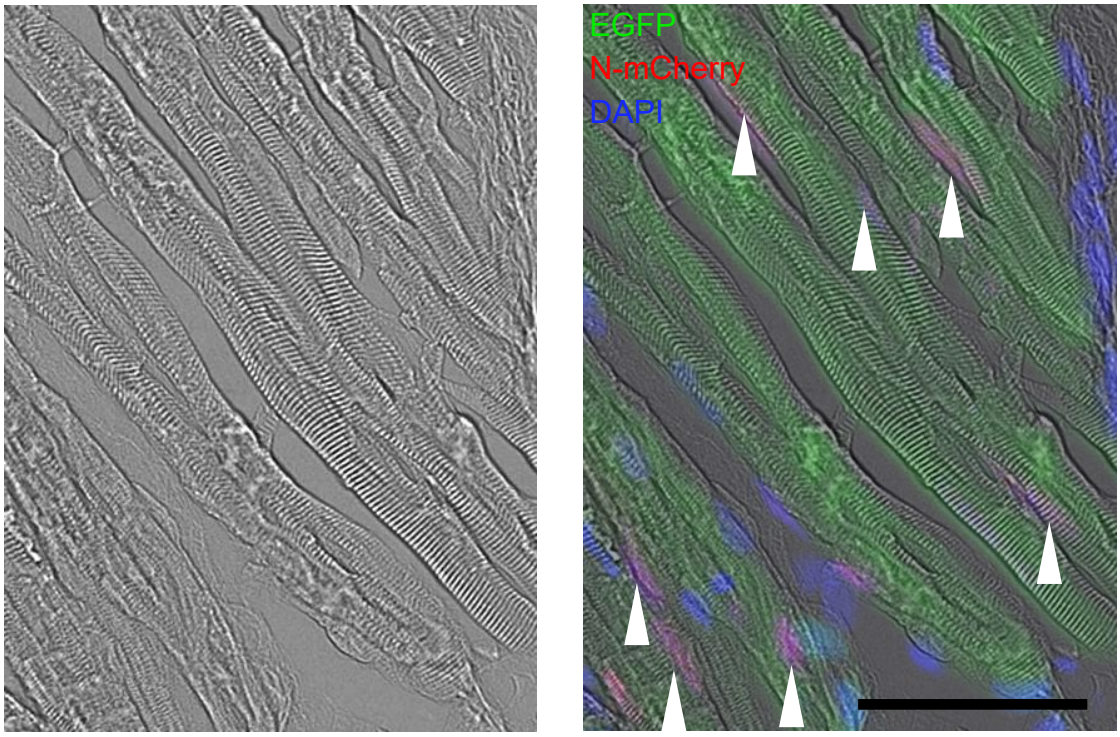

Figure 9. Muscle fiber-specific expression of N-mCherry. Magnified images in boxes of figure 8. Left panel is a transmitted light image of a section of the forelimb. Of note, right panel is a merged image of EGFP, N-mCherry and DAPI (nuclei) as well as transmitted light image. Showing a clearly beads on string appearance. Scale bar, 100 μm.

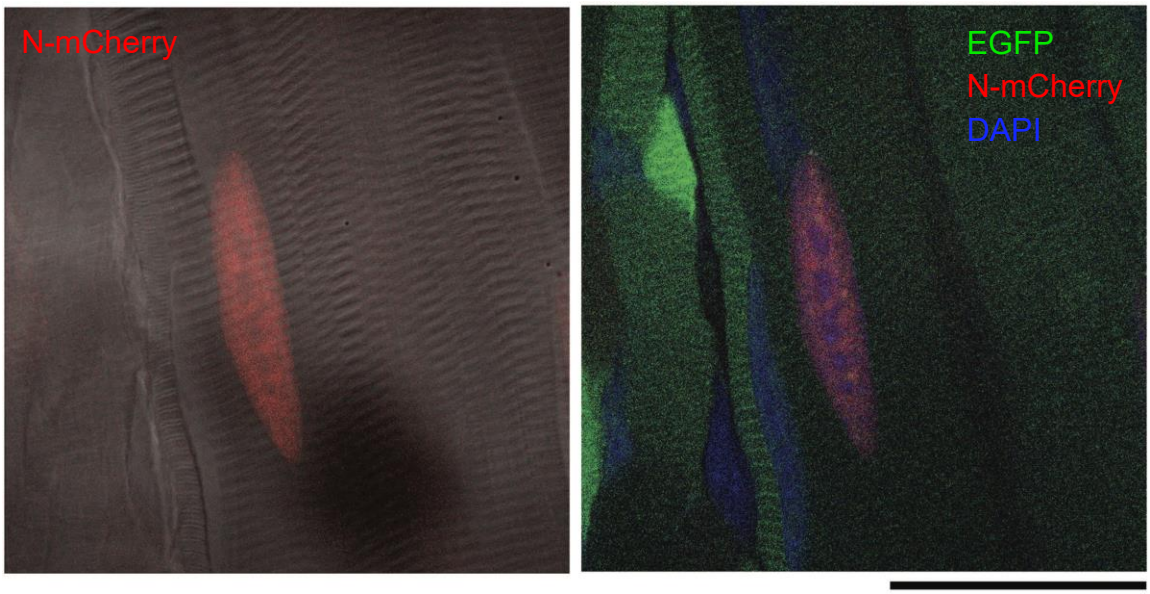

Figure 10. Muscle fiber-specific expression of N-mCherry. Representative confocal images showing nuclear localization of N-mCherry in muscle fibers of forelimbs in juveniles (*n*=20). Left panel is a merge of N-mCherry fluorescence on a transmitted light image. Sarcomeres are found in skeletal muscle fibers. Right panel is a merged image of EGFP, N-mCherry and DAPI (nuclei) fluorescence.

Scale bar: 40 μm.

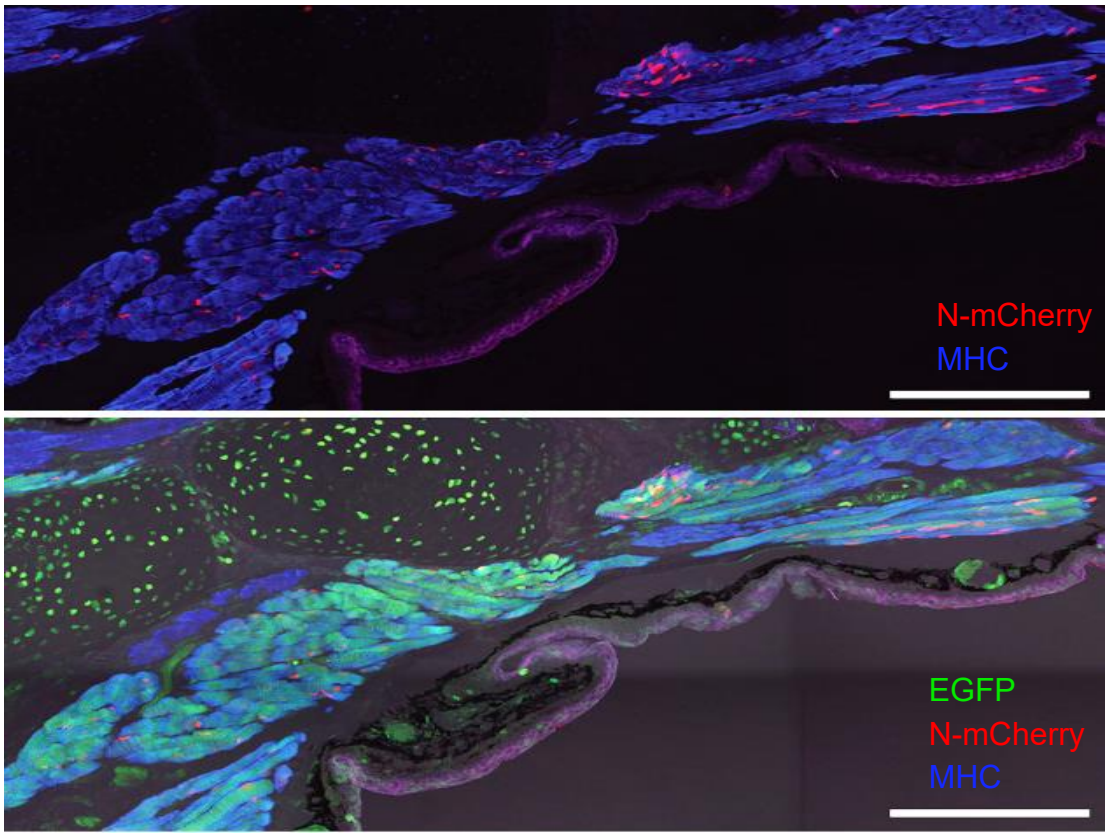

Figure 11. Muscle fiber-specific expression of N-mCherry. A representative confocal image showing localization of N-mCherry in adult forelimbs (*n*=4). Upper image is a muscle heavy chain (MHC) immunofluorescence image merged with N-mCherry fluorescence. Lower image is a merge of EGFP, N-mCherry and MHC fluorescence on a transmitted light image. Scale bar: 500 μm.

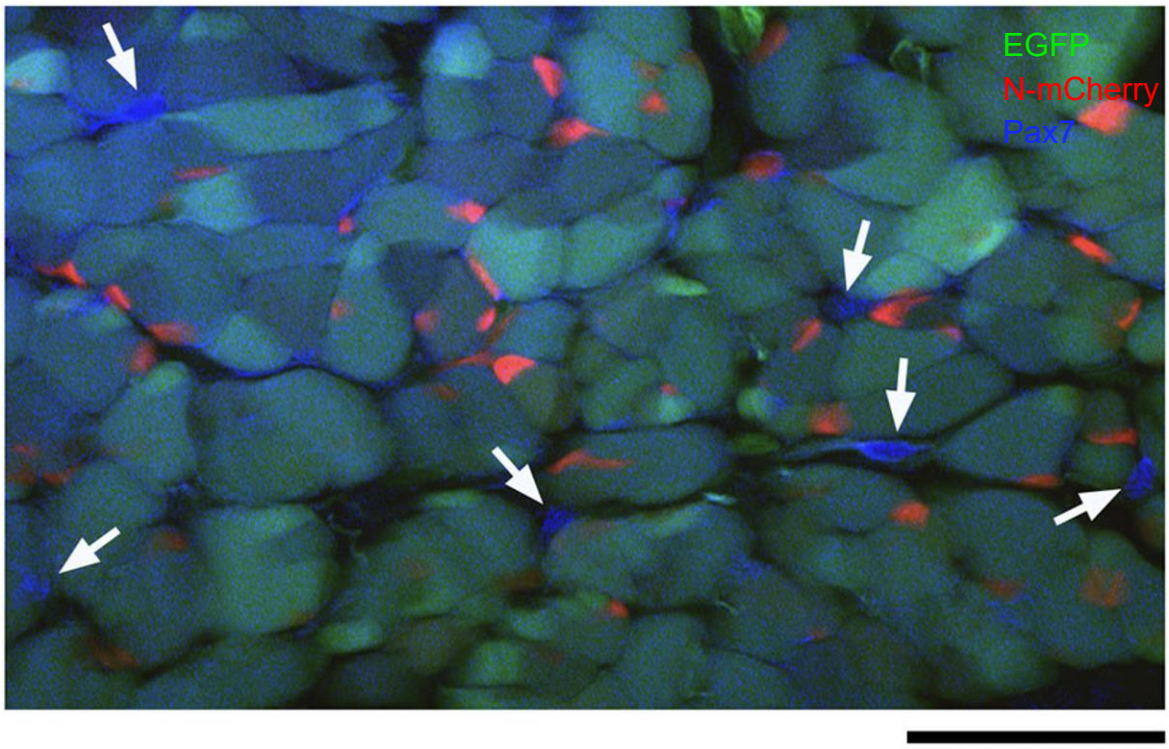

Figure 12. Labeling specificity. A representative confocal image of transverse sections of limb muscle showing uniform expression of EGFP. Immunohistochemistry showed that satellite cells, which are resident myogenic stem cells, that express Pax7 (blue), were never labelled by N-mCherry. Therefore, muscle originated cells are tracked in this system, but not residual stem cells. Scale bar, 100 μm.

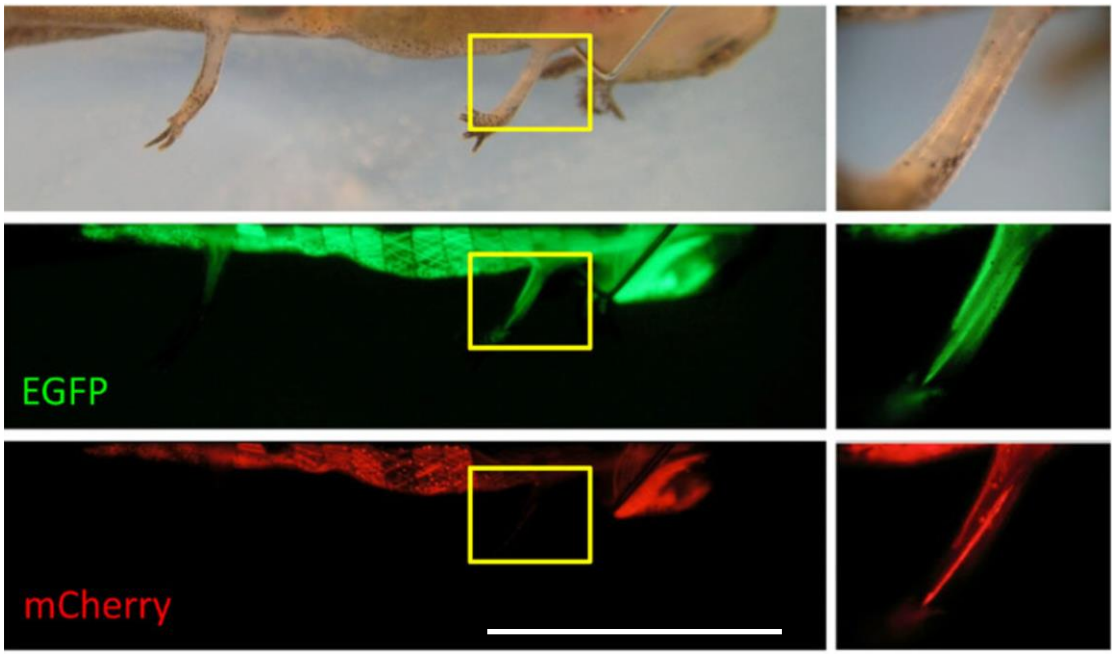

Figure 13. Cytoplasmic muscle tracking system. (Adapted from Tanaka et al., 2016). Representative images from a cytoplasmic muscle tracking larva newt demonstrated here created by our laboratory recently. Images showing a 2 cm larva newt. Muscle fiber could be tracked by cytoplasmic mCherry fluorescence. Scale bar, 1 cm.

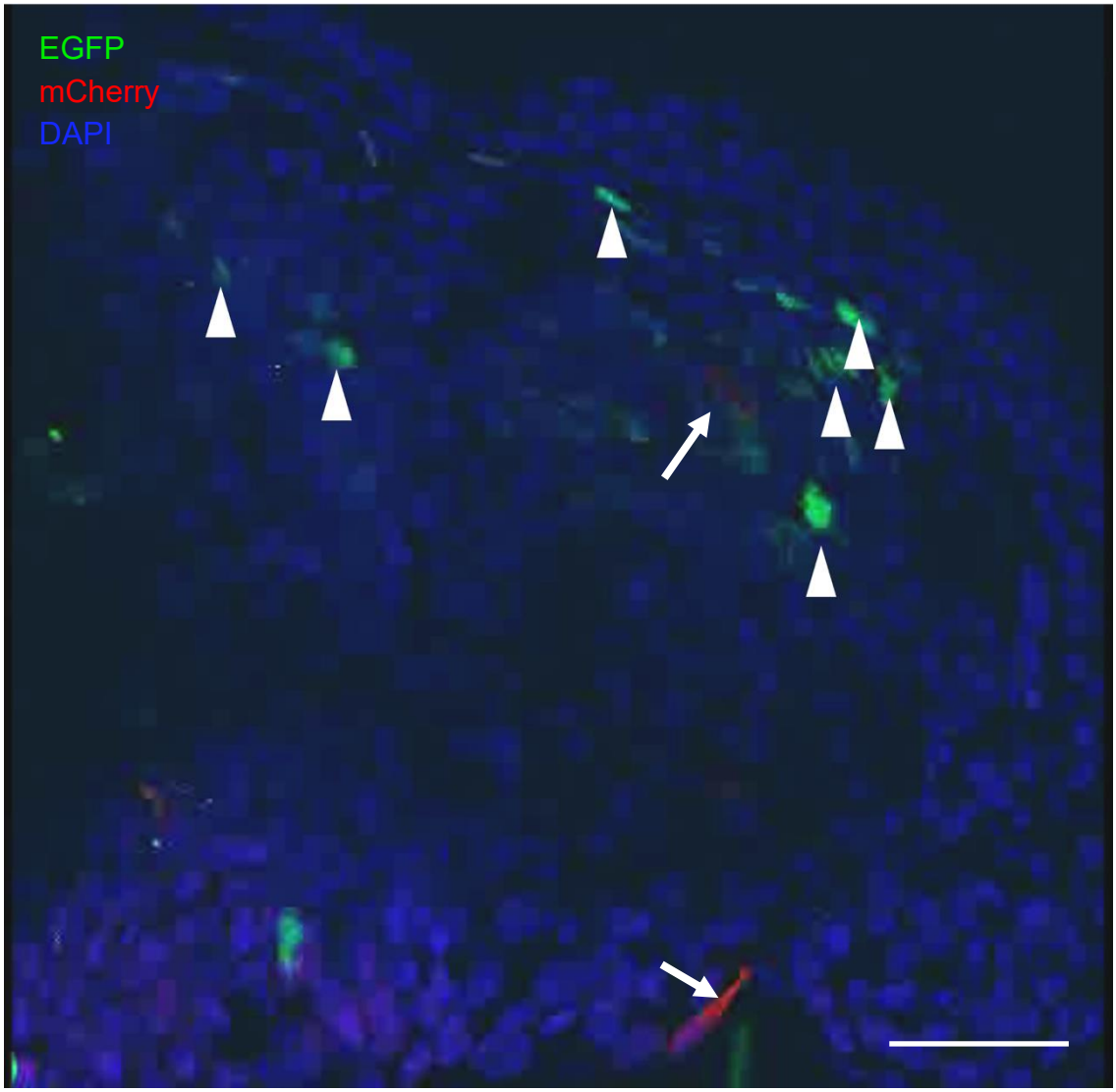

Figure 14. A 3D tissue section of an adult blastema (adapted from Tanaka et al., 2016). Whole blastema tissue showed here. Arrows pointing mCherry fluorescent cells. Arrowheads pointing fragmented muscle cells located on the top of blastema region. Muscle cells which containing EGFP and mCherry fluorescence showing fragmented appearance. Therefore, it was difficult to identify and localize muscle originated cells. Scale bar, 100 μm.

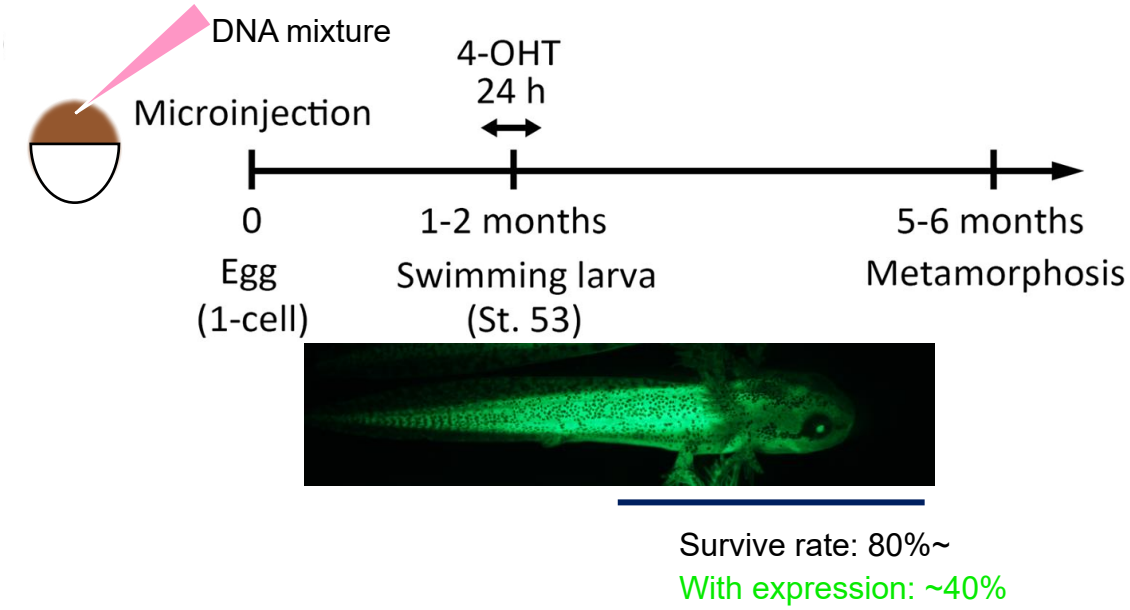

Figure 15. Experiment timeline. Creating transgenic newts. The construct was injected into one-cell stage embryos of albino F1 and wild-type F0. To induce recombination, swimming larvae at St. 53 (1-2 months old), which only had three of five digits on the hind limbs, were incubated in tap water containing 4-OHT for 24 h. Of note, survival rate of transgenic newts was higher than 80%, and among those normally developing newts, up to 40% showed EGFP fluorescence. Scale bar, 1 cm.

Figure 16. Albino F1 muscle tracking newts grown in the laboratory. Eggs obtained from albino parental newts (F0) and combined with muscle nucleus-tracking system, so these albino newts (F1) were used for living monitor of skeletal muscle fiber nuclei which showing N-mCherry. Scale bar, 3 cm.

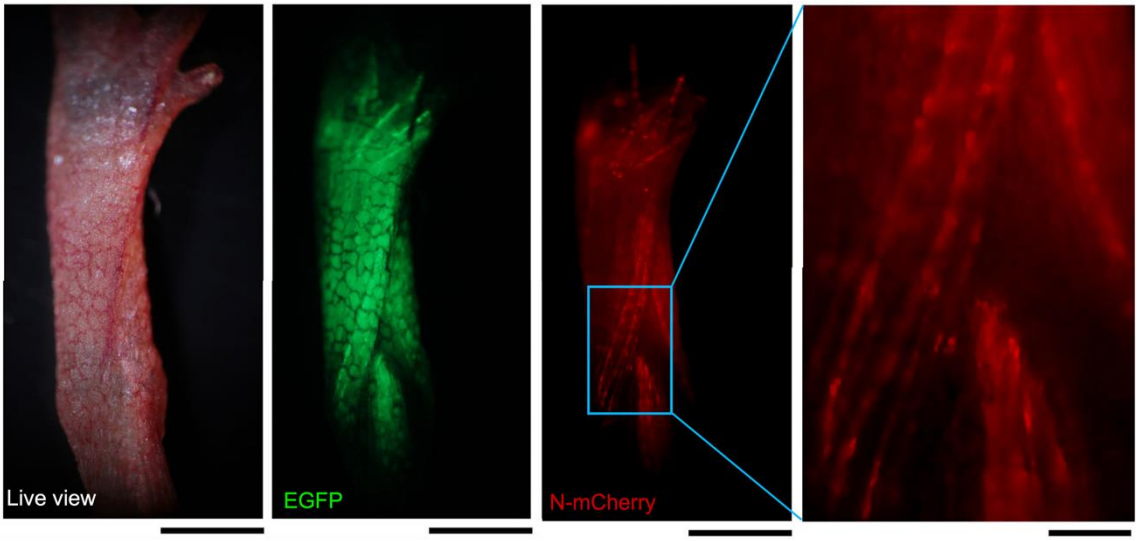

Figure 17. Representative images of an albino newt limb. Images showing the expression of EGFP and N-mCherry in the forelimbs of albino juveniles. A large number of N-mCherry nuclei were observed along the muscle fibers. Albino newt enables muscle cells live monitor because they lost pigments. Scale bar, 200 μm, 100 μm for magnified image at right panel.

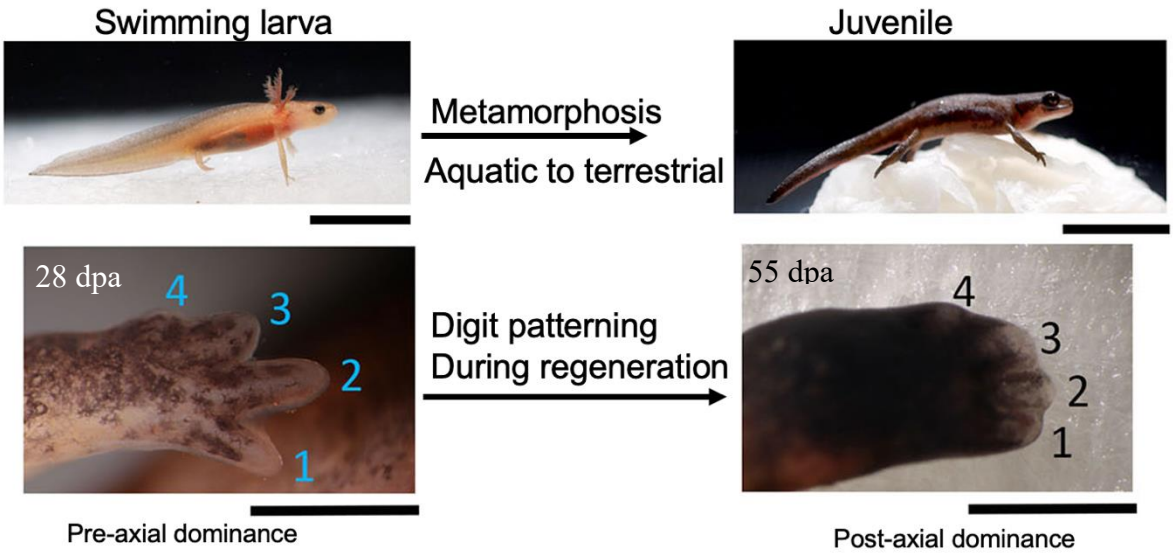

Figure 18. Digit patterning changed during regeneration after metamorphosis.

Images at left side are from a swimming larva newt. Newt digits patterning during limb regeneration followed the rule of pre-axial dominance. Images in right panel are from a juvenile newt, its digits patterning switches to post-axial dominance. In each developmental stage, a forelimb was amputated at a midpoint of the lower arm. dpa: day post amputation. Scale bar, 1 cm for newts, 1 mm for their hands. Numbers, finger counting.

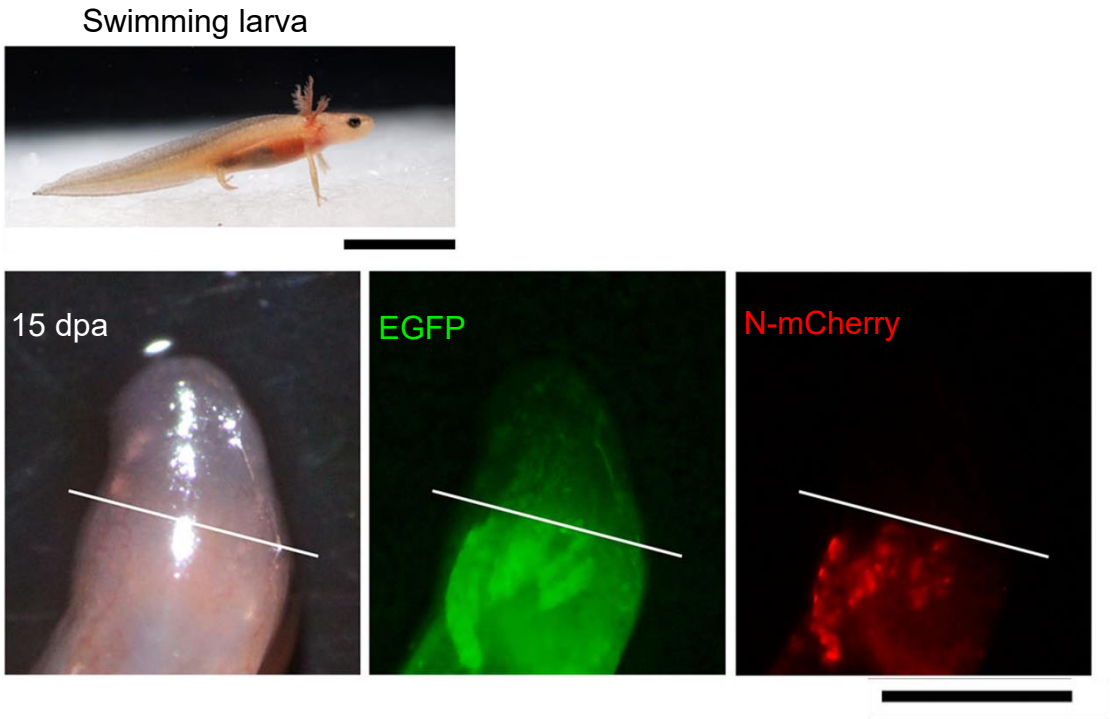

Figure 19. Live images of a larval blastema. Muscle tracking in swimming larvae at St. 58 (age: 2-3 months; total body length: ~3 cm). Nuclei with N-mCherry fluorescence were not observed in the larval blastema. White line, amputation plane. Scale bar, 1cm for upper image, 0.5 mm for lower images.

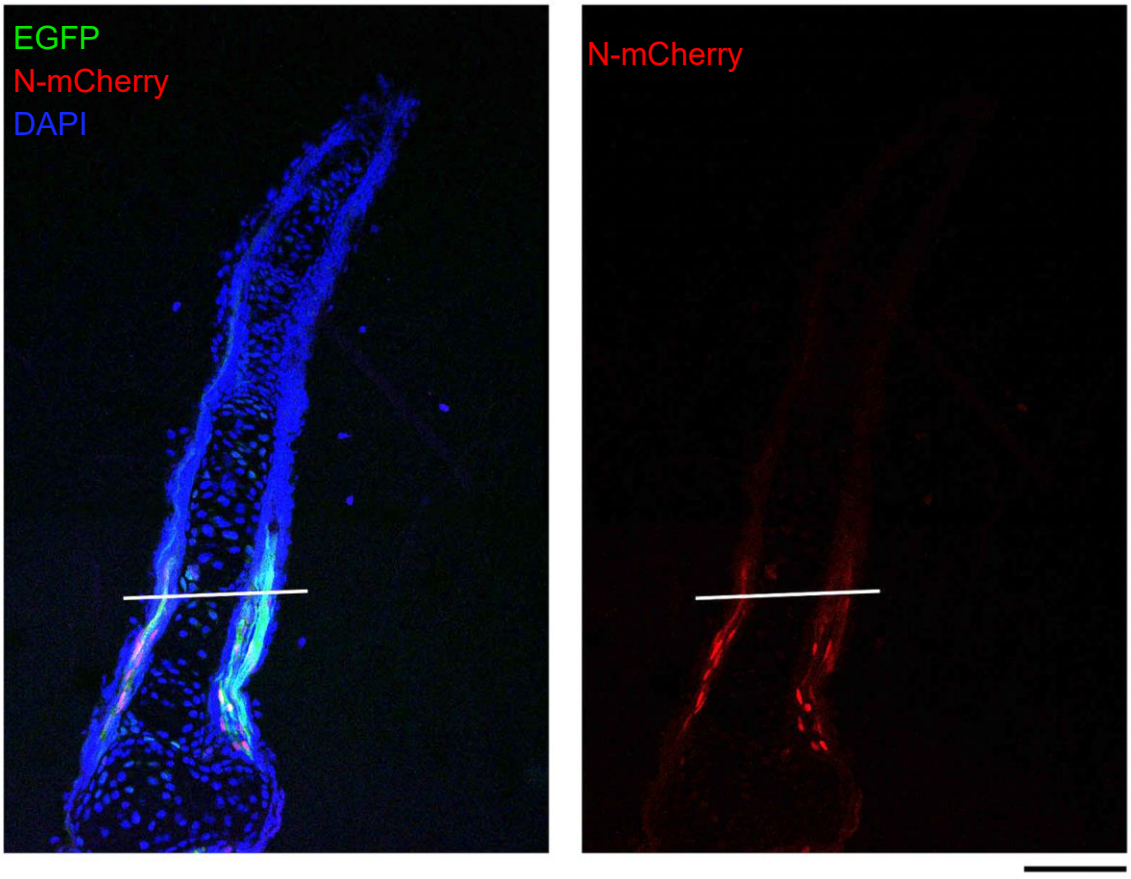

Figure 20. Distribution pattern of N-mCherry nuclei in regenerating forelimbs of swimming larvae. A representative image of sections of late regenerating limbs in swimming larvae at St. 58. This section was obtained from a limb at 16 days after amputation, in which digit formation had started. The limb was sectioned along the dorsoventral axis. Nuclei with N-mCherry fluorescence were not observed in the tissues distal to the amputation plane (white line) (*n*=5). Scale bar, 200 μm.

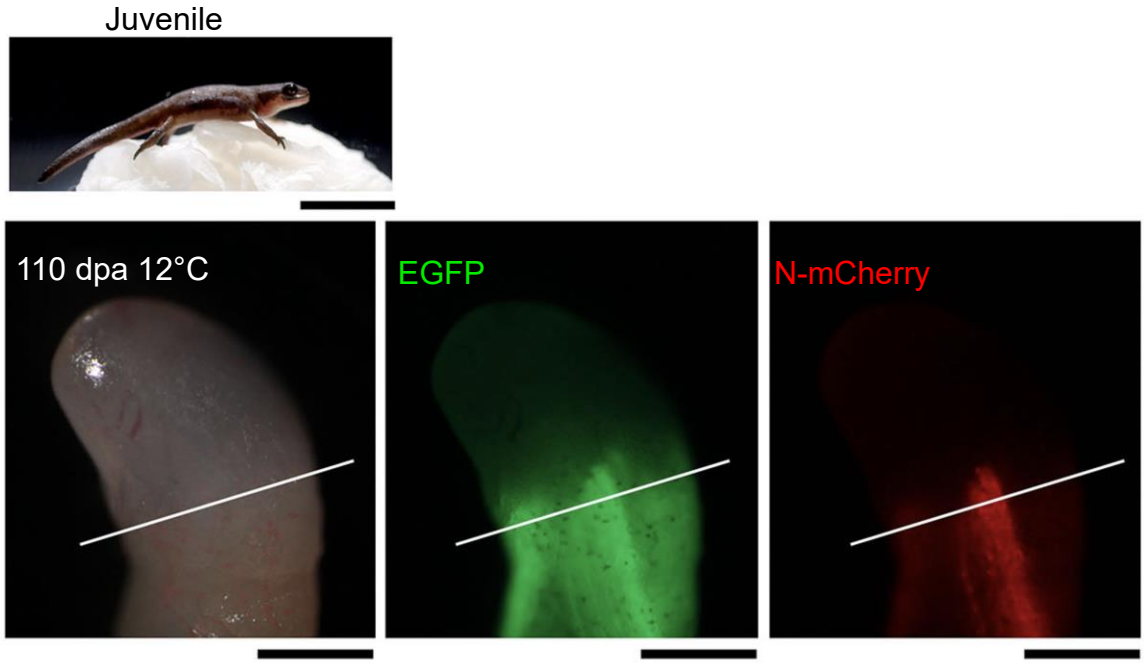

Figure 21. Live images of a juvenile's blastema. Muscle tracking in juveniles (age: 5-6 months; total body length: ~3 cm). Note that the animal showed herein was a mosaic in which EGFP was exclusively expressed in muscle fibers, and reared after limb amputation at 12 °C to explore mono-SMFCs during blastema formation and growth with an increased time resolution (see Methods; for the blastema at the standard rearing temperature, see Figure 22). Nuclei with N-mCherry fluorescence were not observed in the larval blastema. White line, amputation plane. Scale bar, 1cm for upper image, 0.5 mm for lower images.

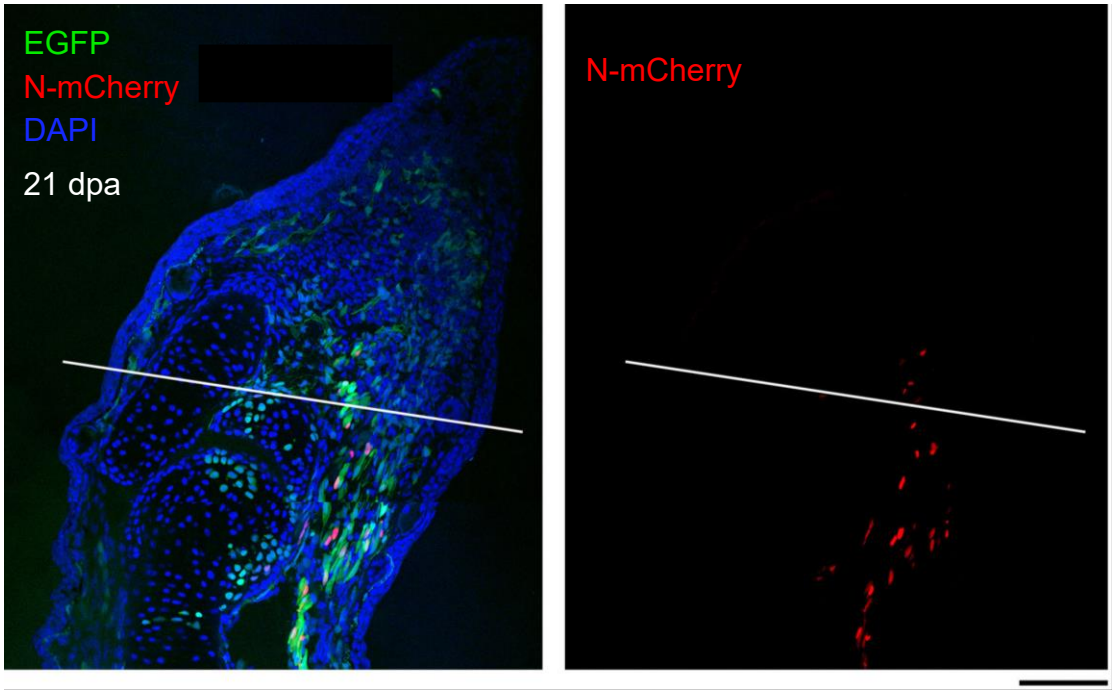

Figure 22. Distribution pattern of N-mCherry nuclei in regenerating forelimbs of juveniles. A representative image of sections of the blastema in juveniles. The animals were kept at the standard rearing temperature (18-20°C) after the limb amputation. This section was obtained from a limb at 21 days after amputation. The limb was sectioned along the anterior-posterior axis. Mono-SMFCs were never observed in the blastema of juveniles (*n*=20) and in a transitional stage between juvenile and preadolescence (*n*=5). Scale bar: 200 μm.

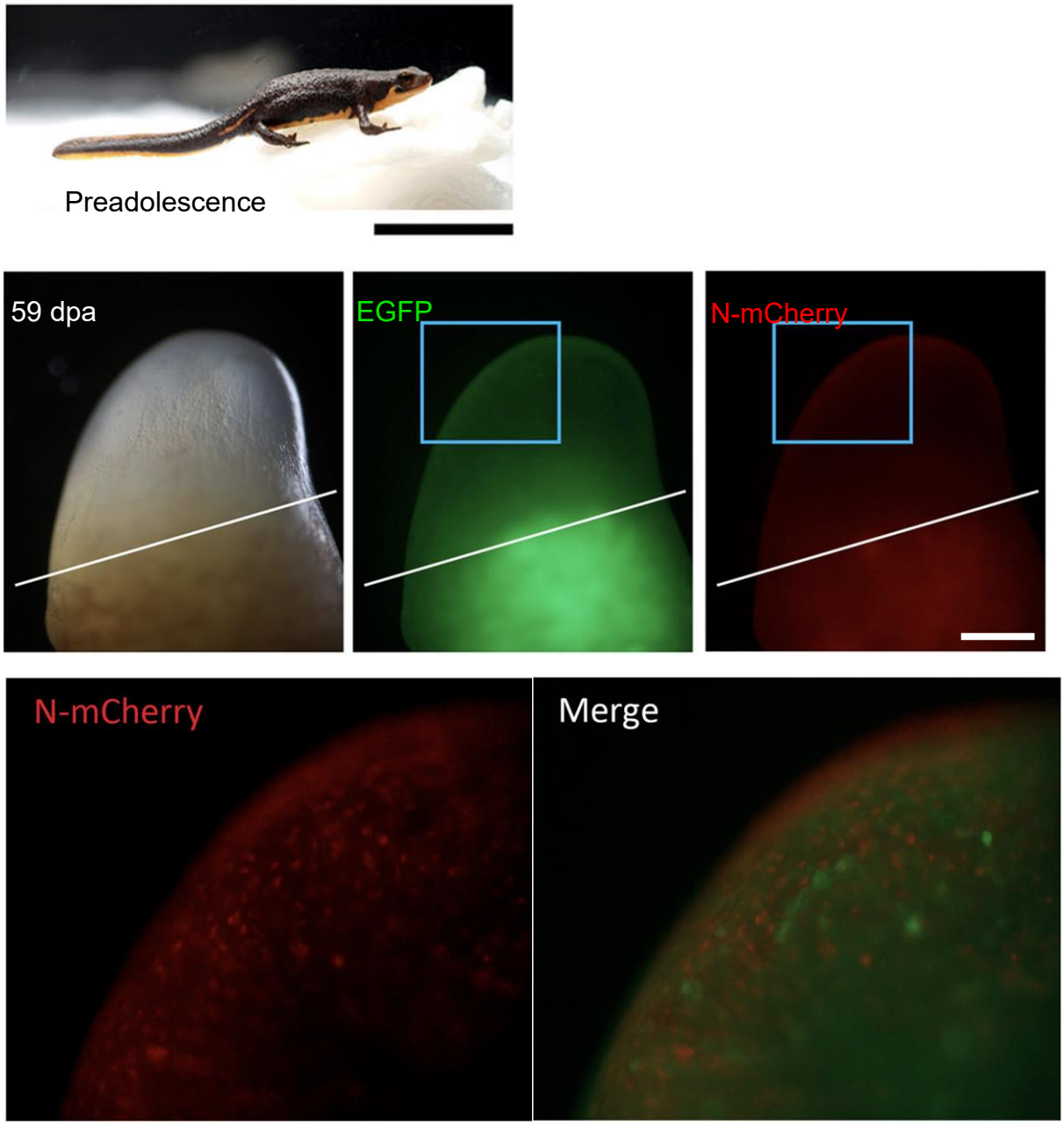

Figure 23. Live images of a preadolescence's blastema. Muscle tracking in preadolescences (age: 1.1 years; total body length: ~6 cm). In all animals at preadolescence stage (albino, *n*=1; wild color, *n*=4), a large number of mono-SMFCs appeared in the blastema (sections images see below). Lower images are enlargements of the areas of the boxes. White line, amputation plane. Scale bar, 2 cm for upper, 0.5 mm for middle, 100 μm for lower.

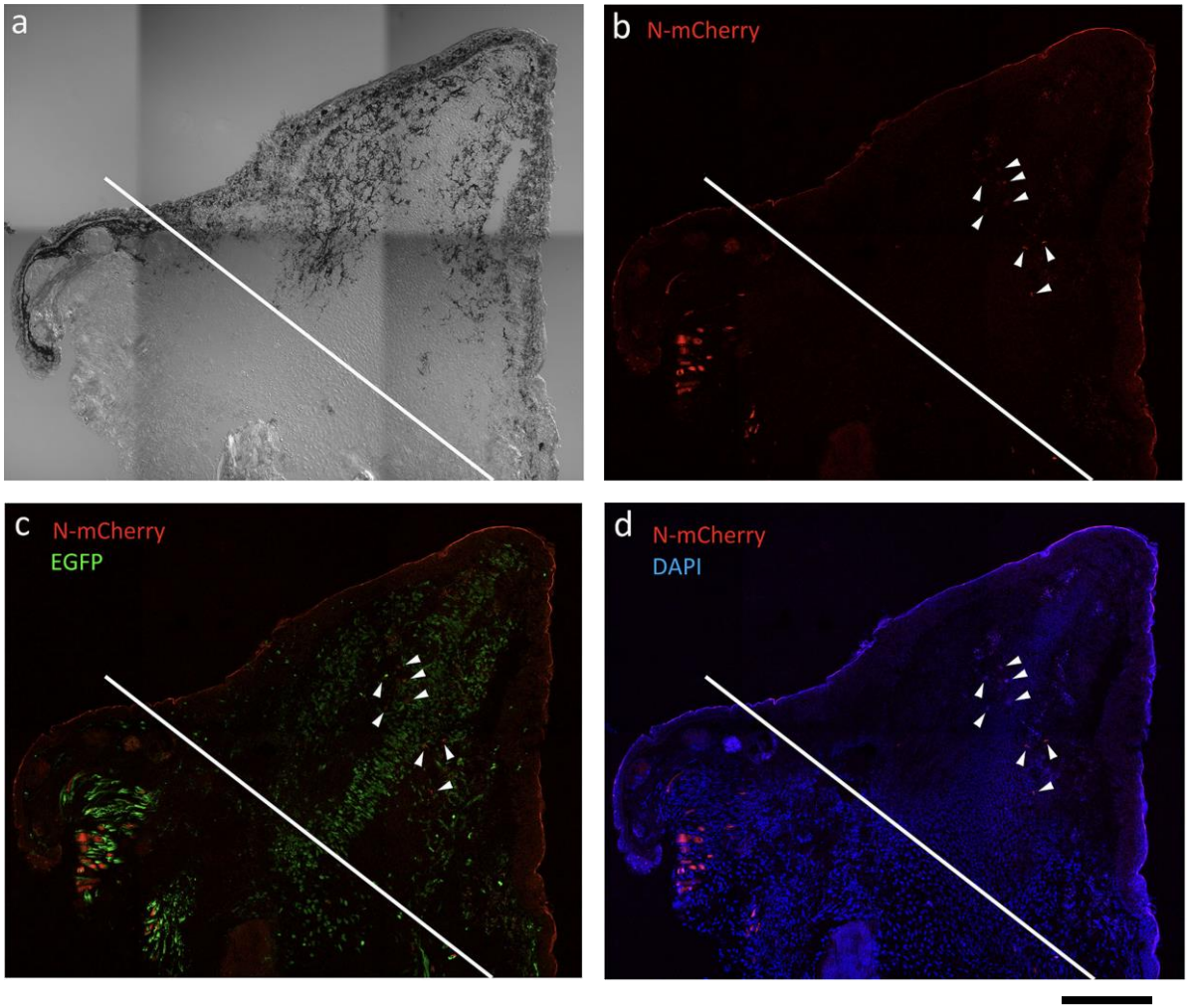

Figure 24. A representative set of images showing mono-SMFCs in blastema of the forelimbs of preadolescences. This animal is not albino. (**a**) A transmitted light image of a section of the blastema. (**b**) N-mcherry fluorescence. (**c**) Merge of N-mCherry and EGFP fluorescence. (**d**) Merge of N-mCherry and DAPI (nuclei) fluorescence. Arrowheads: N-mCherry+ nuclei. White lines: amputation plane. Scale bar: 500 μm. Though the number of mono-SMFCs in blastema region varied among sections possibly due to the difference in distribution pattern of N-mCherry muscle fibers in the stump, I observed mono-SMFCs in all animals examined (n=4).

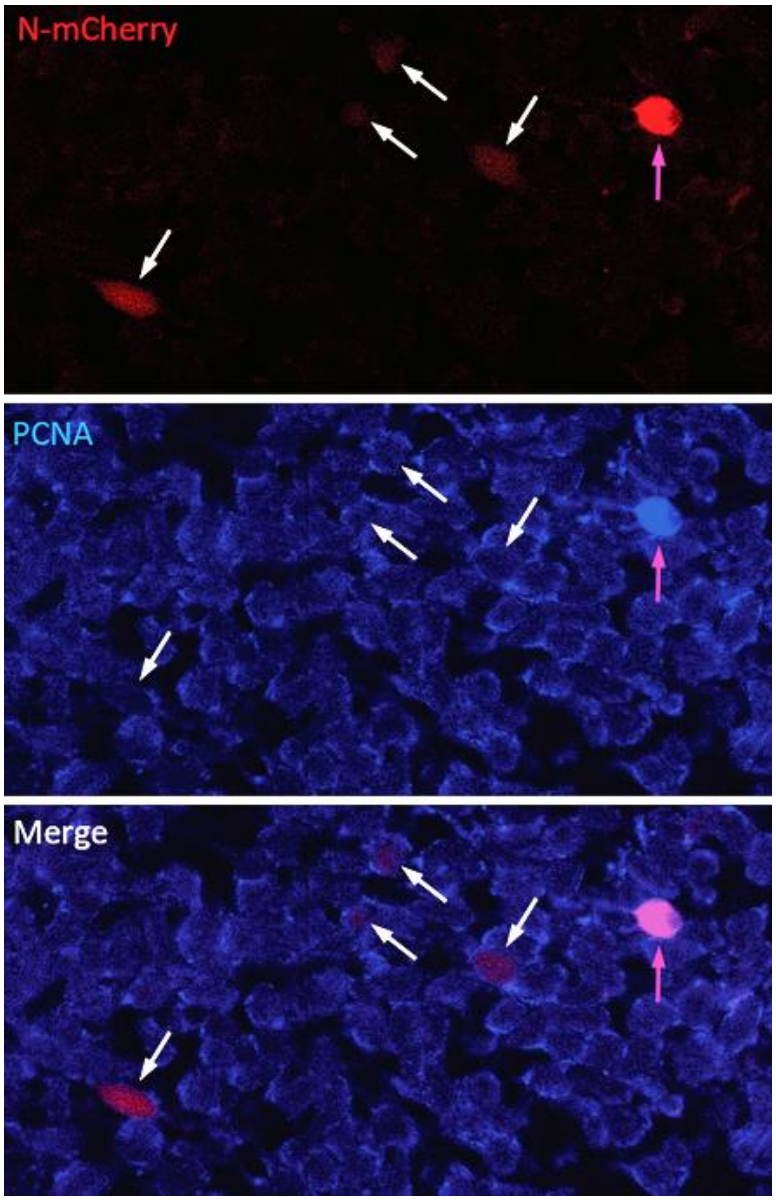

Figure 25. A representative set of confocal images showing cell cycle entry of mono-SMFCs in blastema of the forelimbs of preadolescences (*n*=4). This area was near the amputation plane. Magenta arrow: a mono-SMFC (N-mCherry+) with PCNA immunoreactivity (blue). White arrows: mono-SMFCs without PCNA immunoreactivity. Scale bar: 100 μm.

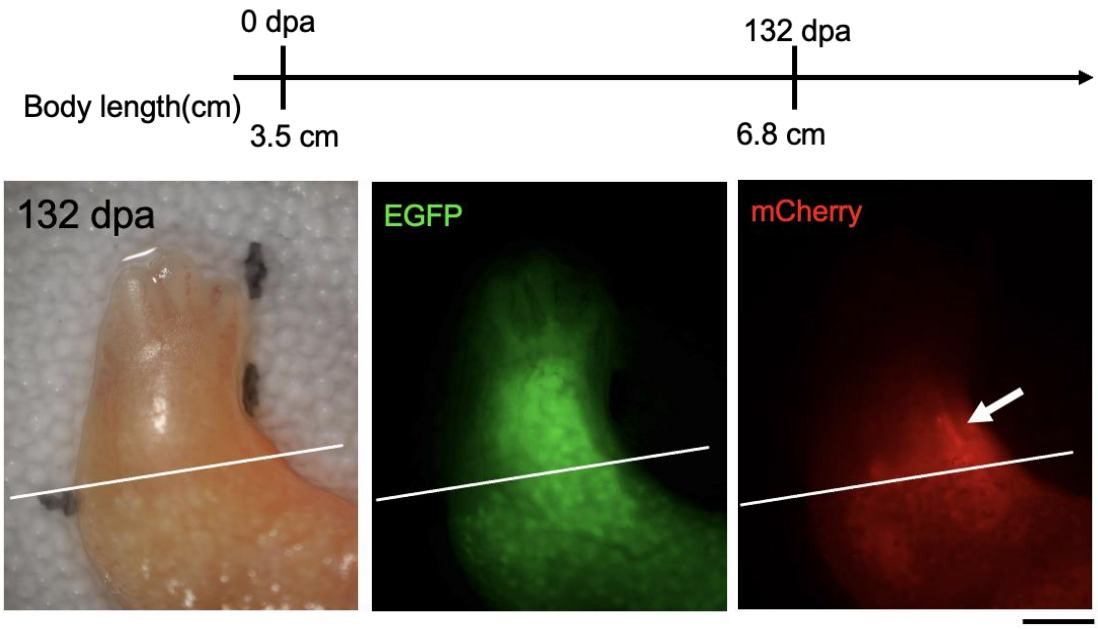

Figure 26. live images of an aged but small-sized newt's regenerated limb.

Juvenile newt was reared at 12 °C, a temperature lower than the standard rearing temperature (18-20°C). This condition slows its body growth while maintaining their aging. When animal reached age of 1.1 years (related to preadolescence), amputation was performed and transferred newt back to 20°C. In this condition, body growth speeded up, as did limb regeneration. However, as in juvenile limb regeneration, mono-SMFCs were not detected during live monitoring of the regenerating limb over 130 days. As in the regenerating limb of the juvenile, N-mCherry nuclei appeared along muscle fibers as they extended distally from the amputation plane (white line), although the number of extended muscle fibers obviously increased. For example, the arrow indicates the distal margin of the extended muscle fibers.

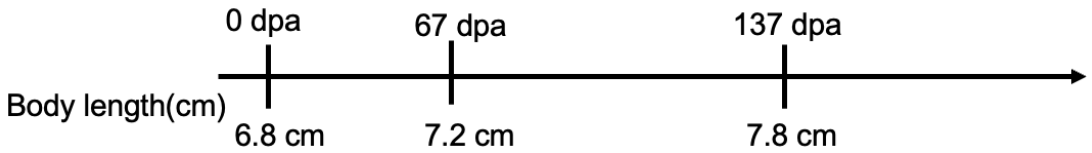
0 dpa
67 dpa
137 dpa
Body length(cm)
6.8 cm
7.2 cm
7.8 cm

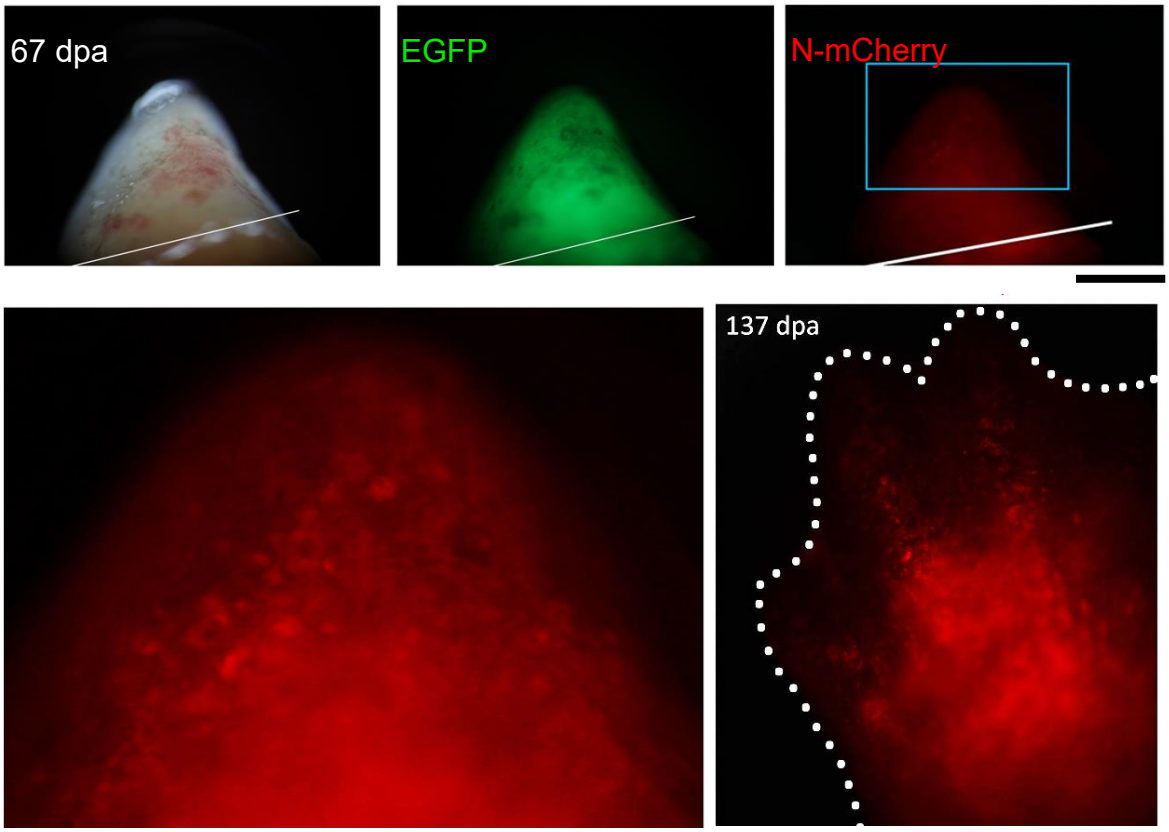
67 dpa
EGFP
N-mCherry
137 dpa

Figure 27. live images of a size released newt's regeneration. Take advantage of newts repeatedly regeneration ability, I examined the same individual's regeneration. To examine whether the grown newt at 132 dpa (age: almost 1.4 years; total body length: 6.8 cm) showed muscle dedifferentiation, the forelimb was amputated at a midpoint in between the elbow and the shoulder. The middle images are the blastema at 67 dpa, and that an enlargement of the box at low left. The white line indicates the amputation plane. As in the normal preadolescence shown in Figure 24, the blastema of this animal contained a large number of mono-SMFCs. Furthermore, N-mCherry nuclei were distributed in the regenerating hand, see the low right image. Scale bars: 1 mm for middle, 300 μm for lower panels.

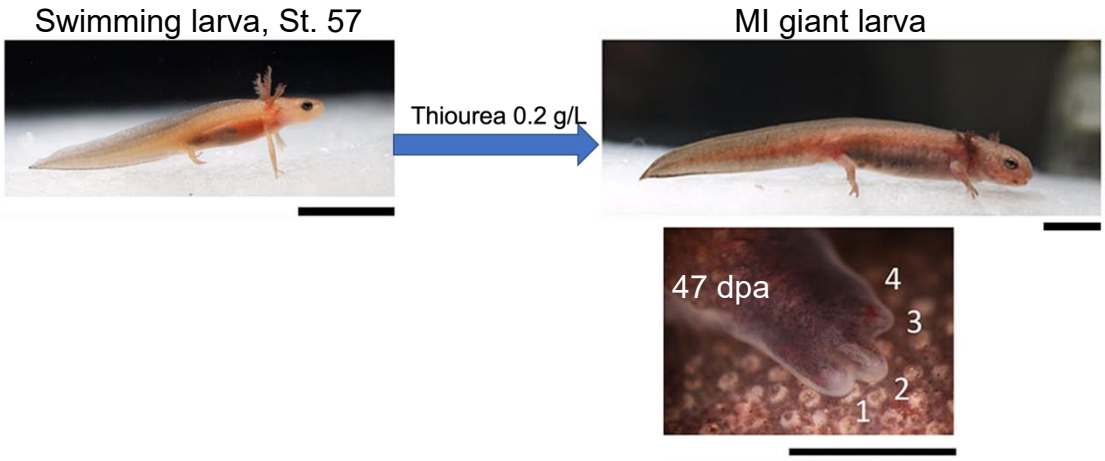

Figure 28. Preparation of metamorphosis-inhibited giant larva. Swimming larvae were reared in water containing 0.2 g/L Thiourea since St. 57. MI giant larva that reached preadolescent size were used for further examinations. Of note, giant larvae digits patterning during limb regeneration are pre-axial dominance, that is a larval feature. Scale bars, 1cm for upper, 2 mm for lower.

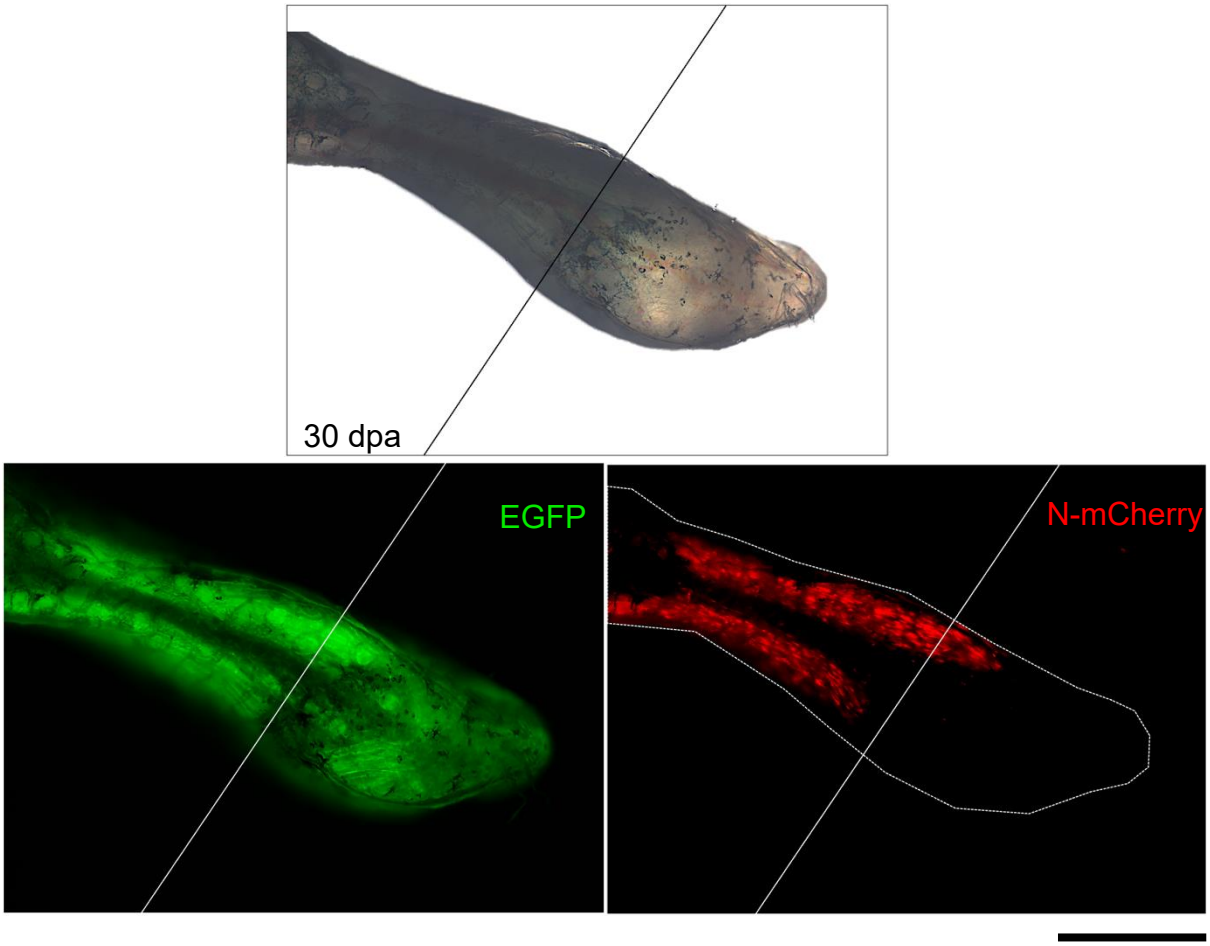

Figure 29. Live images of MI giant larva newt's blastema. One particular case showing here, a metamorphosis-inhibited newt, reached growth conditions related to preadolescence (age, 1.1 years, body size, 6 cm), having extremely strong fluorescence expression, but very few pigmentations on its skin. It enables live monitor of muscle nuclei. Clearly, mono-SMFCs were not detected during live monitoring of limb regeneration. White and black lines indicate amputation plain. Scale bar, 200 μm.

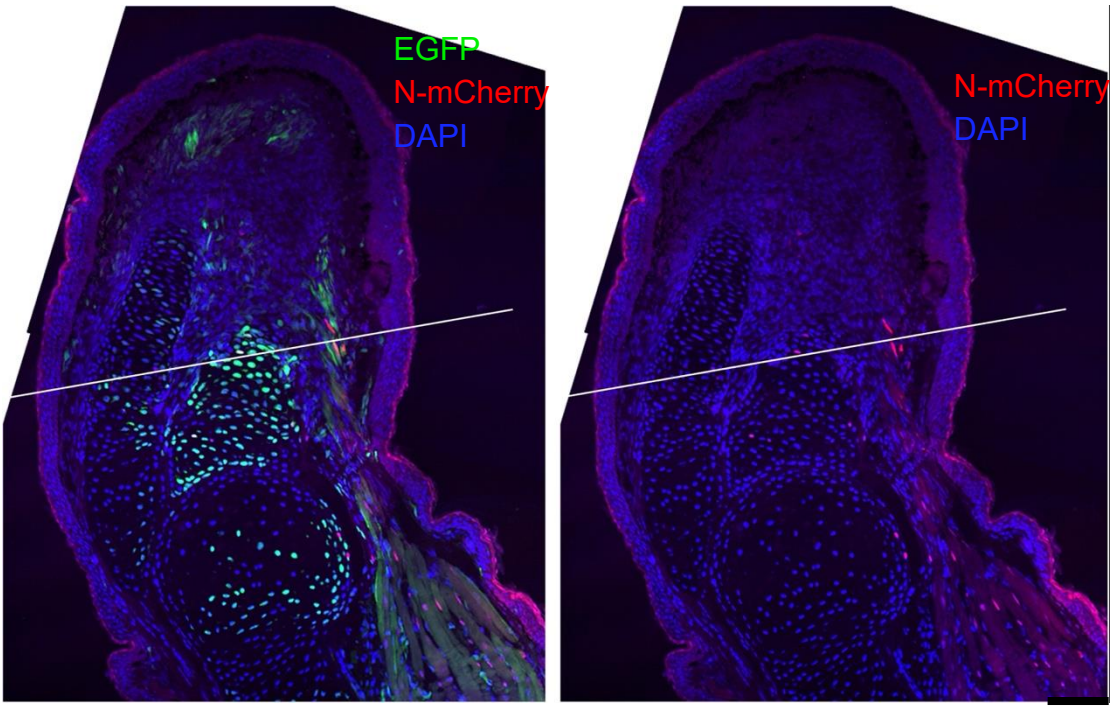

Figure 30. Contribution of muscle dedifferentiation to limb regeneration in MI giant larvae. The images are representative of blastema in MI giant larvae. Mono-SMFCs were not detected in the blastema (*n*=8). Note that in both MI giant larvae and MIR juveniles (see below), the ulna and radius, which were still cartilage, regenerated quickly by growing distally. Even at the blastema stage, the distal ends of the ulna and radius were observed inside the blastema. White line, amputation plane. Scale bar, 200 μm.

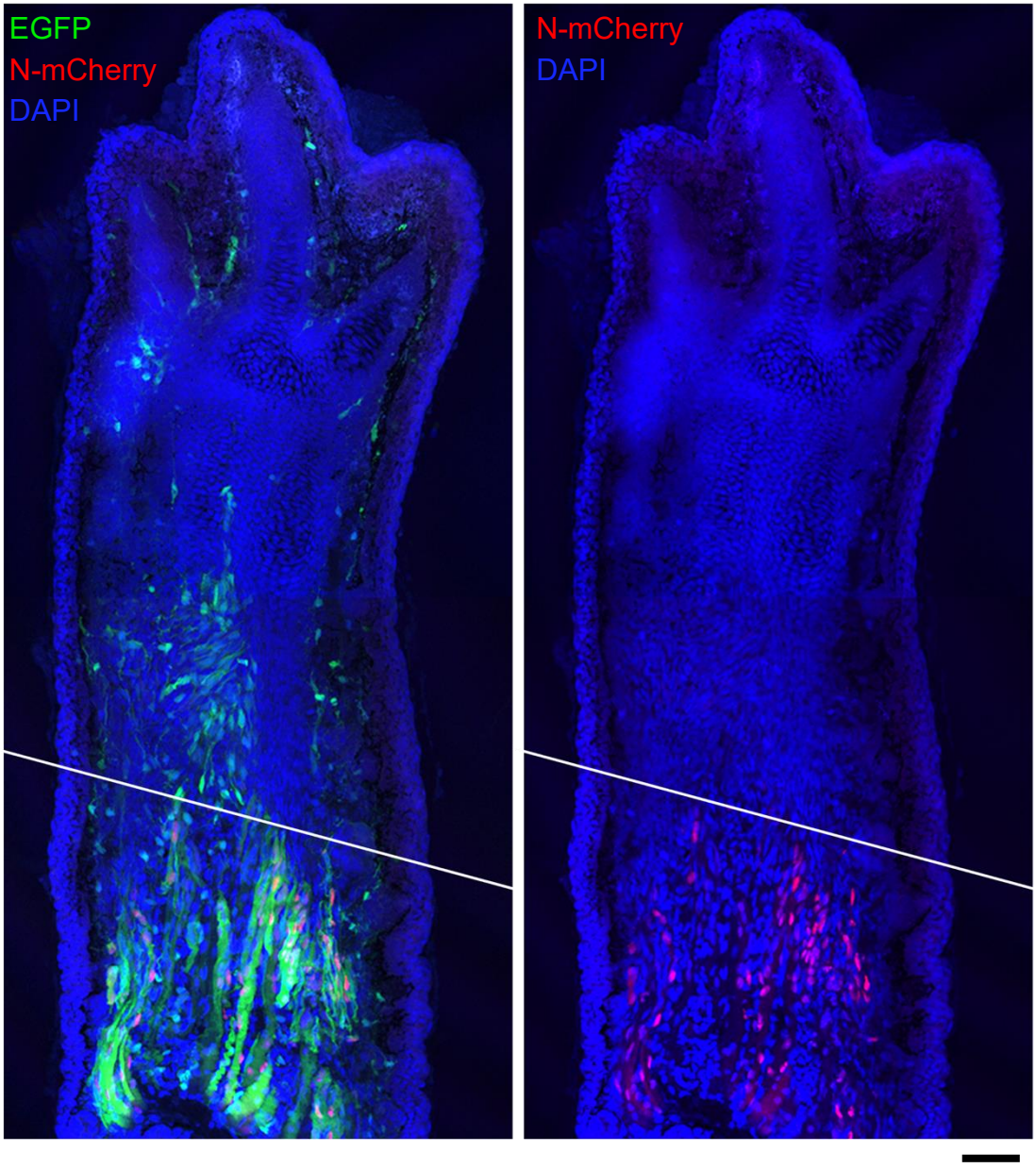

Figure 31. Contribution of muscle dedifferentiation to limb regeneration in MI giant larvae. The images are representative of regenerated limb in MI giant larvae. Mono-SMFCs were not detected in the blastema (*n*=8). White line, amputation plane. Scale bar, 200 μm.

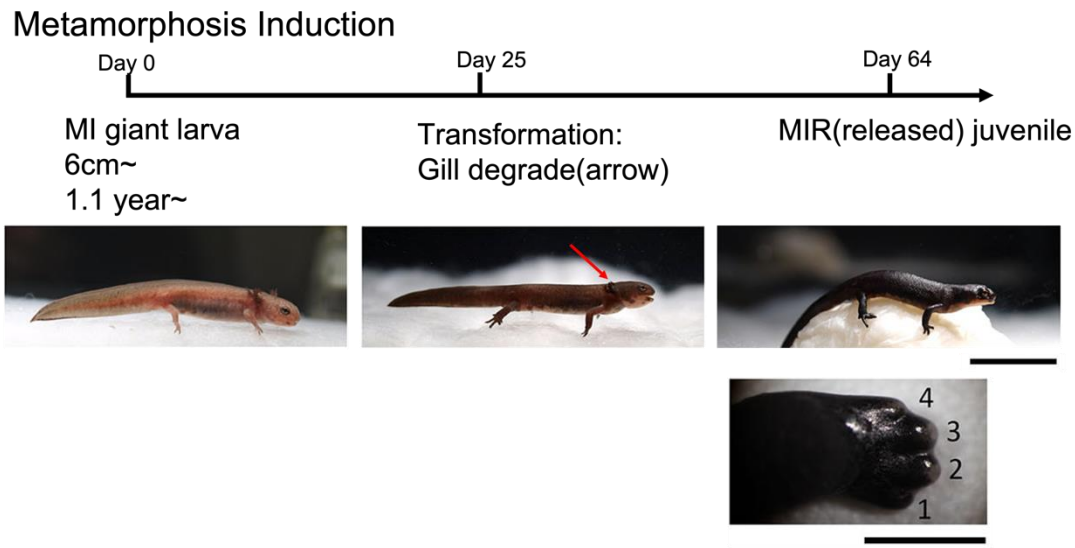

Figure 32. Induction of metamorphosis in metamorphosis-inhibited (MI) giant larvae. Representative set of images obtained from the same individual show above. For this experiment, animals were grown to ~6 cm (total body length) in tap water containing 0.2 g/l thiourea for 1.1 year while preserving their larval characteristics such as gills and tail fin (age and body size corresponded to those of preadolescence). 1 month later, transformation begin, for example, respiratory organ, gill showed degradation. MI giant larvae metamorphosed over ~2 months after they were transferred into plain tap water. These animals are referred to as MI-released (MIR) juveniles. MIR juvenile showing an adult feature that digit regenerate post-axially. Numbers are digits counting. Scale bars, 2 cm for newt, 2 mm for a hand.

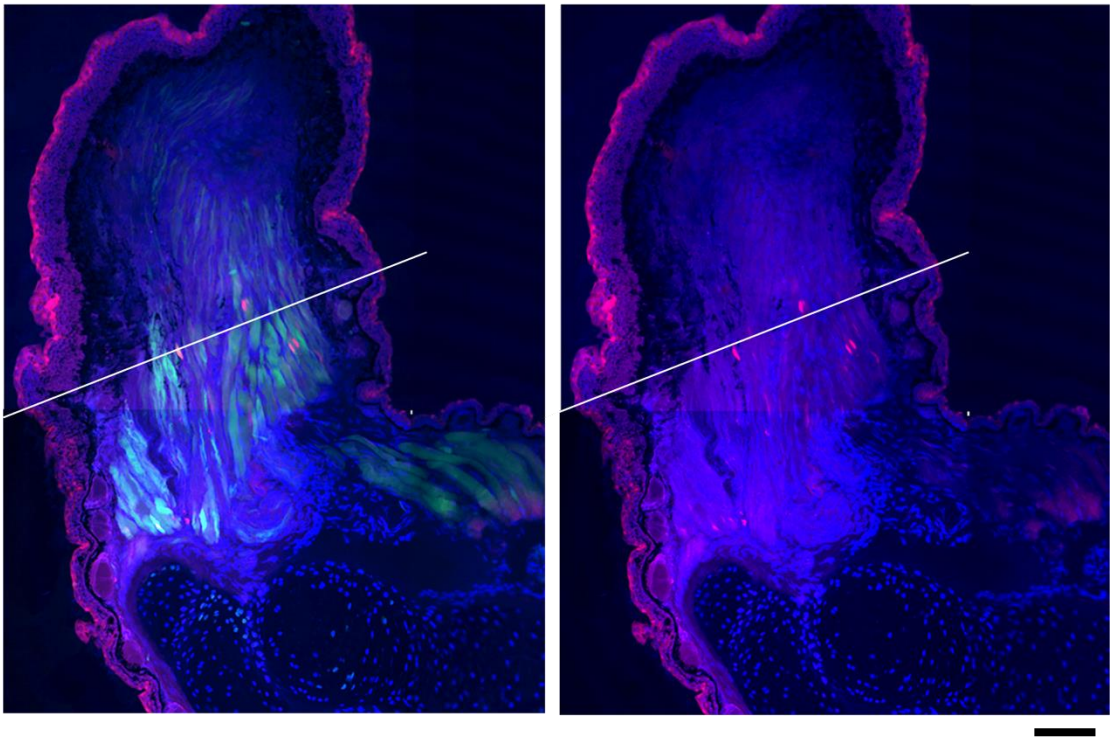

Figure 33. Contribution of muscle dedifferentiation to limb regeneration in MIR juveniles. The images are representative of blastema in MIR juveniles. Unexpected, mono-SMFCs were not detected in the blastema (*n*=8). White line, amputation plane. Scale bar, 200 μm.

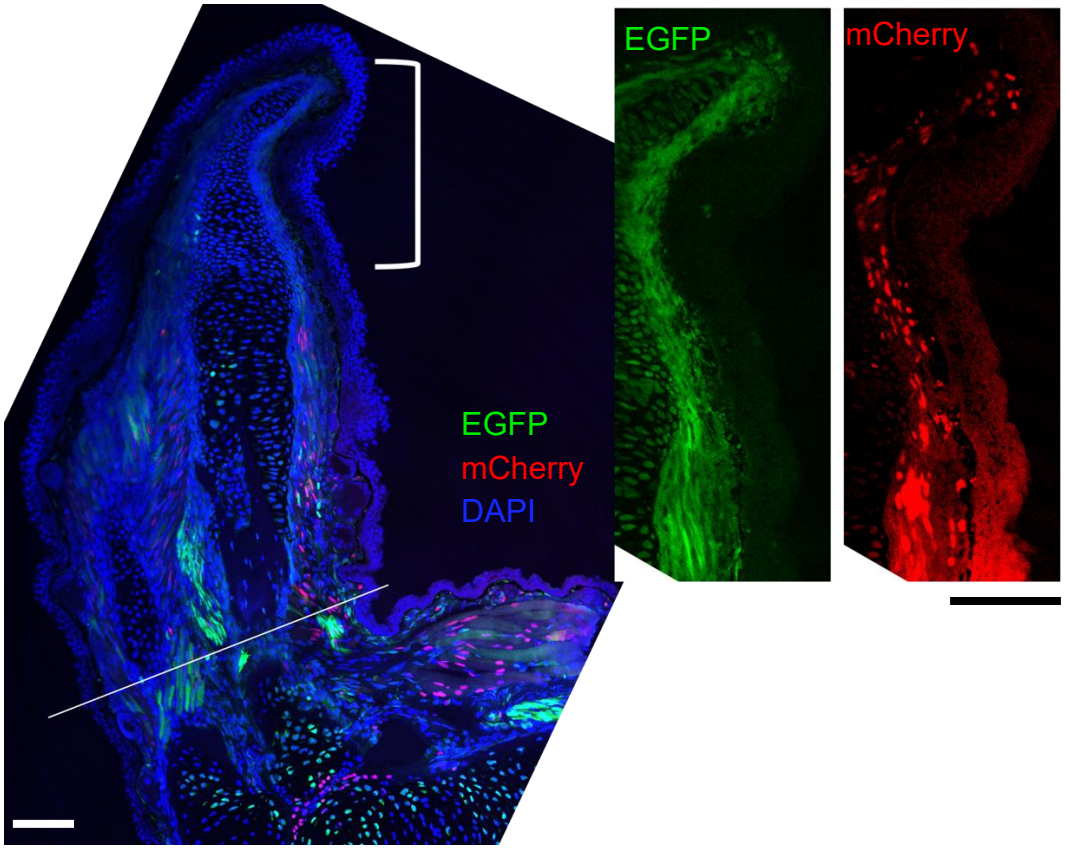

Figure 34. Contribution of muscle dedifferentiation to limb regeneration in MIR juveniles. The images are representative of almost regenerated limb in MIR juveniles. Even though mono-SMFCs were not detected in the blastema (see Figure 33), a large number of mesenchymal cells with N-mCherry nuclei appeared along the space under the skin of a distal part of the regenerating limb, when autopod (hand) formation started in the regenerating limb (n=6). At this stage, as in normal juveniles, muscle fibers with N-mCherry nuclei had already extended distally from the amputation region. Note that the animals used here were mosaics that expressed EGFP at least in muscle. White line, amputation plane. Scale bars, 200 μm.

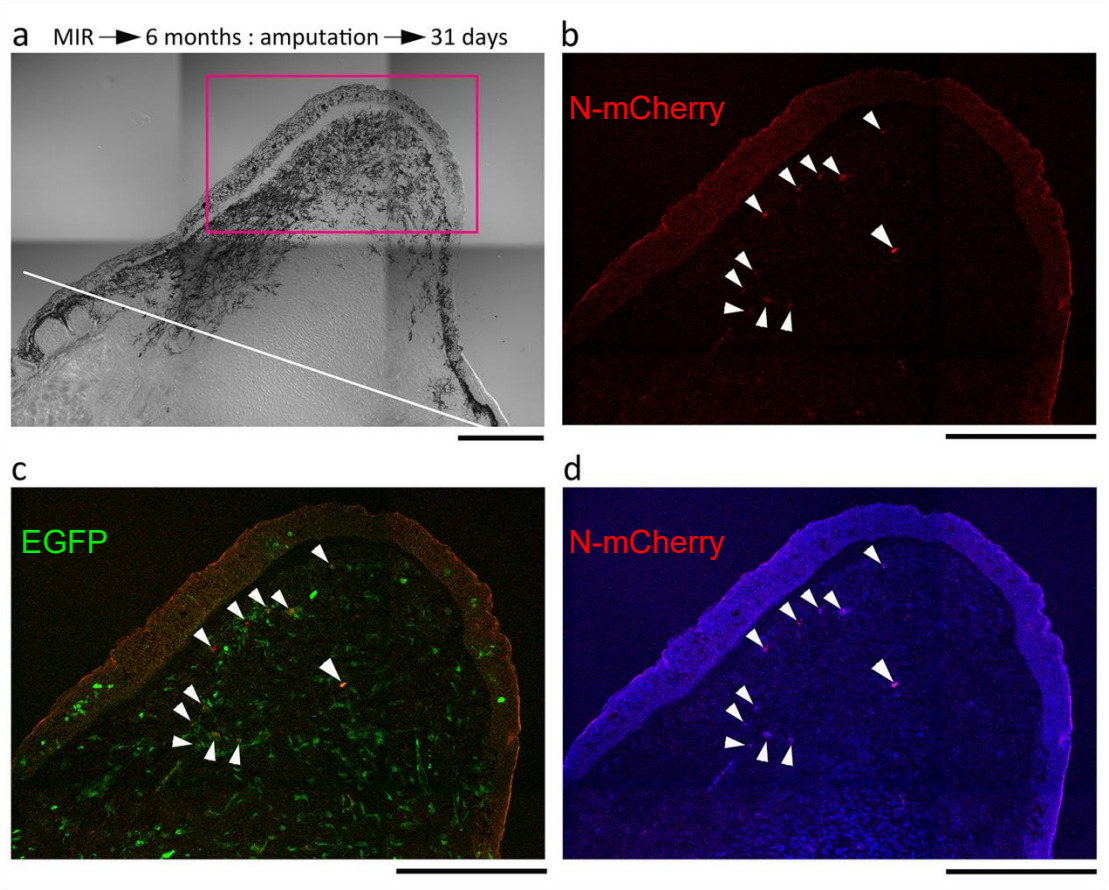

Figure 35. A representative set of images showing mono-SMFCs in blastema of the forelimb of a MIR individual. This animal was reared for 6 months after released from metamorphosis inhibition, and thereafter its forelimb was amputated. The total body length of this animal had reached 7.5 cm immediately before limb amputation. (**a**) A transmitted light image of a section of the blastema at 31 days after amputation. White line: amputation plane. (**b**) N-mcherry fluorescence in the area enclosed by a rectangle in (**a**). (**c**) Merge of N-mCherry and EGFP fluorescence. (**d**) Merge of N-mCherry and DAPI (nuclei) fluorescence. Arrowheads: N-mCherry+ nuclei. Scale bars: 500 μm.

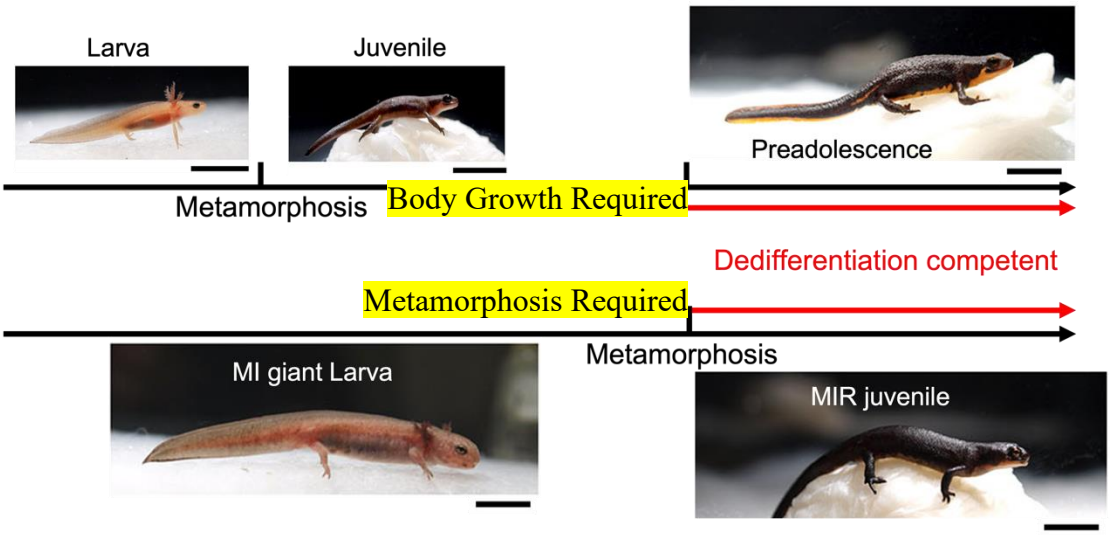

Figure 36. Conclusion. By examine natural developing newts, even animals undergone metamorphosis, body growth (reach size as preadolescence) still required. In other hand, by examine metamorphosis inhibition (MI) newts, no matter how big size they reached, still requiring metamorphosis to switch on muscle dedifferentiation. Taken together, I conclude that a combination of metamorphosis and body growth is required for muscle dedifferentiation.

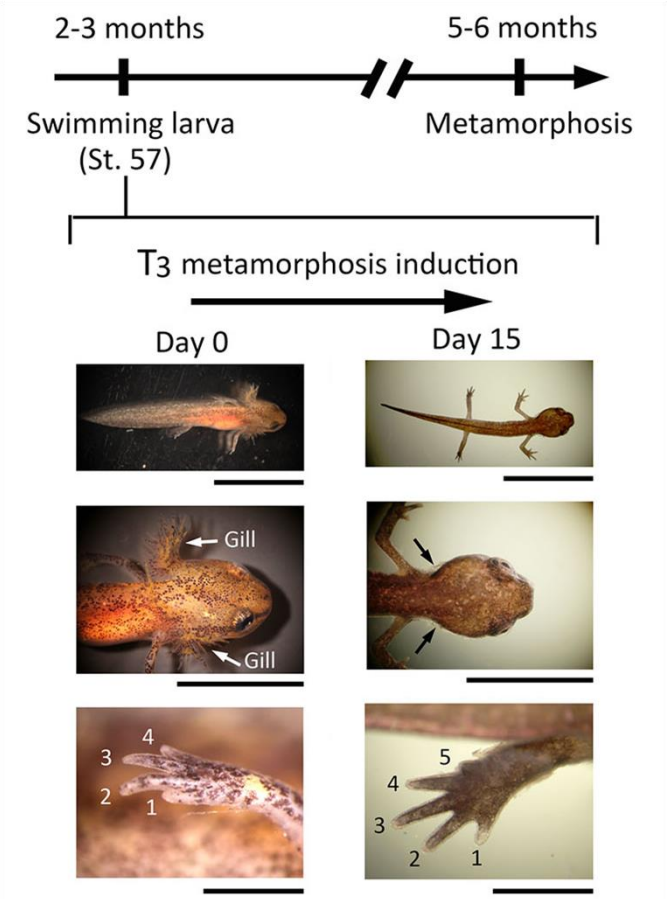

Figure 37. Competency of swimming larvae at St. 57 to metamorphose in response to triiodothyronine (T_3). 2 weeks after T_3 administration, larvae completely metamorphosed. Arrows point to the location of the gills. Degradation of gills indicates metamorphosis. Numbers in lower panels indicate number of fingers as the sign of stage determination. Scale bars from upper to lower are 1 cm, 5 mm, 1 mm.

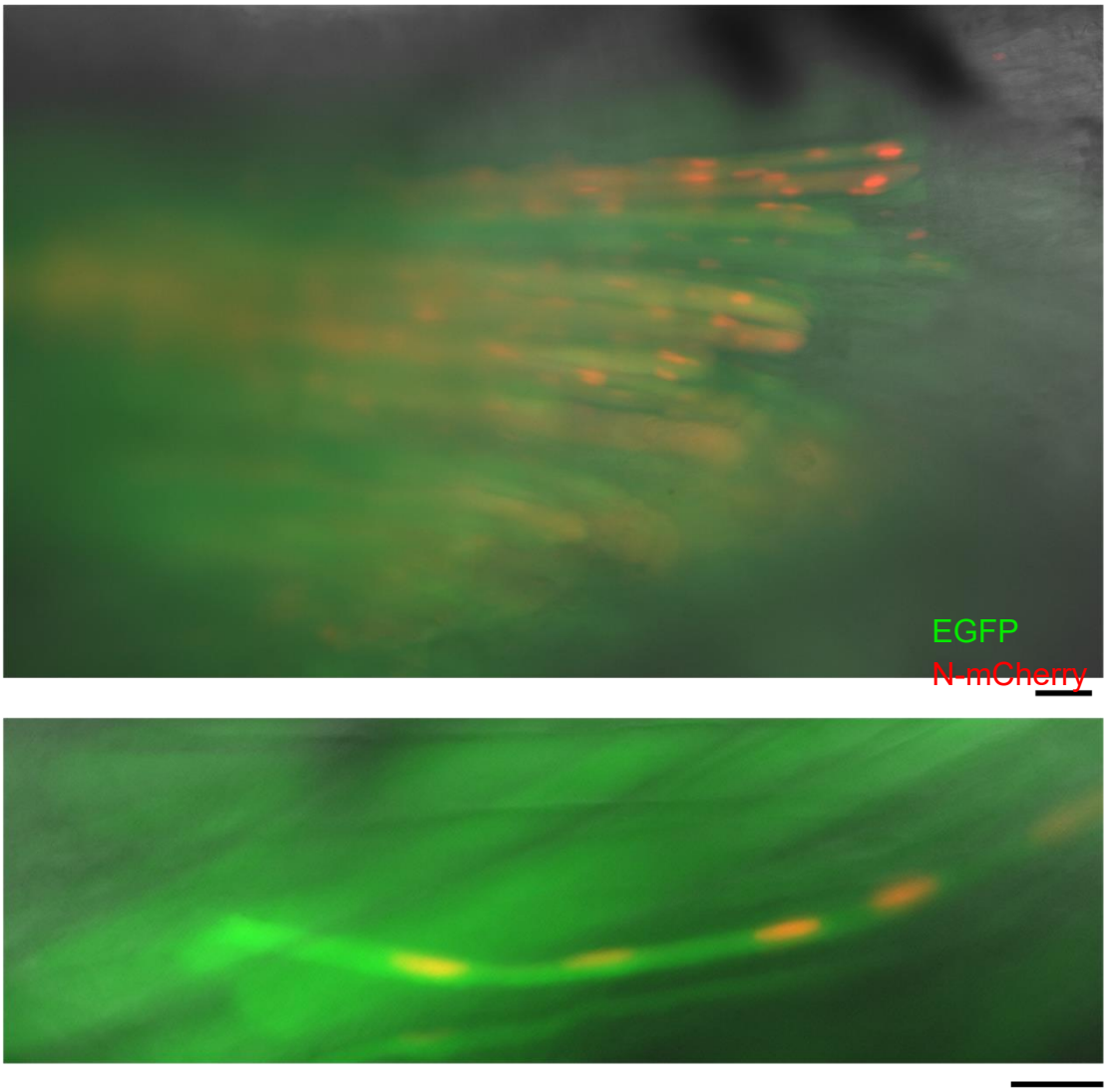

Figure 38. Muscle fiber-specific expression of N-mCherry. Representative images showing N-mCherry expression in nuclei of muscle fibers in swimming larvae at St. 58. Recombination was induced by 4-OHT at St. 53. The images are of live muscles in dissected forelimbs, that was observed under the KEYENCE BZ-X800 fluorescence microscope before being harvested for explant culture.

Scale bar: 100 μm.

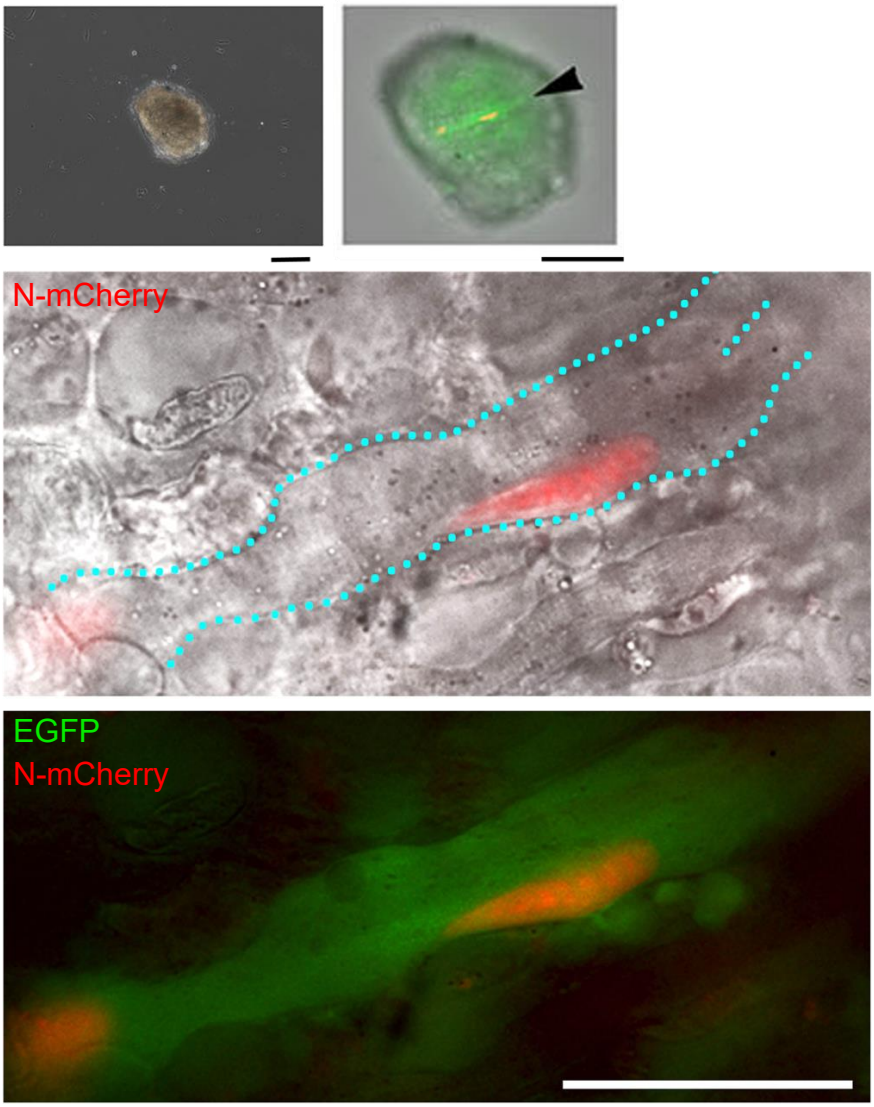

Figure 39. Representative images of adhered muscle explant at day 7. Upper images are an example of adhered muscle explant. In this case, one muscle fiber attached to the substrate with two N-mCherry nuclei (black arrowhead points). Lower panels show attached muscle fiber with fluorescence as well as a striped pattern indicates mature muscle mature striated muscle feature. Dotted line, outline of the muscle fiber. Scale bars, upper: 200 μm; lower: 50 μm.

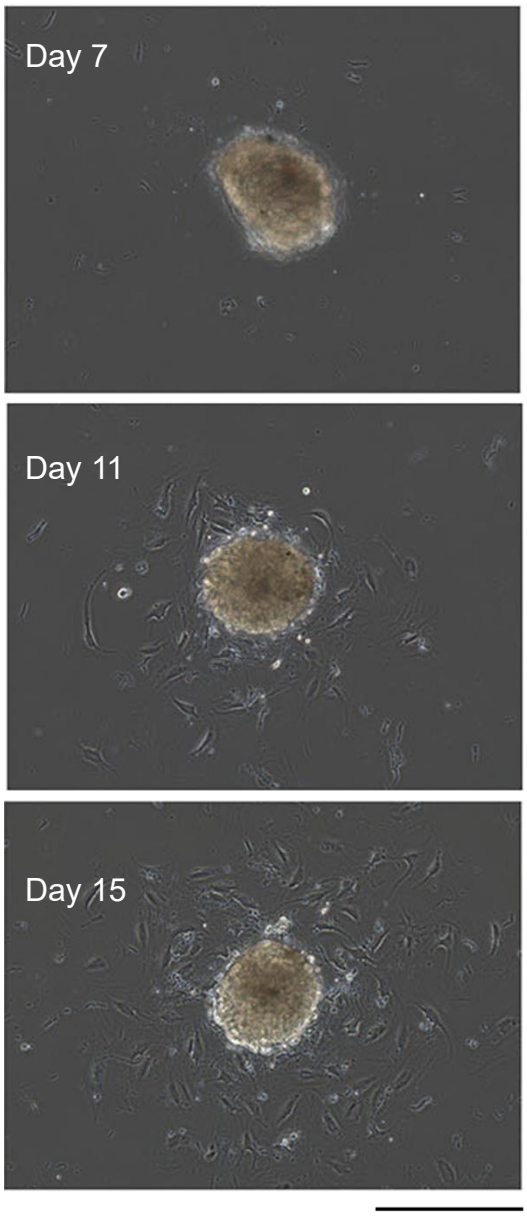

Figure 40. Representative images of an explant in culture. Regardless of T_3 administration, fibroblast-like mesenchymal cells started migration immediately after the explant adhered to the dish in 7 days. Scale bar: 500 μm.

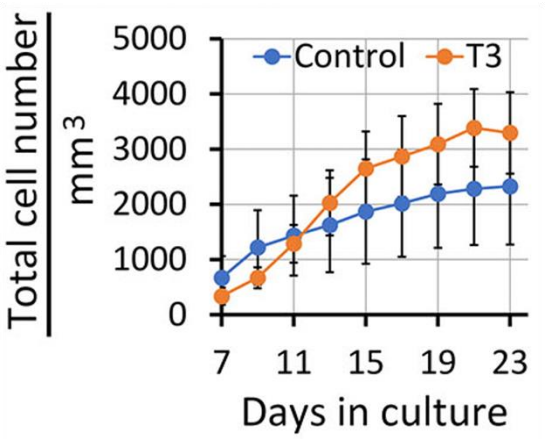

Figure 41. Changes of the total number of migrating cells during culture. The number of cells counted on each day was normalized with explant volume, which was estimated on day 7. The mean values on each day were not statistically different between control (n=4) and T_3 (n=5) conditions.

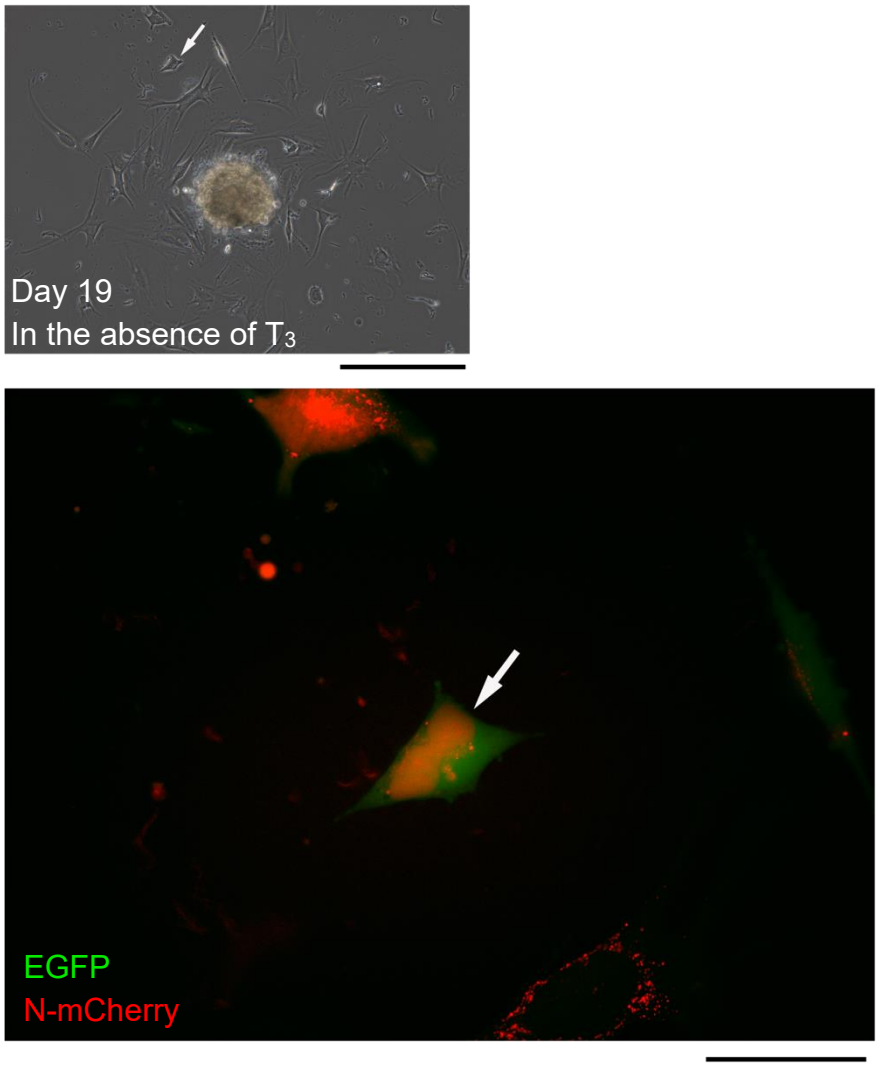

Figure 42. Iv-mono-SMFCs migrated from a larval muscle explant during culture. A representative of iv-mono-SMFCs in the absence of T_3 culture condition. Images were taken on day 19. The fluorescence image of the cell, which is indicated by the arrow. Lower panel was enlarged image of those cells. The cells expressed both N-mCherry in its nucleus and EGFP in its cytoplasm. Scale bars, upper: 500 μm; lower: 100 μm.

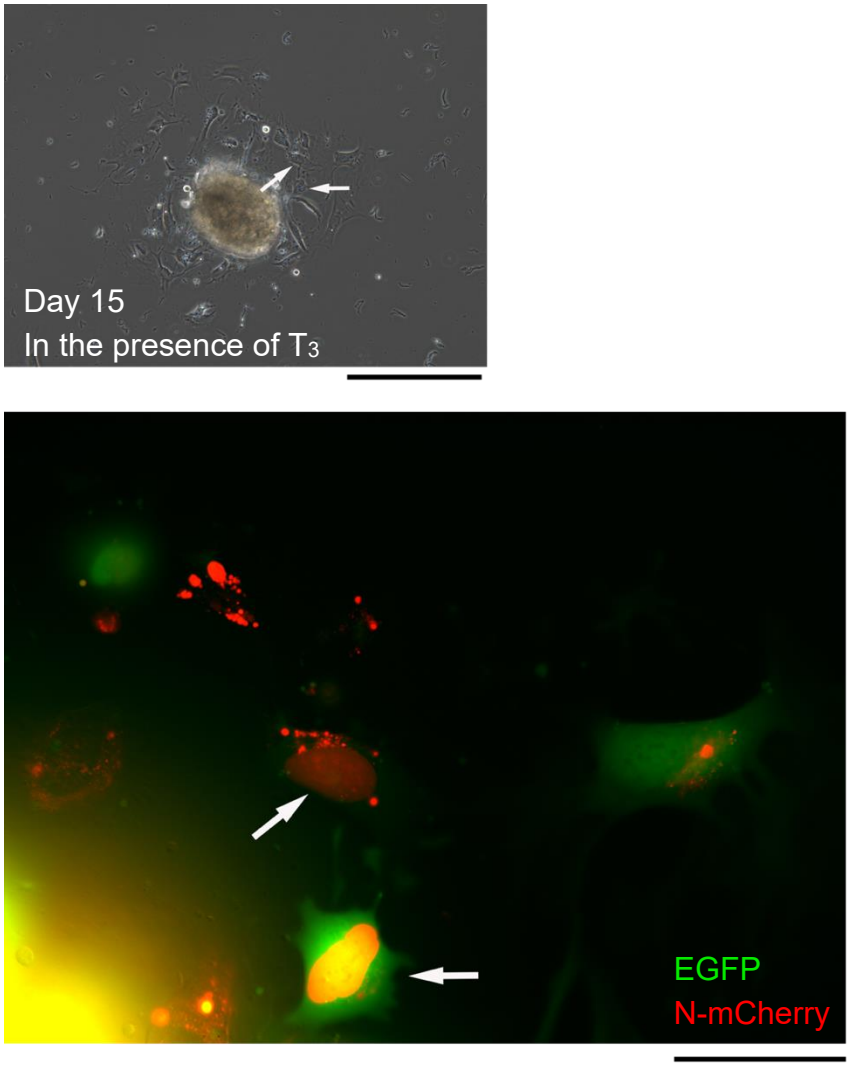

Figure 43. Iv-mono-SMFCs migrated from a larval muscle explant during culture. Representatives of iv-mono-SMFCs in the presence of T_3 culture condition. Images were taken on day 15. The fluorescence image of the cells, which are indicated by the arrows, was enlarged in lower panel. One cell (upper) had low EGFP fluorescence in its cytoplasm, and expressed N-mCherry in its nucleus. The other one (lower) intensely expressed both N-mCherry in its nucleus and EGFP in its cytoplasm. Scale bars, upper: 500 μm; lower: 100 μm.

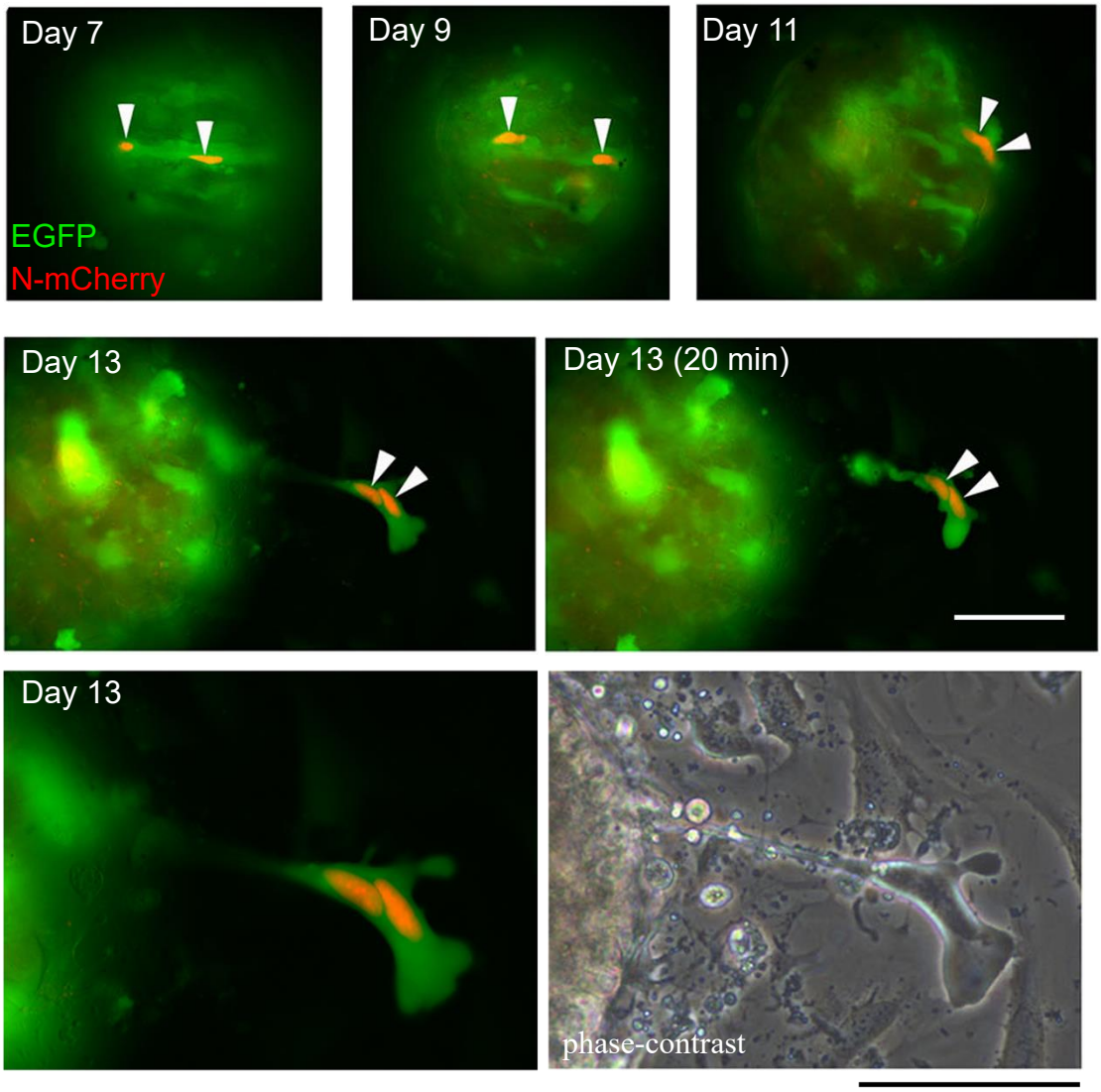
Day 7
EGFP
N-mCherry
Day 9
Day 11
Day 13
Day 13 (20 min)
Day 13
phase-contrast

Figure 44. Tracking of the muscle fiber during culture. This is a case in the presence of T_3. Arrowheads indicate the nuclei. At day 7, one muscle fiber attached to the bottom. And two nuclei migrate along the muscle fiber towards periphery of explant, finally met at the peripheral end of explant at day 11. Then, at day 13, a protrusion formation was observed, which contained two N-mCherry fluorescent nuclei. The resulting cell with two nuclei stayed at the same place for as long as 2 hours but finally disappeared. at day 13, a protrusion formed, since the striated pattern of the muscle fiber disappeared, this may an indicator of muscle fiber dedifferentiation. Scale bar, 100 μm.

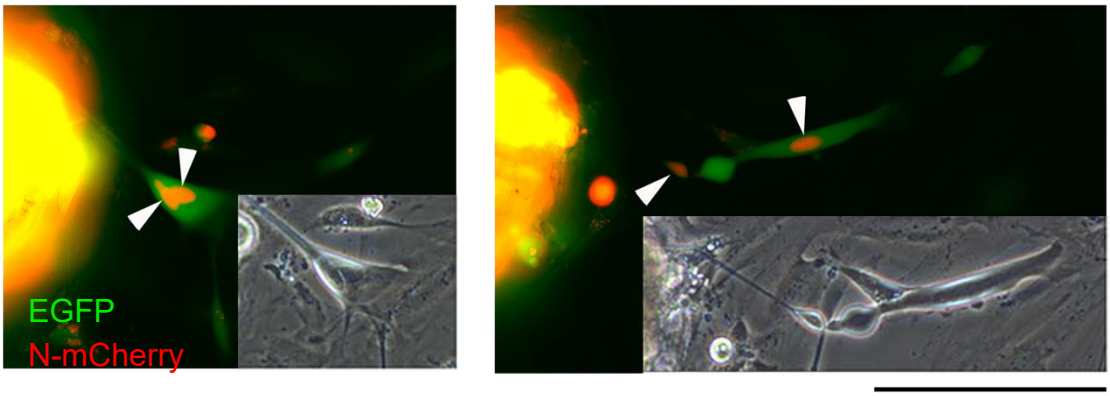

Figure 45. Tracking a protrusion of muscle fiber. Arrowheads indicate the nuclei. Insets indicate phase-contrast images. In this case, the muscle explant was cultured in the absence of T_3 condition. The protrusion contained two nuclei in its leading end on day 19. It gave rise to two mononucleated cells on day 20. One of those (right-hand cell) had an elongated shape and survived (for detail, see Figure 46).

Scale bar: 200 μm.

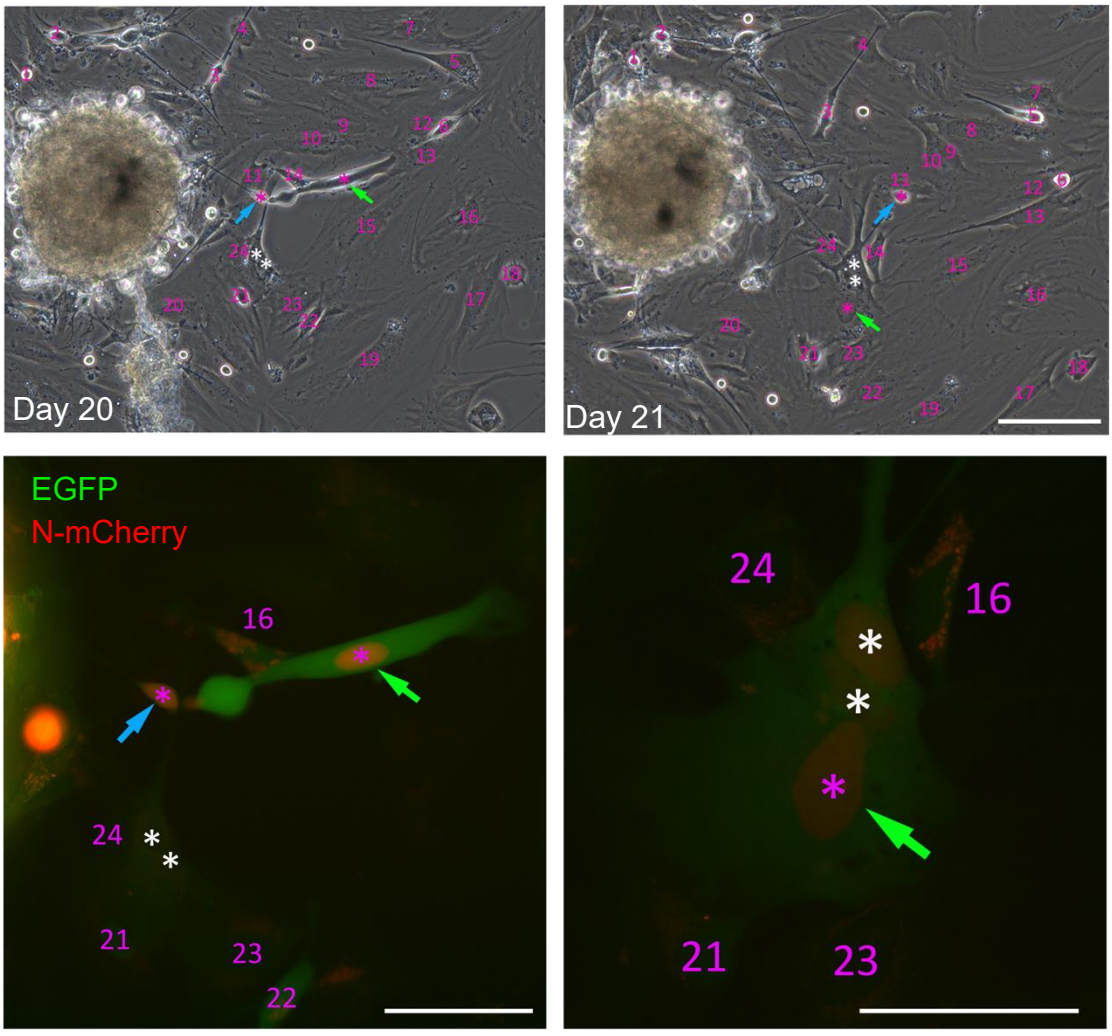
Day 20
Day 21
EGFP
N-mCherry
16
24
21
23
22

Figure 46. Further tracking of the iv-mono-SMFC shown in Figure 45. Left penal are images on day 20. Right penal are Images on day 21. Magenta asterisks indicate the position of the two N-mCherry nuclei which were originally located in the protrusion of a muscle fiber in the explant. The protrusion gave rise to two iv-mono-SMFCs. One (blue arrow) shrank and eventually died. The other one (green arrow), which initially showed an elongated (or tube-like) shape with EGFP in its cytoplasm (day 20), dynamically migrated and fused to another migrating mesenchymal cell with two nuclei (white asterisks) within 24 h (day 21). The recipient cell did not have fluorescence in either cytoplasm or nuclei before fusion (white asterisks in left image). However, after fusion with the iv-mono-SMFC (green arrow in right image), the cytoplasm and nuclei of the fused cell became fluorescent with EGFP and N-mCherry, respectively. Numbers in magenta indicate the ID number of nuclei in migrating cells. Note that in the current culture conditions, red autofluorescence appeared in the cytoplasm of some migrating cells (e.g., the cell with nucleus No. 16). Scale bars: 500 μm for upper images; 50 μm for lower images.

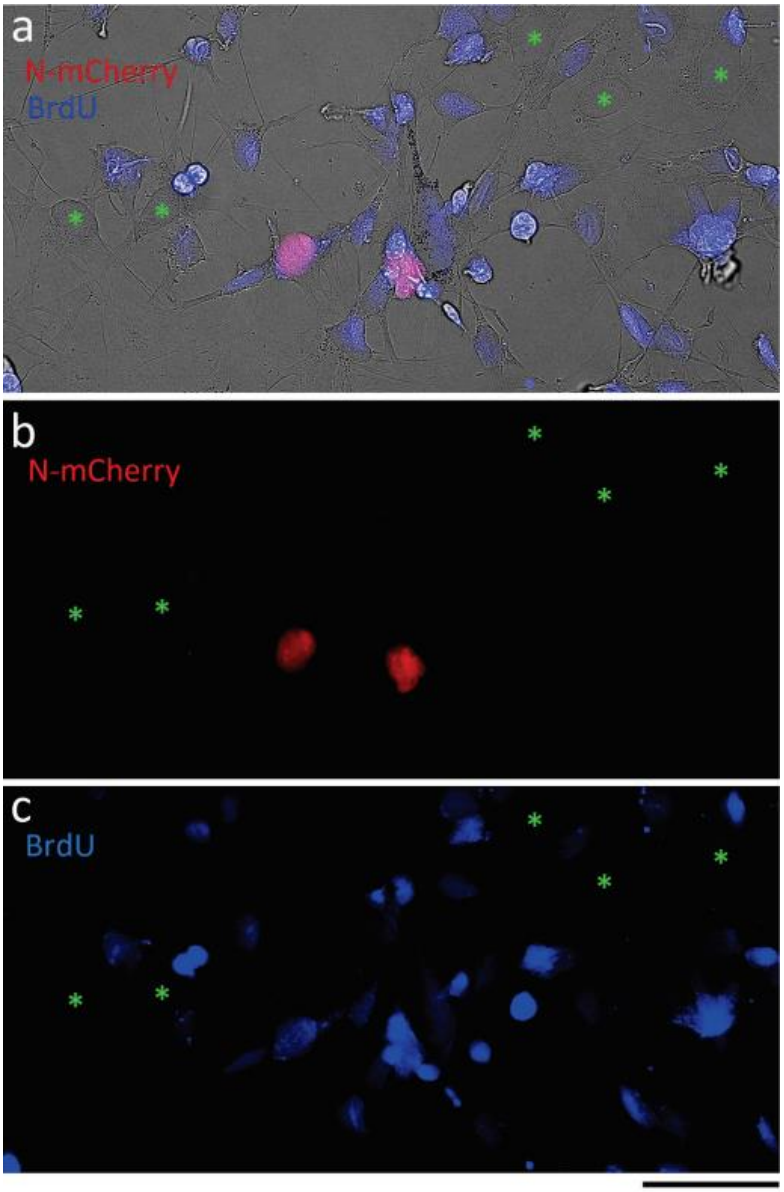

Figure 47. Cell cycle entry of iv-mono-SMFCs. Iv-mono-SMFCs migrated from a muscle explant during culture for 23 days were further cultured in the presence of 10 μM BrdU for 15 hours. In this culture condition, the medium contained 10% normal fetal bovine serum. (a) A merge of N-mCherry fluorescence (b) and BrdU immunofluorescence (c) on a transmitted light image. Asterisks: nuclei without BrdU labelling. Scale bars: 100μm.

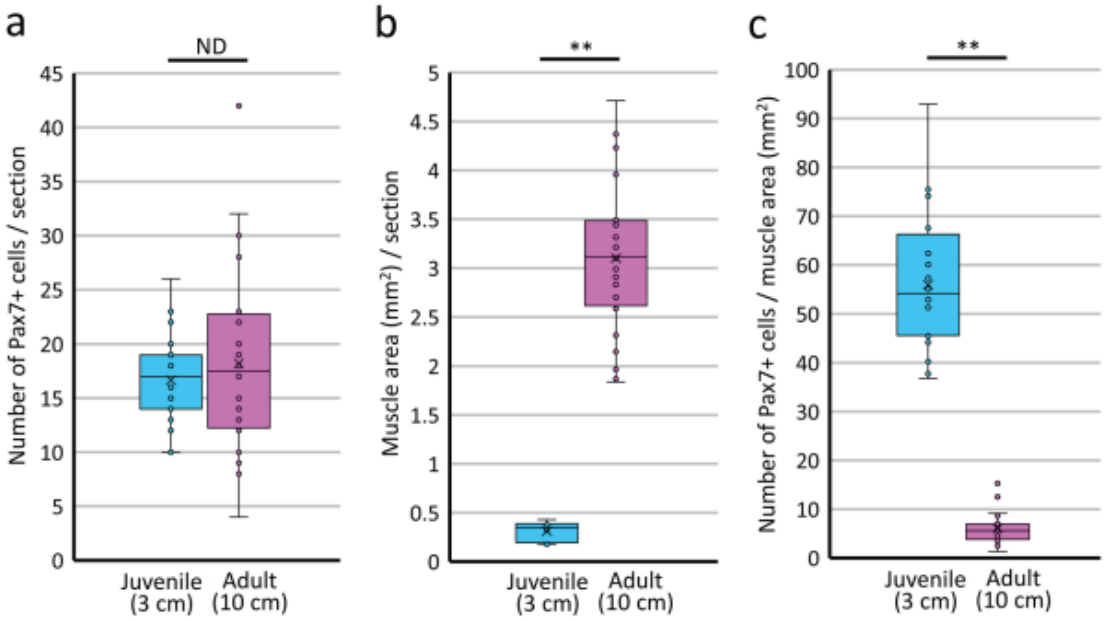

Figure 48. Boxplots showing the comparisons of the density of satellite cells in muscles between juveniles and adults. I prepared transverse sections (8 serial sections, each 20 μm) of the forearm near the elbow and visualized satellite cells by Pax7 immunohistochemistry. Here I compared the number of Pax7+ cells/section (a), muscle area (mm^2)/section (b) and the number of Pax7+ cells/muscle area (mm^2) (c) between juveniles (3 cm; n=3) and adults (10 cm; n=3). Although the total number of Pax7+ cells per section was not significantly different between juveniles annd adults (a), the number of Pax7+ cells/muscle area (mm^2) was significantly reduced in adults (c) due to the increase of muscle size as the body grows (b). These results suggest that the density of satellite cells in adult muscle is much lower than that in juvenile muscle. ND: no difference. **: Welch's t-test, p<0.001.

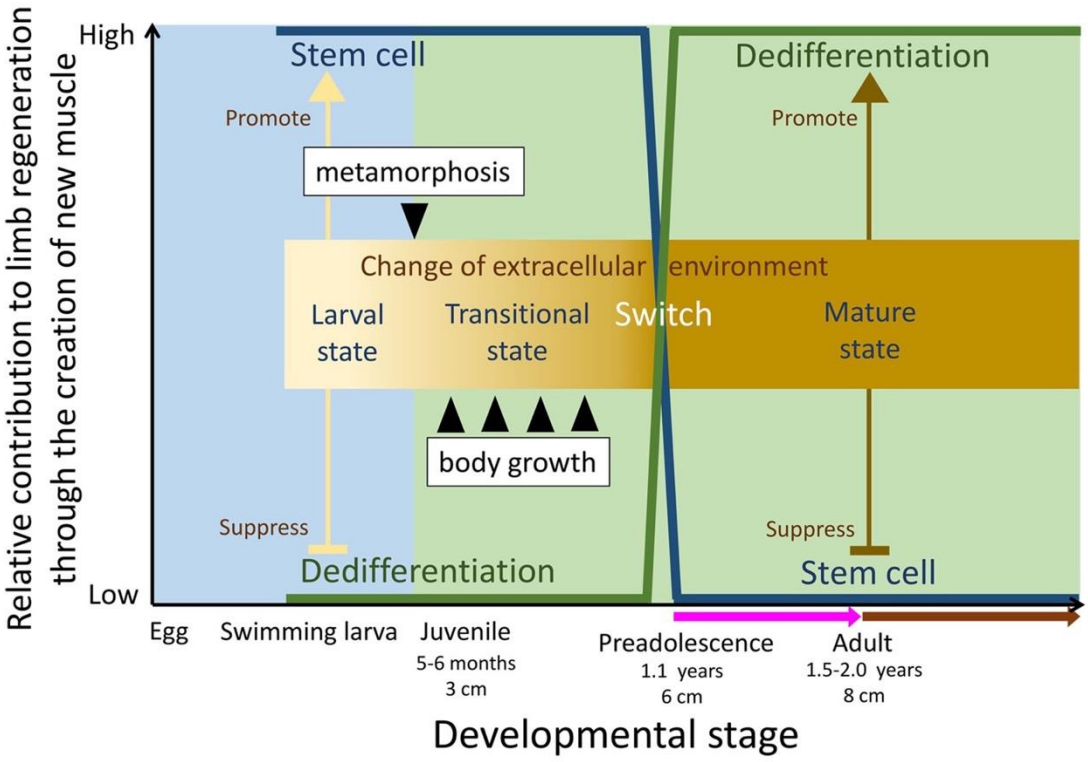
Relative contribution to limb regeneration through the creation of new muscle
High
Low
Stem cell
Promote
metamorphosis
Change of extracellular environment
Larval state
Transitional state
Switch
Mature state
body growth
Suppress
Dedifferentiation
Dedifferentiation
Promote
Suppress
Stem cell
Egg
Swimming larva
Juvenile
5-6 months
3 cm
Preadolescence
1.1 years
6 cm
Adult
1.5-2.0 years
8 cm
Developmental stage

Figure 49. Hypothesis. Relative contribution of myogenic stem cells and dedifferentiation of muscle fibers to limb regeneration through the creation of new muscle is switched prior to the preadolescence stage. Metamorphosis and body growth regulate this switch, possibly by changing the extracellular environment (niche) in the limb from the larval state to the mature state. The extracellular environment in the larval state allows the myogenic stem cells to exert their capacity to create muscle while suppressing the intrinsic ability of muscle fibers to dedifferentiate. When the newt grows to preadolescence beyond metamorphosis, the extracellular environment transits to the mature state and the situation becomes opposite such that the muscle fibers are allowed to exert their dedifferentiation capacity for muscle creation, while the performance of the myogenic stem cells were eliminated. It must be noted that it has not yet been determined in what proportion dedifferentiation and stem cells contribute to muscle creation in post-preadolescence newts.

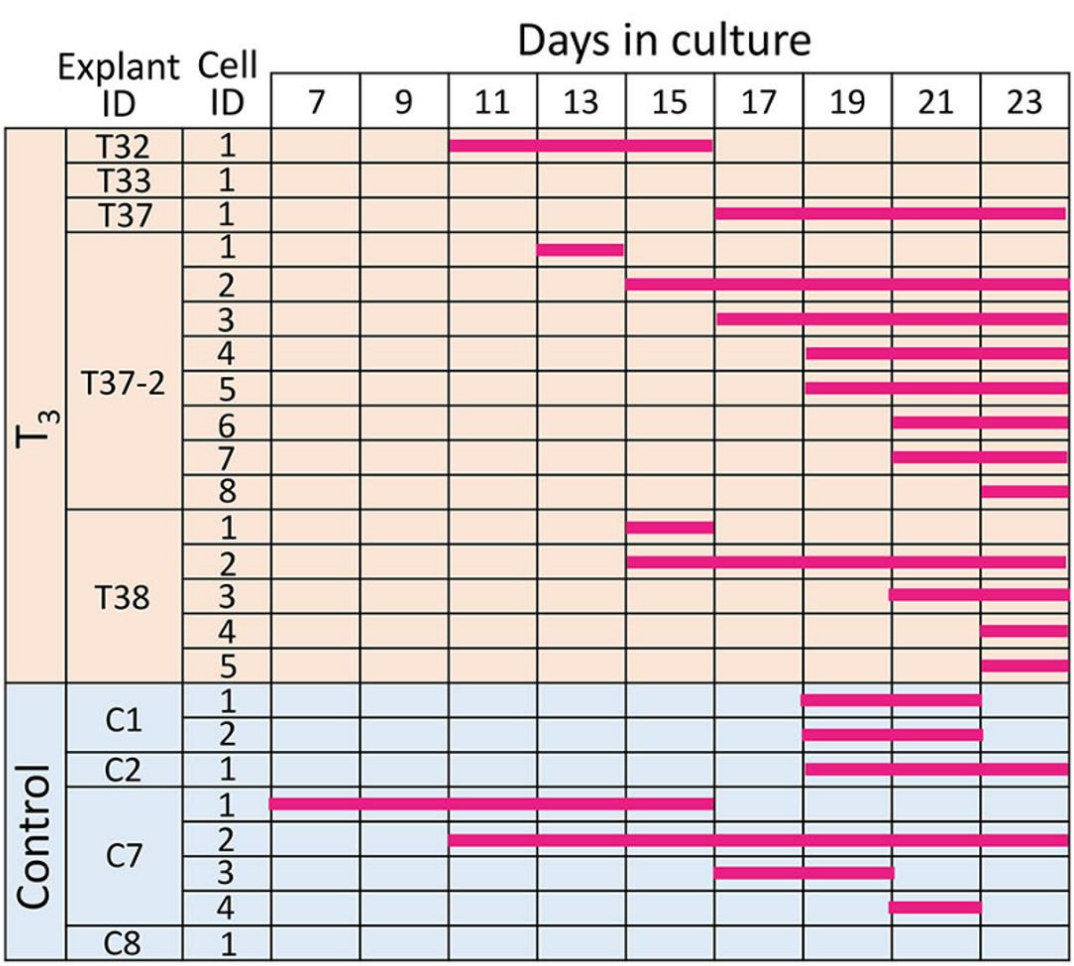

Table 1. Summary of iv-mono-SMFC tracking during culture. Horizontal bars indicate the period between the day of appearance and the day the cell could no longer be followed. Note that the cells, except for cell 1 of explant T37-2 (see Figure 44) and cell 1 of explant C2 (see Figure 45), were already a single mesenchymal cell with one nucleus when I discovered them near the explant.

7. Acknowledgements

First and foremost, I would like to express my deepest gratitude and appreciation to Dr. Chikafumi Chiba, for giving me the opportunity to study in Japan, and conduct research in his laboratory. For all of the invaluable advice, support, motivation, and teachings to continue improving myself, I give my thanks to him.

I appreciate Dr. Takeshima, for him kindly providing albino newt to create live monitor system. I appreciate Dr. Shiga for supporting me in completing *in vitro* experiments. I appreciate Dr. Martin for lots of discussion. I appreciate Dr. Tanaka, H. V helped me start in laboratory. I am grateful to my lab members, who helped me by providing insight and discussions in my study. I appreciate all members of imorinosato, for communications and inspirations.

I appreciate all members of Koga-Rotary club, not just for commercial support and also showed to me China-Japan friendship and world-wide social-responsibility. Also appreciated Dr. Tatsuzaki Jin and Tokiwa Phytochemical which allowed me a new life journey.

I also appreciate Dr. Nakada, Dr. Hashimoto and Dr. Sakamoto, for reviewing my thesis draft, and providing valuable feedback and supporting me to make my doctoral thesis better.

I would like to say thank you and love to my mother (Wang jie), my father (Yu xinguo), and my love (Dr. Chen xutong) for all their unconditional support, encouragement, and love. I am nothing without you.